1. Report No. FHWA/TX-09/0-5089-1	2. Government Accession No.	3. Recipient's Catalog No.
4. Title and Subtitle DEVELOPMENT OF MEASURES TO IMPROVE FIELD PERFORMANCE OF RETROREFLECTIVE RAISED PAVEMENT MARKERS		5. Report Date Published: February 2009
		6. Performing Organization Code
7. Author(s) Yunlong Zhang, Jiaxin Tong, Paul Carlson, Gene Hawkins, and Peter Keating		8. Performing Organization Report No. Report 0-5089-1
9. Performing Organization Name and Address Texas Transportation Institute The Texas A&M University System College Station, Texas 77843-3135		10. Work Unit No. (TRAIS)
		11. Contract or Grant No. Project 0-5089
12. Sponsoring Agency Name and Address Texas Department of Transportation Research and Technology Implementation Office P.O. Box 5080 Austin, Texas 78763-5080		13. Type of Report and Period Covered Technical Report: September 2004 – August 2007
		14. Sponsoring Agency Code
15. Supplementary Notes Project performed in cooperation with the Texas Department of Transportation and the Federal Highway Administration. Project Title: Raised Pavement Marker Improvements URL: http://tti.tamu.edu/documents/0-5089-1.pdf		

16. Abstract

Retroreflective raised pavement markers (RRPMs) are routinely used in Texas to supplement highway pavement markings. In recent years, problems of marker failure such as poor retention on pavements, physical damage, and loss of retroreflectivity are common.

All marker models used in Texas meet the requirements set by American Society of Testing and Materials (ASTM) specifications. However, their performance varies significantly. The results from existing testing methods also do not correlate with field performance. It is therefore critical to identify or develop new lab testing methods that can accurately predict marker performance in the field.

This report presents the research conducted over the three-year period to develop new lab tests that can predict marker field performance. Four field test decks were installed and monitored. Retroreflectivity and physical condition data were collected on six selected RRPM models at four deck locations that were selected based on traffic condition, pavement surface type, geographic and other environmental factors. Currently recommended ASTM tests, modified ASTM tests, and other new lab tests were conducted. Finite element modeling (FEM) of RRPMs under tire-marker impact and lab setting testing was also conducted. The marker performances from the test decks, under lab tests, and in simulation are compared. Based on the results of comparisons, a new lab test that best correlates with the field performance of the RRPMs is recommended.

17. Key Words Raised Pavement Markers, Retroreflectivity, Durability, Lab Tests	18. Distribution Statement No restrictions. This document is available to the public through NTIS: National Technical Information Service Springfield, Virginia 22161 http://www.ntis.gov		
19. Security Classif.(of this report) Unclassified	20. Security Classif.(of this page) Unclassified	21. No. of Pages 204	22. Price

Form DOT F 1700.7 (8-72)   **Reproduction of completed page authorized**

DEVELOPMENT OF MEASURES TO IMPROVE FIELD PERFORMANCE OF RETROREFLECTIVE RAISED PAVEMENT MARKERS

by

Yunlong Zhang
Assistant Research Scientist
Texas Transportation Institute

Jiaxin Tong
Graduate Assistant, Research
Texas Transportation Institute

Paul Carlson
Research Engineer
Texas Transportation Institute

Gene Hawkins
Research Engineer
Texas Transportation Institute

and

Peter Keating
Associate Research Engineer
Texas Transportation Institute

DISCLAIMER

The contents of this report reflect the views of the authors, who are responsible for the facts and accuracy of the data presented herein. The contents do not necessarily reflect the official views and policies of the Texas Department of Transportation (TxDOT) or the Federal Highway Administration (FHWA). This report does not constitute a standard, specification, or regulation. The objective of this project is to develop and recommend lab test procedures for raised pavement markers for the Texas Department of Transportation. The project does not endorse or recommend individual marker manufacturers or marker brands. The researcher in charge of this project is Yunlong Zhang.

ACKNOWLEDGMENTS

TABLE OF CONTENTS

LIST OF FIGURES

xii

xiii

xiv

LIST OF TABLES

CHAPTER 1. INTRODUCTION

Retroreflective raised pavement markers (RRPMs) provide delineation on highways. The *Manual on Uniform Traffic Control Devices* (*MUTCD*) defines an RRPM as "a device with a height of at least 10 mm (0.4 in) mounted on or in a road surface that is intended to be used as a positioning guide or to supplement or substitute for pavement markings or to mark the position of a fire hydrant" (*1*). They are especially useful during nighttime and in rainy conditions when applied pavement markings lose their effectiveness at providing guidance to drivers (*2*). In addition, the rumbling effect of RRPMs reminds drivers to align themselves appropriately in their respective lanes.

RRPMs are diverse with varied configurations. They are available in different shapes. For example, they may be wedge, round, and oval. They are also available in different colors. They can be classified as mono-directional or bidirectional depending on the purpose they serve. One can also classify them as snowplowable and non-snowplowable. The snowplowable markers are used in the areas where snow precipitation occurs.

It is expected that RRPMs would remain in the installed locations and have sufficient retroreflectivity over time. However, markers can lose most of their effectiveness on highways with high traffic volume in a short period of time after installation due to poor retention and durability (*2, 3, 4, 5*). The major problems of marker failure are poor retention on pavements, breaking of marker body or lens, and loss of retroreflectivity. Various factors responsible for these failures include high traffic volume, high loading (such as trucks), sand abrasion, and environmental factors like temperature, humidity, and ultraviolet radiation. Several research agencies suggested that poor manufacturing and inadequate application quality also contributed to the poor durability of markers (*2, 3, 4, 5*).

PROBLEM STATEMENT

It has been reported in the literature that RRPM performance varied with many external conditions. RRPMs often underperform with respect to their expected service life. It would be highly desirable that markers stay on the pavement surface and remain retroreflectively functional for a long duration of two to three years. The reality is, however, that they do not stay

that long. Many RRPMs on high traffic roads will be deficient in retroreflectivity, be structurally damaged, or entirely disappear after less than a year. Several TxDOT districts have reported mass failures of RRPMs. In those reported mass failures, a significant percentage of markers disappeared only weeks after installation. Considering the factors of marker cost, installation cost, and traffic control cost, the poor RRPM durability problem has a significant impact on capital and maintenance costs for departments of transportation (DOTs). It is very important that the factors affecting marker durability be studied.

In addition to marker quality and various external factors, the underperformance of RRPMs can be attributed to the lack of appropriate laboratory testing standards for testing the adequacy of markers to perform well in the field. The existing laboratory testing procedures recommended by the American Society of Testing and Materials (ASTM) have problems in several areas (6). First, RRPMs are generally tested to particular loading levels (pass or fail). Moreover, the existing testing procedures are unable to simulate all the scenarios of tire-marker impact in the field, i.e., contact with angle and offset. The problem remains, however, that RRPMs passing the tests have displayed markedly different field performances. Therefore, it is necessary to examine the existing testing procedures and develop new testing procedures that could better simulate certain field scenarios.

The development of new lab testing procedures requires that these new procedures yield results that correlate RRPM performance in the field. Field testing therefore is critical to this project. Since the performance of RRPMs varies with area type (urban or rural), pavement type (concrete, asphalt, or seal coat), traffic (average daily traffic [ADT] and truck percentage), and environmental conditions, multiple field test decks need to be installed to provide RRPM performance under various conditions.

In addition to field evaluation results that can be used to validate developed testing procedures, a theoretical modeling approach is also considered in this project. The evaluation and recommendation of laboratory testing procedures require that the critical locations and magnitudes of stress inside RRPMs be identified during the tire-marker impact in the field. Therefore, the dynamic process of tire-marker impact has to be studied to determine the stress generated inside markers during the impact. While previous studies mainly tried to discover the factors affecting performance of RRPMs, little work had been carried out to find the critical locations and magnitudes of the stress generated inside markers during the tire-marker impact.

Moreover, measuring the stress multiple times (and including various factors) in the field is not feasible. However, with the advent of finite element modeling (FEM) technology, it is possible to model and simulate the tire-marker impact dynamically and microscopically. It is a very popular method used currently for analyzing real applications in structures and mechanics.

Finite element modeling, simulation, and analysis of tire-marker impact would give information on the critical locations and magnitudes of stresses during the impact. A computer simulation gives the flexibility to analyze the tire-marker impact varying different factors such as tire load and tire velocity, which would not be practical in the field. In addition to these advantages it is also time and cost efficient. This research applies the finite element computational techniques for the simulation and analysis of tire-marker impact in real-world conditions. Field study and laboratory tests of RRPMs are also conducted to help correlate the type and location of damage on markers identified from the two activities and thus recommend ideal laboratory tests for RRPMs.

It has been observed in the field where test RRPMs were installed on both rigid (concrete) and flexible (asphalt) pavement that several RRPM brands had different damage types on these pavement types. Such field observation especially highlights the necessity of examining the stress inside markers during the tire-marker impact on both rigid and flexible pavement. Considering the different applications of pavement on roadways in the United States, it is valuable to evaluate tire-marker impact based on different types of pavement such that the existing and new laboratory testing procedures can be investigated and developed on a more comprehensive basis.

RESEARCH OBJECTIVES

The ultimate goal of this research is to recommend laboratory testing procedures in order to improve the testing standards for RRPMs. FEM and simulation of tire-marker impact, field study, and laboratory tests are used to fulfill the research objectives, which specifically are:

1. to evaluate the marker conditions at the designated field decks over time regarding RRPMs' structural damage and loss of retroreflectivity;
2. to model the tire-marker impact system on both rigid and flexible pavement using finite element tools;

3. to use the model to simulate tire-marker impact and discover the critical locations and magnitudes of stress generated inside the markers during impact;

4. to analyze the effects of varying external factors, i.e., tire load, tire speed, contact angle, and contact location, on the stress generated inside the markers during the impact and identify the factors that have to be evaluated in a laboratory testing procedure;

5. to investigate if the same test is suitable for markers on both rigid and flexible pavement and if there is a need to distinguish laboratory testing procedures for RRPMs based on the pavement type;

6. to evaluate the existing laboratory testing procedures and recommend additional testing procedures in simulation based on the achievements of the prior objectives;

7. to conduct laboratory tests of RRPMs and correlate the results from laboratory tests, field evaluation, and finite element simulation so as to recommend ideal laboratory testing procedures; and

8. to assess an installation process and its effect on marker durability.

RESEARCH BENEFITS

The project will research and recommend lab procedures for testing RRPMs. With good lab testing procedures that can better predict the performance of the markers in the field, TxDOT can test and select marker brands for inclusion in the approved product list. Even though this project does not evaluate individual RRPM manufacturers or brands, both the lab and field tests use common RRPM models. The performance of these markers can be used by TxDOT for vendor selection. It is expected that this research will lead to better marker durability in the field, which will translate into significant savings for the state considering the quantity of annual usage and the current service life of RRPMs.

REPORT ORGANIZATION

After this introductory chapter, a comprehensive review of the state-of-the-art and state-of-the-practice is provided in Chapter 2. This review includes basic knowledge of RRPMs, the previous studies and results of RRPM performance, and current testing practice. In Chapter 3,

finite element modeling of RRPMs is described. The FEM studies the tire-marker impact on asphalt and concrete surfaces and describes the stresses inside markers under different loading conditions. The common lab testing procedures and some modified versions of those procedures are also modeled with FEM for their respective stress conditions inside the markers. Chapter 4 provides the results of FEM and provides a theoretical evaluation of various lab testing procedures based on the comparisons of stress conditions with tire-marker impact modeling. Chapter 5 provides detailed results of field evaluation. The performance of the RRPMs by location, roadway type, traffic condition, and surface type are compared and discussed. Chapter 6 describes various lab tests that have been evaluated and their respective results. A ranking of lab tests is provided based on the correlation between lab test results and field test results. Chapter 7 provides final recommendations and concludes the report.

CHAPTER 2. STATE-OF-THE-ART AND STATE-OF-THE-PRACTICE

This chapter is a review of the state-of-the-art and state-of-the-practice concerning RRPMs. First, it introduces pavement markings and retroreflectivity. Then, it describes RRPMs, their types, functions, and manufacturing processes. The next section concerns the previous research conducted on the durability of RRPMs. In addition, the researchers describe some important results from the district surveys conducted as part of this research project, followed by the existing testing practices for RRPMs. The next section is a brief overview of research conducted on the impact of tires with small obstructions on pavement. The last section describes the basics of finite element analysis (FEA) and introduces some of the FEA tools used in this research.

PAVEMENT MARKINGS

Pavement markings are used as traffic control devices to provide 'information' and 'guidance' to road users (*1*). They are used either as stand-alone devices or to supplement other traffic control devices such as signs, signals, and other markings. Markings have retroreflectivity to make them visible at night.

Retroreflectivity is the phenomenon of light reflecting from a surface (retroreflector) back to the source. A perfect retroreflector will reflect the entire light incident on it back to the source. With no light reflected back to the driver, that would do little to make it visible during night conditions. Fortunately, in real-world conditions, that does not happen and some of the light from the source is scattered in the environment, which makes the reflector and surroundings visible (*7*). Figure 1 graphically shows the phenomenon of retroreflectivity and the variation between theoretical and actual reflection. Retroreflectivity is quite useful in providing guidance in wet weather as well, when standing water might obscure other pavement markings.
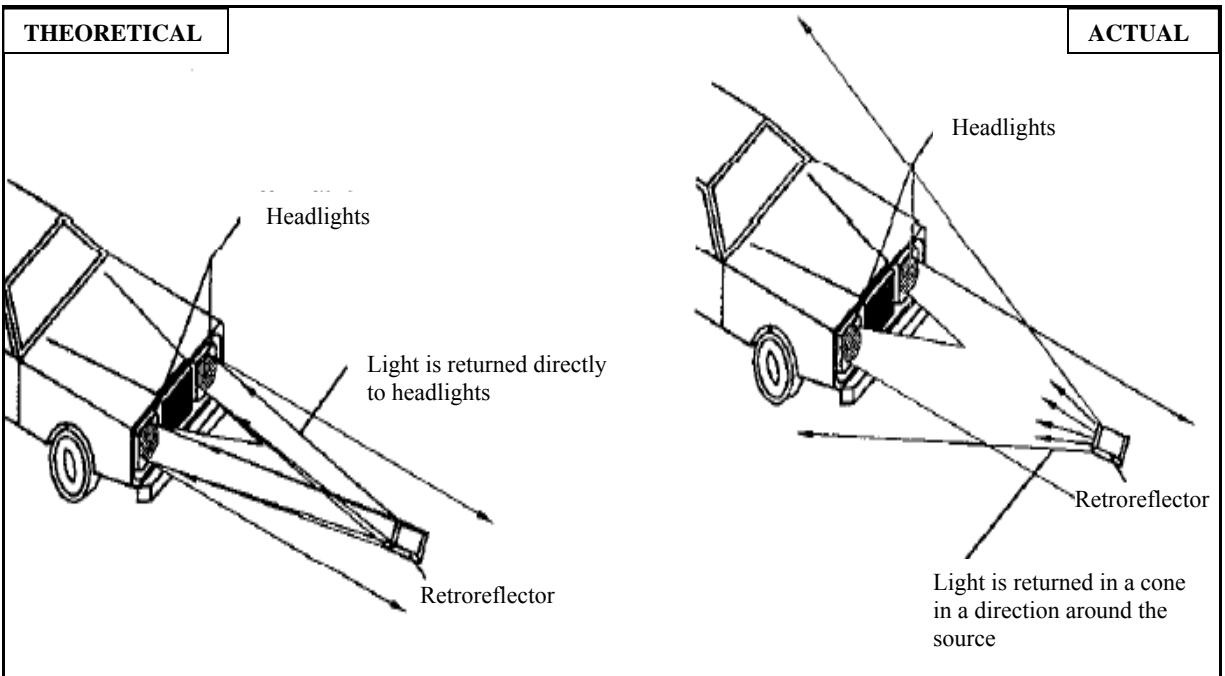
Figure 1. Difference between Theoretical and Actual Retroreflection (*7*).

RETROREFLECTIVE RAISED PAVEMENT MARKERS

The *MUTCD* defines a raised pavement marker (RPM) as "a device with a height of at least 10 mm (0.4 in) mounted on or in a road surface that is intended to be used as a positioning guide or to supplement or substitute for pavement markings or to mark the position of a fire hydrant" (*1*). According to the *MUTCD*, the color of raised pavement markers under both daylight and nighttime conditions shall conform to the color of the marking for which they serve as a positioning guide, or for which they supplement or substitute.

RRPMs are used to supplement other pavement markings. California traffic authorities introduced the RRPMs in 1954 as convex buttons with glass beads on top, applied on concrete pavements using epoxy adhesive. They were called 'botts-dots' (*7*). Their initial application was to supplement traffic control devices during nighttime and wet weather. Currently, wedge-shaped RRPMs are used. This kind of rectangular RRPM was developed around 1955 to improve durability on asphalt pavement. The wedge-shaped markers did not submerge in water. They also allowed one- and two-way delineation. Non-retroreflective ceramic buttons supplement these RRPMs (*7*). Typical retroreflective raised pavement markers are shown in Figure 2.

8

Figure 2. Typical Retroreflective Raised Pavement Markers.

Functions

The inability of conventional pavement markings to provide enough retroreflectivity in wet weather and poor light caused the need for RRPMs. RRPMs have been very effective in providing guidance to drivers in these conditions. Since they are raised above the ground to some height, they can be effective even when a water layer covers other pavement markings. They are also effective at demanding locations like entry and exit ramps, curves, bridge approaches, lane transitions, construction zones, etc. where the roadway geometry hinders proper guidance for drivers.

RRPMs can provide directional information because of their color configuration. For instance, the white and yellow colors in RRPMs inform drivers of the right direction of travel, while the red color represents the wrong direction of travel. The blue RRPMs indicate the locations of fire hydrants. RRPMs also remind drivers to remain in their lanes. This happens when drivers stray over a lane line and strike the RRPMs with their vehicles' tires, which produces a rumbling sound and vibration in vehicles and reminds drivers to remain in their lanes (8).

The disadvantage of using RRPMs is the fact that they are expensive compared to pavement markings. The initial cost of installing RRPMs is very high, compared to applied markings (7). Their reduced durability, as seen in the last few years, reduces their cost-effectiveness, which makes their usage typically limited to high volume roads.

The *MUTCD* details the guidelines for color, positioning, and spacing (Figure 3) between the markers. The figure shows how the RRPMs are positioned as substitutes or supplements to pavement stripes. In the figure, N is equal to 80 feet. The reader may refer to the *Traffic Control Devices Handbook* (8), *Roadway Delineation Practices Handbook* (7), and *Guidelines for the Use of Raised Pavement Markers* (9) for more details on these aspects.
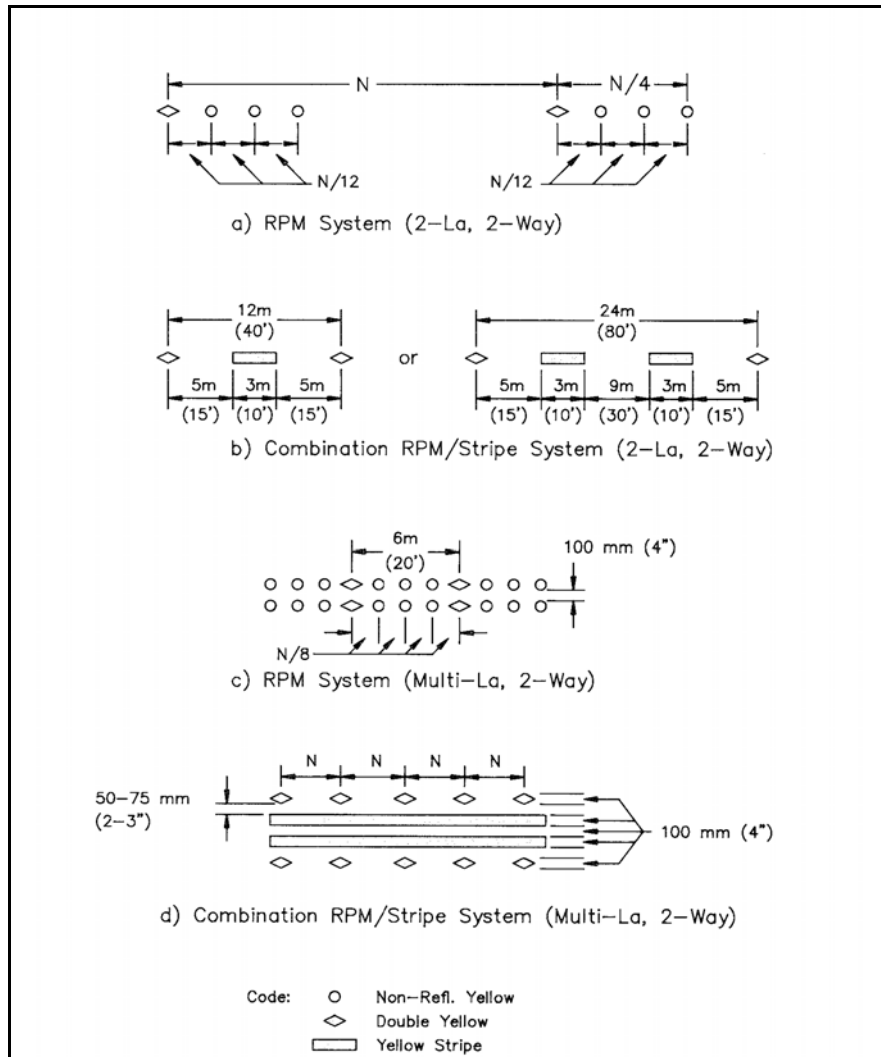
Figure 3. Typical Arrangements of RRPMs on Tangent Sections (8).

Types

There are many different kinds of RPMs. They can be classified based on:

1. *Retroreflective capability.* They can be both retroreflective and non-retroreflective. The non-retroreflective markers, known as just raised pavement markers, are used to supplement retroreflective markings or RRPMs.

2. *Shape, size, and material.* RRPMs can be wedge shaped, round, or oval.

3. Figure 4 shows two markers of different shapes. RRPMs can also be made of different materials, as discussed in the next section.

11
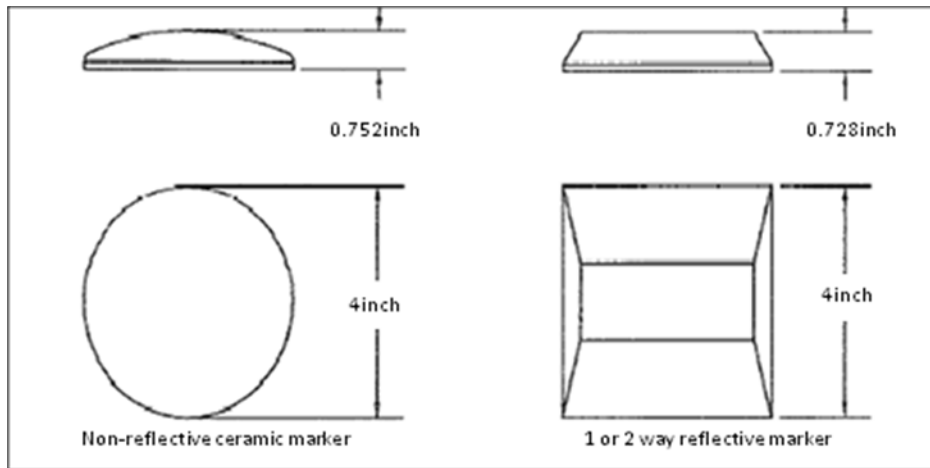
Figure 4. Typical RRPM Configurations (7).

4. *Directional configuration.* The RRPMs can be mono-directional or bidirectional depending on the purpose they serve. Mono-directional RRPMs serve only one direction of traffic, while bidirectional RRPMs serve both directions of traffic.

5. *Color.* RRPMs can come in many colors and configurations. Generally, an RRPM can be white only, red only, two-way white, white-red, one-way yellow, two-way yellow or blue depending on the purpose it serves. For example, a white-red RRPM is a bidirectional RRPM with white and red retroreflective lenses on opposite sides. Yellow markers are used as centerline markers, while blue markers are used to mark fire hydrants.

6. *Lane position.* RRPMs can be edge lines or centerlines depending on their position on the highway.

7. *Snowplowability.* One can also classify RRPMs as snowplowable or non-snowplowable. The snowplowable markers are used in the areas where snow precipitation occurs, for instance, in the northern United States. Areas without snow precipitation use non-snowplowable RRPMs.

Manufacturing

The production design and manufacturing process for RRPMs have evolved over the years. Traditionally RRPMs have had two components: an acrylic shell integrated with a lens and polyurethane resin as the filler. The interior of the shell in the area of the prism array is given a thin coating of aluminum as a mirrored surface. The filler then fills the shell. Some brands have a very thin glass surface bonded to the face of the prism array. More recently, companies have developed markers with no filler and a body made up of impact-graded acrylonitrile butadiene styrene (ABS). The lens is again composed of methyl methacrylate with cube corner technology embedded.

Figure 5 shows the components of a marker. The RRPMs are applied on the pavements using epoxy (generally used for concrete pavements) or bitumen (generally used for asphalt pavements).
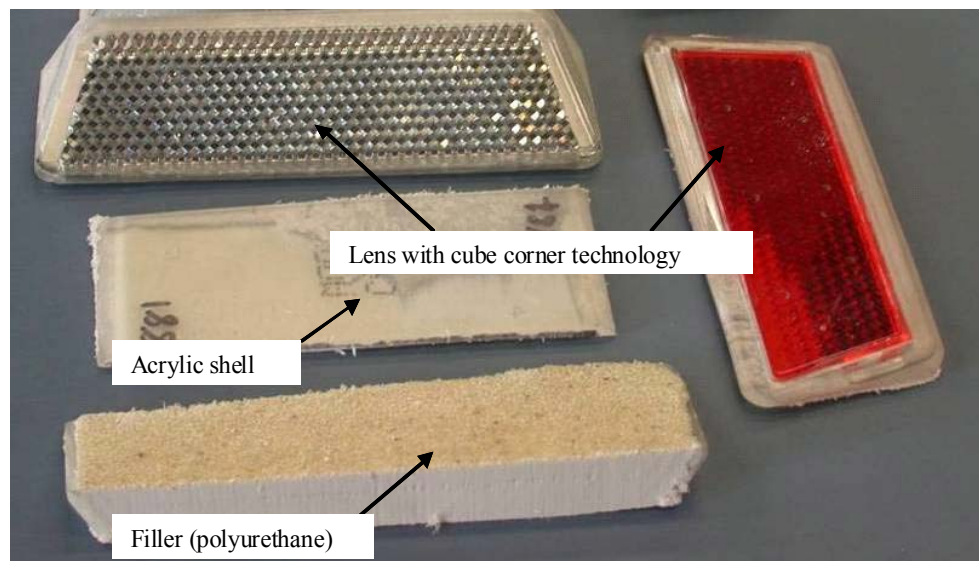
Figure 5. Synthesized RRPM.

RRPMs make use of retroreflective technology that includes the cube corner prism array. In this technology, three mirrored surfaces are arranged at 90-degree angles. They receive the rays of headlights on one of the three mirrors. It reflects the ray to the second, which reflects it to third. This results in the ray returning in exactly the opposite direction from which it entered.

Approximately 360 retroreflective corner cubes are contained in the face of an RRPM (*7*). Figure 6 illustrates the concept.
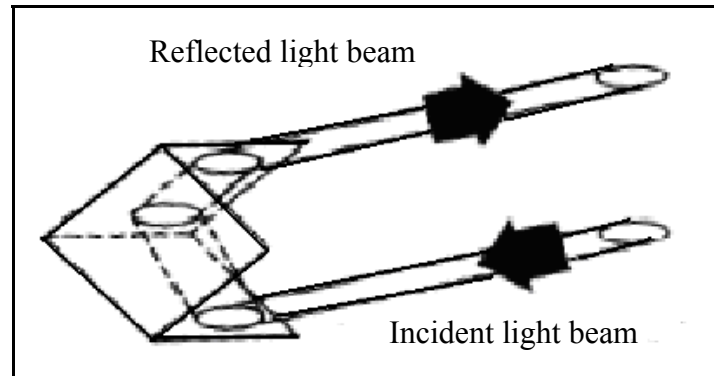
Figure 6. Cube Corner Retroreflection Principle (*8*).

PREVIOUS RESEARCH ON DURABILITY OF RRPMS

Some state traffic agencies have sponsored research on the durability of RRPMs (*2, 3, 4, 5*). Two major problems associated with RRPMs have been poor retention on pavements and loss of retroreflectivity. Traffic agencies have expressed concerns that markers lose most of their effectiveness on high traffic volume highways in a short time after installation because of poor retention and durability.

Lower Durability

There is little published research about the reasons behind the poor durability of markers. The Louisiana Department of Transportation and Development sponsored a study regarding the evaluation of raised pavement markers in which Rushing et al. (*10*) developed a method of simulating field wear and tear on RRPMs. They developed a circular concrete test track on which they installed marker specimens. A tire with a certain load revolved over these markers. The researchers observed the deterioration of marker specimens under these conditions. They recommended developing this test for better field simulation of performance of RRPMs (*10*).

Pigman et al. (*11*) conducted another evaluation of RRPMs for the Kentucky Transportation Cabinet (then called the Kentucky Department of Transportation). They found

RRPMs to be very effective for roadway delineation. The study also resulted in the revision of specifications relating to RRPMs.

The Mississippi State Highway Department also sponsored a similar evaluation of RRPMs (12). They recommended some measures to reduce RRPM replacement costs, a few of which are given here:

- increase spacing between RRPMs,
- test asphalt to determine factors that lead to early failure, and
- make more low profile (lowered height) RRPMs.

The Texas Transportation Institute's (TTI) McNees and Noel (2, 13, 14, 15) conducted research for TxDOT (then called the Texas State Department of Highway and Public Transportation). The researchers identified four problem areas with RRPMs: retention, resistance to wear and tear, high installation and maintenance costs, and early loss of retroreflectivity. They classified marker failures as:

- failure in pavement,
- adhesive-pavement failure,
- adhesive failure,
- adhesive-marker failure,
- marker failure/wear, and
- loss of retroreflectivity (15).

The major external factors causing the failures were:

- traffic volume;
- length of time on the road;
- location of markers, e.g., centerline or lane line; and
- truck traffic.

Other factors responsible for the failures were type of marker, bond size, temperature, humidity, marker height and slope, bond area, tire pressure, tire width, contact location across tread, and vehicle speed (2). Defective epoxies (applying watery or improperly cured epoxies), weak pavement materials (e.g., asphalt cement concrete), and deficient installation procedures may have contributed to the failures as well. The deficient installation procedures included:

- applying RRPMs on surfaces with dirt particles,
- using excessively darkened epoxies,

- using inadequately mixed epoxies,

- using an improper ratio of resin to hardener or insufficient epoxy,

- not covering the bonding surfaces completely or uniformly,

- grinding the bonding surface too deeply,

- pushing markers too firmly or pounding markers,

- putting markers over existing stripes, and

- installing markers in hot/cold weather (*2*).

The primary mode of failure on asphalt concrete was shear or tension failure within the pavement material (asphalt) beneath the marker and adhesive (*2*). Tearing forces came from impacts that tended to twist, slide, and/or rock the RRPM. The study observed that compression was predominant during tire-marker impacts. Pavement can bear compression although pure compression can punch a marker into the pavement.

Any time a resultant downward force on a marker passes outside the center third of the bonded area between the marker and pavement, the adhesive at the opposite edge of the marker will be subjected to simple tension (*2*). This is evident as the marker rolls about an axis in the bonded plane. Adhesive and pavement are least resistant to tension, so the tension causes a bond failure or a pavement failure (*2*). Loads that are not directly vertical may cause shear stresses. Horizontal stresses may be induced because of the shape of the marker or because of vehicle turning, accelerations, or decelerations. This may cause the curved surfaces cupped under the marker to slide (analogous to sliding failures of sloping soil) (*2*).

The most damaging impact occurs when a tire side wall strikes a glancing blow on the nearly vertical side (non-reflective, parallel to traffic) of a marker, such as would be experienced during a turning-passing maneuver. Here the maximum force will tend to displace the marker laterally, twist it about its vertical axis, and rotate it about its longitudinal (traffic direction) axis. The higher the marker, the greater these lateral and twisting forces will be. In addition, a greater slope of the marker wall with the pavement will increase the severity of these forces. So a smoothly contoured low profile marker with a large bond area to the pavement would be desired. A tall marker with nearly vertical sides and small bond area is not recommended (*14*).

The loss of markers from pavements is primarily due to their inability to repeatedly absorb the total force imposed on them and transmit it to the pavement. Environmental and material-related factors aid fracture in the pavement around the epoxy pad holding the markers to

the surface. After some hits, the RRPM, along with some adhesive and asphalt, comes off the surface. Some of the treatments like strengthening the pavement, redesigning the marker to reduce impact forces, and using an adhesive that better absorbs shock forces may increase retention of RRPMs (14).

Tielking and Noel (3) performed a study to increase the retention time of RRPMs on asphalt concrete pavement surfaces. They observed the fatigue characteristics of asphalt pavements under the repetitive loads imparted by tires. The study hypothesized that a fatigue failure in the pavement surface limits a marker's retention time. A fatigue test was also designed to simulate the repetitive loads that a marker imparts to the pavement when hit by a car or truck tire. The test consisted of alternating loads that imparted a rocking motion to the marker installed on the asphalt surface. This generated both compressive and tensile stresses in asphalt under the plate (3). It was also found that the adhesive used to attach the marker influenced the fatigue strength of asphalt concrete. A softer adhesive such as bitumen would give RRPMs (on new asphalt pavement, a more flexible pavement) longer fatigue life than a hard adhesive like epoxy. The advantages of bitumen decrease as pavement stiffness and the input stress level increases. This meant that on high traffic roads, bitumen would be less effective (3).

Tielking and Noel also conducted high speed photography to evaluate the kinematics of tire-marker impacts. They found that a small, high pressure car tire did not bound over the marker but instead stayed in contact over the entire top surface of the marker and remained in contact over the sloping exit surface. A truck tire was more likely to remain on top of a marker than a passenger car tire (3). An instrumented hit marker was also developed as part of this study to measure the number of hits a marker receives. This helped to relate the laboratory fatigue studies to retention time on a highway (3).

In the same study, the authors established that the most critical condition for pavement in terms of negative moment produced is the application of a vertical force on the edge of the non-reflectorized side. Assuming a marker completely rigid and perfectly attached to the surface of the pavement, the pavement force pattern would be like a uniform load of P/L (P being the tire load and L being the width of the marker) and a triangular load of M on the marker top (3). Figure 7 and Figure 8 illustrate this concept.
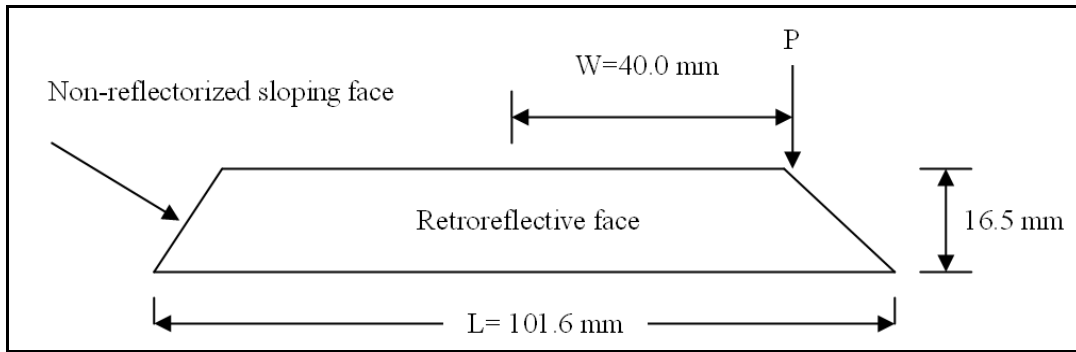
Figure 7. One Critical Force Condition during Tire-Marker Impact (3).
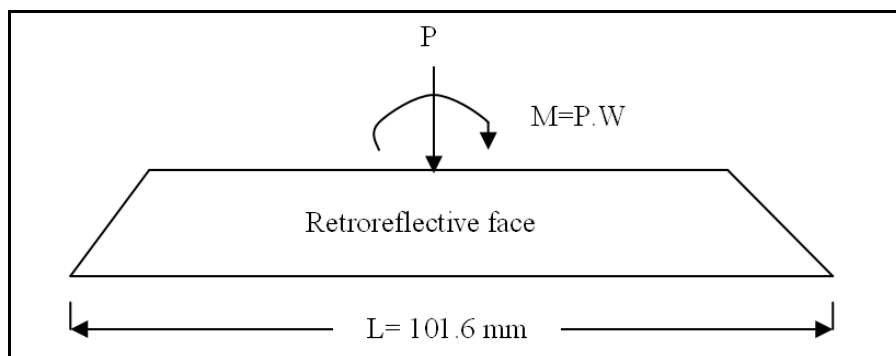
Figure 8. Force Translation for Critical Force Condition (3).

Loss of Retroreflectivity

The primary causes of loss of retroreflectivity in RRPMs are abrasion of the retroreflective surfaces, dirt accumulation, extruded adhesives on the retroreflective surfaces, and structural deterioration causing wear and breakage. Retroreflectivity loss may occur because of worn, missing, dirt-covered, or cracked lenses, or due to softening of filler in hot weather. The loss of retroreflectivity directly relates to the problem of retention; hence, high volume and high truck traffic are detrimental to retroreflectivity as well. Other factors are humidity (improper sealing can allow seepage of water into the marker causing reduction in retroreflectivity) and poor drainage (causing submergence of markers). In rainy seasons, the retroreflectivity may increase due to the cleanup of dirt (13).

Pezoldt (4) conducted a study evaluating the retroreflectivity decay of RRPMs. He observed that physical damage to the retroreflective surface was the primary factor for decline in retroreflectivity. He found that glass-faced markers fared better than plastic ones. On the plastic-

faced RRPMs subjected to abrasion, myriads of scratches scatter light instead of transmitting it directly to the reflective cube corner prism array, hence causing loss in retroreflectivity. However, the glass-faced markers can get shattered with tire-marker impacts, thus causing loss in their retroreflectivities. The plastic face beneath the glass surface in the lens acts like an original all-plastic RRPM. Thus, a glass-faced marker with several chipped or broken areas may still perform better than a plastic-faced marker (4).

Ullman (5, 16, 17) did a two-year evaluation of retroreflectivity of RRPMs in Texas and tried to correlate the field measurements and laboratory tests of retroreflectivities. The major findings were:

- Loss of retroreflectivity was largely dependent on the number of tire impacts, which is a function of traffic volume, especially truck traffic.
- Dirt accumulation was a major cause of loss of retroreflectivity, but it is prominent only in initial degradation in retroreflectivity. After a period, the marker lenses abrade due to a number of impacts.
- The glass-faced RRPMs performed better than the plastic ones.

Pavement Characteristics

In the study conducted by McNees and Noel (14) on the retention of RRPMs, they found that pavement failure is another significant factor causing the poor retention of markers, especially on asphalt pavement. All three types of stresses; tension, compression, and shear, are likely to be generated in pavement under a marker. Pavement is best at supporting the compressive stress that is predominant among these three types of stresses. Adhesives at the opposite edge of the marker undergo tensile stress when the downward force resulting from tire loading is located out of the center one-third of the bonded area between the marker and pavement. The shear stress between the marker and pavement is caused by non-vertical forces that might be produced by vehicle acceleration or deceleration. Furthermore, they revealed that higher RRPM retention can be obtained using bitumen, which gives asphalt pavement longer fatigue life, but such an advantage decreases as pavement stiffness grows and input stress level increases.

Ninety-three percent of U.S. paved roadways are surfaced with asphalt material, which is often called flexible pavement, while rigid pavement, surfaced with Portland cement concrete (PCC), comprises 7 percent of U.S. paved roadways (*18*). In Texas, about 90 percent of the highways are surfaced with asphalt material (*15*). Flexible pavement has a unique structure consisting of several layers of material, with the highest load-bearing material on the top and the lowest one at the bottom (*19*). A typical flexible pavement structure is shown in Figure 9. On the other hand, rigid pavement typically only consists of two layers, the concrete surface and the subgrade (existing soil). The load from vehicle tires distributes differently inside the two types of pavement, which is shown in Figure 10.
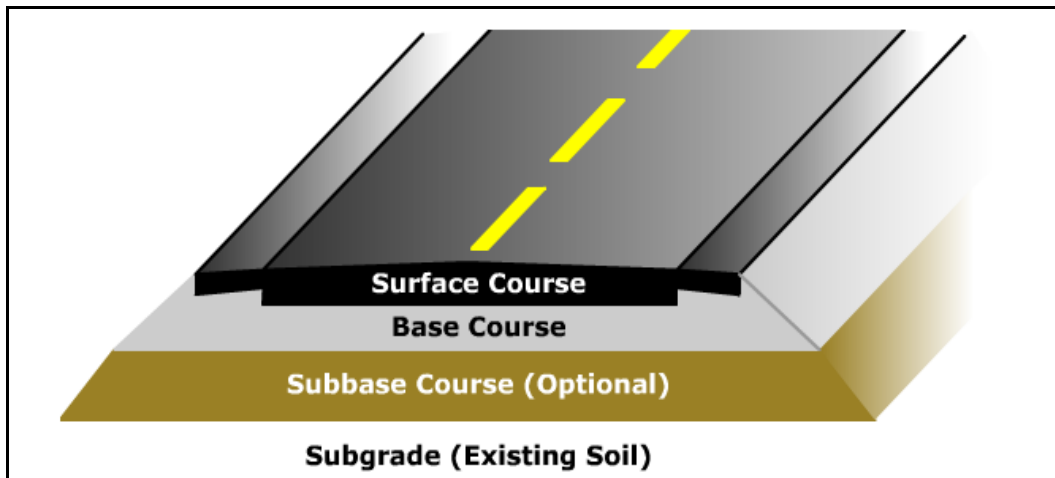
Figure 9. Typical Flexible Pavement Structure (*19*).
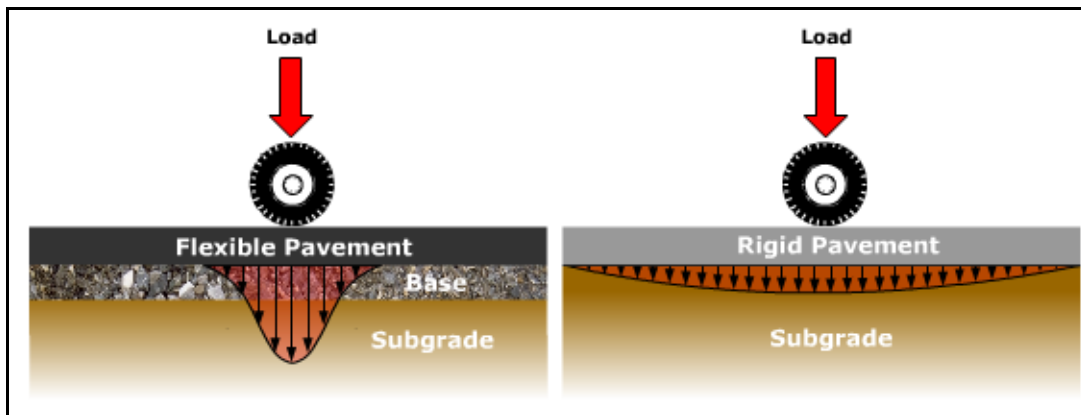
Figure 10. Flexible and Rigid Pavement Loading Distribution (*18*).

DISTRICT SURVEYS

The TTI research project team conducted a survey of TxDOT district staff. The team chose 12 TxDOT districts that represent different areas, climates, area types, roadway surface types, and traffic conditions including annual average daily traffic (AADT) levels and truck percentages. The following are the selected districts:

- Abilene,
- Atlanta,
- Austin,
- Beaumont,
- Corpus Christi,
- Laredo,
- Houston,
- Dallas,
- Odessa,
- Lubbock,
- Bryan, and
- Lufkin.

The team asked the engineers a few questions regarding the state of RRPMs in their respective districts, and to list the main causes that they thought would have caused the deterioration of RRPMs. From their responses, we found the following:

- The markers' performances varied with the traffic on highways. On high volume interstate highways, many markers did not last for more than a year. In some of the districts, the markers did not last for more than six months. Most of the districts replaced or would have preferred to have replaced the markers every year on interstates. On lower volume Farm-to-Market (FM) roads and state highways, the markers lasted for three to five years.

- There was no consensus on the most frequent mode of marker failure. Lens failure, marker loss (off the pavement), and marker breakage were the major failures. A few times the pavement failed beneath the marker, removing the marker, adhesive, and some portion of the pavement.

- The major factors accounting for marker failures were high traffic volume (urban area/intersections) and truck traffic. The type of pavement surface was a factor as well. All the districts had a problem with the seal coat surface treatment, which uses large rocks. Environment was not a major concern, though some districts had problems with hot and rainy weather. The markers could be punched into the pavement in hot weather, while rain could allow moisture to enter RRPMs through cracks, causing retroreflectivity loss.

- A few districts had a mass failure problem on a few projects where many markers failed just after installation. Poor installation practices were the primary cause of these failures (e.g., using bitumen for concrete and epoxy for asphalt pavement surfaces).

- Officials suggested improvements in the durability of lenses. Often the lens was damaged, causing loss of retroreflectivity even though the marker body was intact. They suggested an improvement in laboratory testing procedures for RRPMs. Some officials did not consider the ASTM tests (6) to be adequate tests of the RRPMs. They thought that improved tests were needed that could simulate the vehicular forces on markers.

In addition to the survey by phone, the project team also conducted field visits to the Bryan and Lufkin Districts. During the field visits, the project team had in-depth discussions with TxDOT engineers on marker performance in the respective districts. The team also inspected locations with various marker failure modes. During the visit to the Lufkin District, the team had the opportunity to observe marker installation on a seal coat road. There was an installation quality problem discovered during the field visit.

TESTING PRACTICES

This section discusses various laboratory and field tests performed on RRPMs by different state and national agencies. The agencies performed these tests on samples of markers before they could be installed on the roadways. In this report, the researchers focused on tests that are concerned with the structural performance of RRPMs.

The ASTM provides standard specifications for non-snowplowable RRPMs (6). Most state agencies follow the testing practices provided by ASTM. ASTM standard D 4280 includes a longitudinal flexural test, a compression test, and a resistance to lens cracking test.

In the longitudinal flexural test or three-point bending test, the marker is placed on two steel bars each longer than the width of the marker base (6). The bars are kept at such a distance that they do not protrude beyond the length of the marker. The traffic direction of the marker is perpendicular to the bars. A steel bar, wider than the marker and parallel to the other bars, is placed centered on top of the marker. Elastomeric pads of appropriate dimensions (minimum 3.175 mm [0.125 inch] thick) are provided between the bars and the marker. A load of 5.08 mm (0.2 inches) per minute is applied through the top steel bar until the marker breaks.

Figure 11 shows the experimental setup for this test.
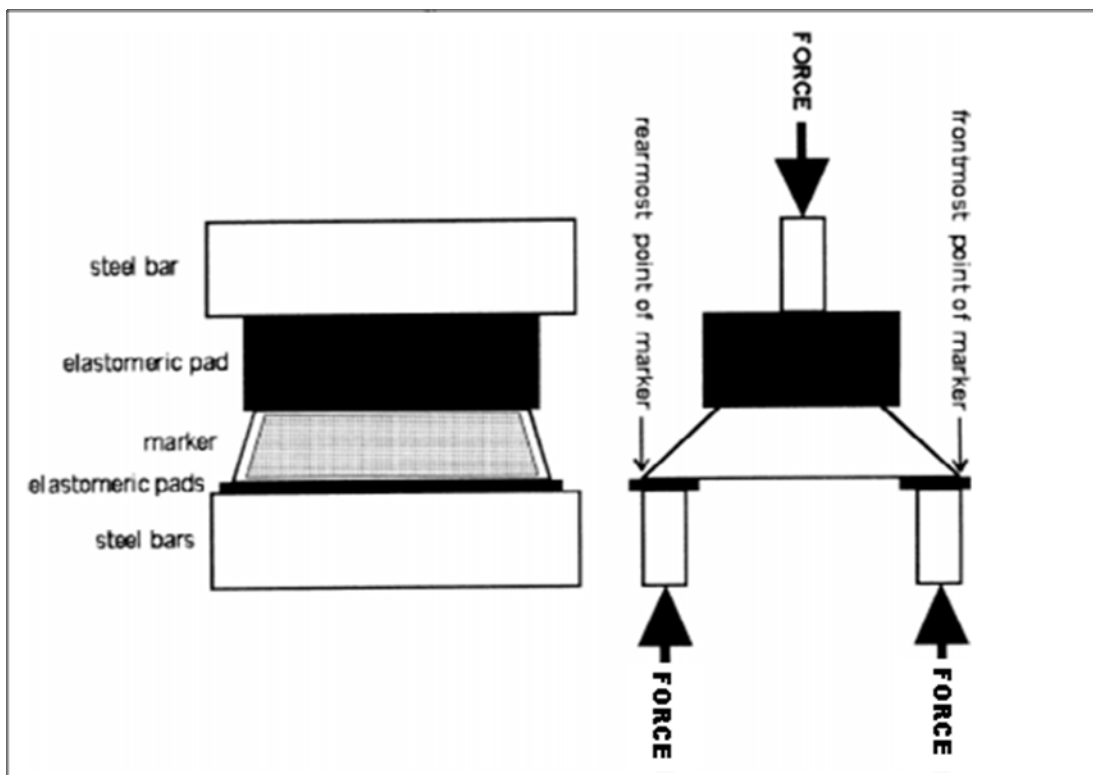
Figure 11. Longitudinal Flexure Test (6).

23

In the compression test (*6*), the marker is placed between two 12.70 mm (0.5 inch) thick steel plates larger than the marker. Elastomeric pads of appropriate dimensions are placed between the marker and the plates. Then, a load is applied at a rate of 2.54 mm (0.1 inch) per minute on the upper plate.

In the resistance to lens cracking test, a 0.19 kg (0.42 lb) dart fitted with a 6.35 mm (0.25 inch) radius semi-spherical head is dropped from a height of 457.20 mm (18 inches), perpendicularly onto the retroreflective surface of the marker (*6*). The marker is placed on a steel fixture designed to hold the retroreflective face horizontal (*6*).

Some states perform other tests in addition to these tests or perform some variations of ASTM tests. For instance, California (*20*) requires a water absorption test in which the marker is kept in water for 48 hours and then examined for any delamination or loss of retroreflection.

The American Association of State Highway and Transportation Officials (AASHTO) voluntarily evaluates the laboratory and field performance of RRPMs (*21*). The plan, known as the National Transportation Product Evaluation Program (NTPEP), evaluates the markers on a 0-5 scale, with 0 for a marker that is absent to 5 for a marker present with structural integrity and retroreflectivity intact. Manufacturers may choose to have their products evaluated by this plan.

TIRE-OBSTRUCTION CONTACT FORCES

To understand the wear of RRPMs by tire impacts, it is important to study the effects of tire forces on small obstructions on roads. Many researchers have tried to understand tire-road interactions (*22, 23, 24, 25, 26, 27*), often using finite element methods. A few have tried to estimate dynamic forces produced when tires encounter large obstacles (*28*) or irregularities (*29*). Bonse and Kuhn (*30*) developed an apparatus for measuring the forces exerted at a point on the road surface by the tires of moving vehicles. They also investigated the influence of tire inflation pressures, speeds, accelerations, tire loads, height of the stud (an obstacle that is small, circular, and 25.4 mm (1 inch) in diameter in this study) above the road surface, etc. on these forces. They concluded that the inflation pressure and stud height influenced the vertical force (Figure 12). The figure shows that an increase in the height of the stud increases the vertical force. In addition, the force increases away from the center of the tread and then decreases at the edges.
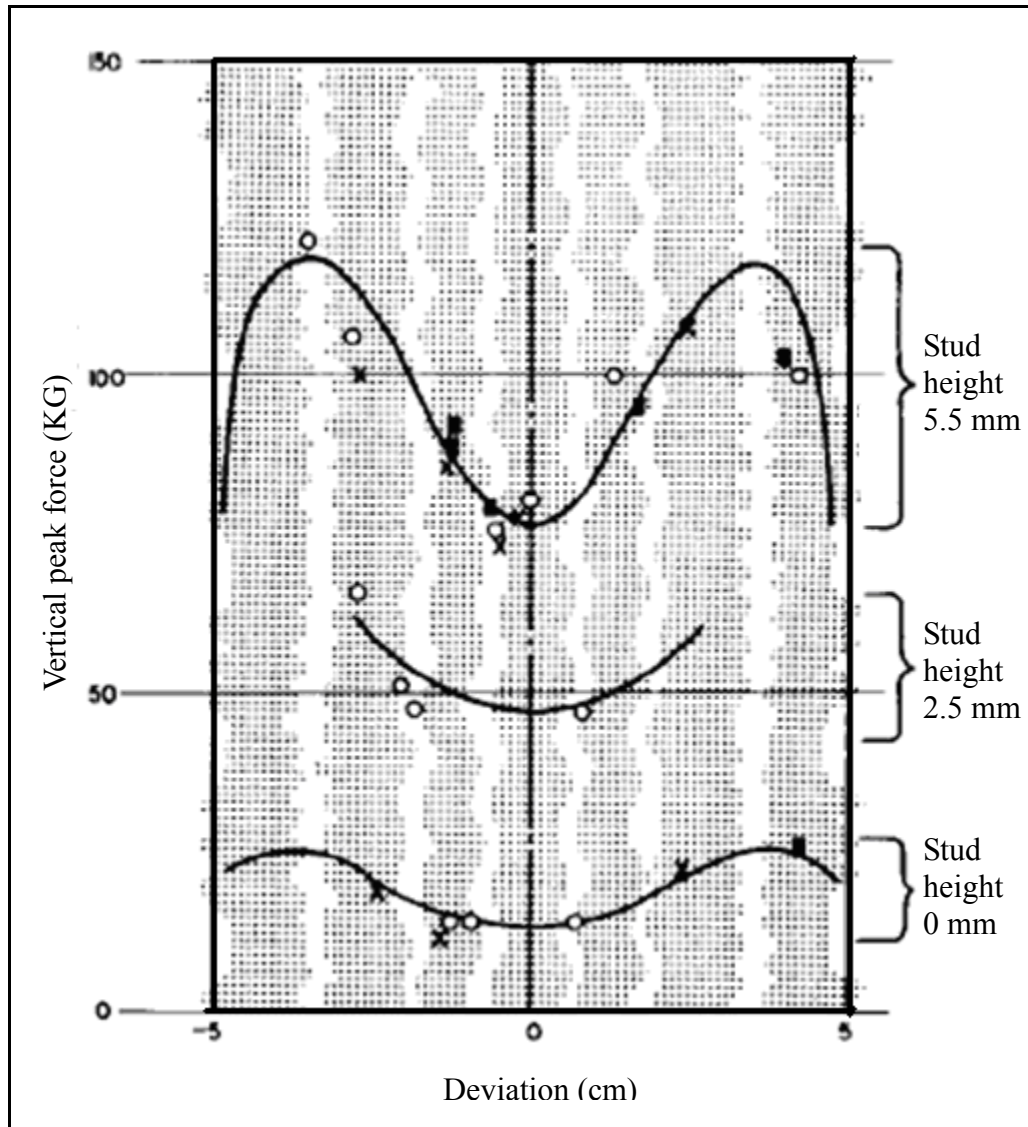
Figure 12. Influence of Stud Height on Transverse Distribution of Vertical Force (*30*).

In another study, Hansen et al. (*31*) found that an increase in the inflation pressure increase (at constant tire load) resulted in an increase in the contact pressure in the tread's central region. Increased tire load (constant inflation pressure) resulted in lengthening of the contact patch (*31*).

FINITE ELEMENT ANALYSIS BASICS

The finite element analysis has been in use for many centuries (*32*). It involves replacing a complex system with a simpler but approximately accurate representation. FEA was initially

used for simple physical problems, but the advent of advanced computer technology allows it to be applied to broad areas and problems. Martin *(32)* has outlined the development of the modern finite element method. Earlier, FEA was used in analyzing static and dynamic problems associated with aircraft. In the 1940s, when jet-powered aircraft appeared, previous analytical techniques became obsolete in the wake of improved speed and design *(32)*. This led to broad application of FEA. Since the solution to complex problems required solving derivatives, which was tedious and difficult, approximate methods like FEA gained importance. In FEA, a differential equation is approximated by expressing derivatives in terms of the formulae obtained by the Taylor series expansion of a function *(32)*. Boundary conditions, based on the solutions at discrete points, are imposed on the resulting algebraic equations *(32)*.

To understand the basic concepts of FEA, let us consider the problem of estimating the circumference of a circle *(32, 33)*. One way this can be done is to break the circumference into easily measurable segments (Figure 13). It is similar to FEA, in which the domain is separated into separate subdomains, the process being called discretization. Each subdomain is called an element. Points, known as nodes, connect the elements. The collection of elements and nodes is called finite element mesh. In this problem, the perimeter of the circle can be approximated as $P = (2R\sin(\theta/2))n$, where R is the radius of the circle and θ or $(2\pi/n)$ is the angle subtended at the center by the element. The error of the solution would be $\varepsilon = 2\pi R - P$, which will converge to zero as n approaches infinity. Hence, the solution improves as the number of finite elements increases *(32, 33)*.
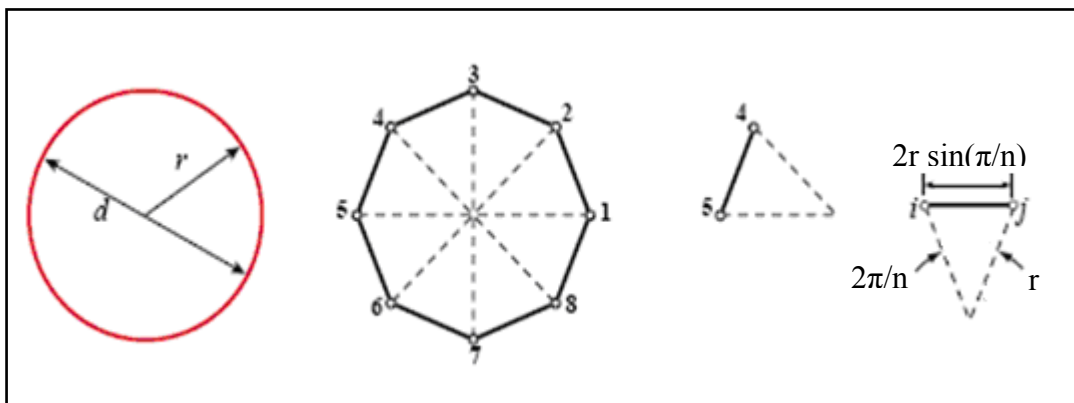
Figure 13. Simple Example Illustrating FEM *(33)*.

FEA allows researchers to handle complex structures, even those with variable material or geometric properties. It can handle nonlinear and time dependent properties. In short, FEA is a very powerful tool to solve boundary-value problems in complex domains (*32*). It has applications in civil engineering structures, aviation, heat conduction, geomechanics, hydraulics, nuclear engineering, biomedical engineering, and mechanical design (*34, 35, 36*).

This study uses FEM (modeling based on the FEA) for understanding tire-marker impacts. The dynamics of these impacts makes it difficult to measure the actual magnitudes and location of stresses generated in markers during impacts. FEM as a proven tool provides an opportunity to analyze these impacts in a cost and time efficient manner. The next chapter details the tools and methodology adopted in this research work.

CHAPTER 3. FINITE ELEMENT MODELING OF RRPMs

This research utilizes finite element tools to simulate tire-marker impact in the real world and then analyzes the results of those simulations to recommend ideal laboratory procedures for RRPM testing. Prior to the start of this research project, the researchers had discussions with the experts at the Center of Excellence in Transportation Computational Mechanics at TTI about finding critical locations and magnitudes of stress inside RRPMs during the tire-marker impact. It was found that the FEM of the tire-marker impact would be a convenient and efficient solution to the problem. Hence the FEM of tire-marker impact was implemented.

Any finite element tool or code has three stages: pre-processing, processing, and post-processing. The finite element tools used in this study are Hypermesh for pre-processing, LS-DYNA for processing, and Hyperview for post-processing. Hypermesh (a finite element meshing tool) is a pre-processor for FEA applications (*37*). Meshing is the process of building a grid of finite elements bound by the model geometry. Hypermesh supports major finite element solvers like LS-DYNA. The LS-DYNA is a general purpose dynamic finite element program (*38*). It can simulate complex real world problems. It is widely used by the automotive industry to analyze vehicle design and by safety researchers for testing strengths of crash barriers. Its applications also lie in the aerospace industry, sheet metal forming, etc. Post-processing was done on Hyperview. Hyperview enables visual and interactive analysis of simulation results (*39*). The researchers chose these tools because they were suitable for simulating dynamic forces on RRPMs as occurs under real-world conditions.

In addition to the computer simulation and finite element analysis, a field study of RRPMs has been conducted throughout the duration of this project. Tests of RRPMs in a laboratory environment have been performed as well. Both of these work as complements to the finite element modeling in the course of developing laboratory testing procedures.

This chapter first describes the finite element modeling process, which includes preliminary modeling and input parameter collection for the final model. Next, this chapter describes the calibration of the model to get accurate estimates of material properties. Furthermore, the modeling of pavement properties based on the preliminary tire-marker impact model is introduced, followed by the simulation of tire-marker impact. The last section discusses

the simulation of laboratory conditions, which the researchers developed and modeled in an attempt to replicate the stress generated in markers during the tire-marker impact.

PRELIMINARY MODELING

As a part of this task, the researchers first obtained a preliminary tire-RRPM model and gathered information required to initiate the modeling and simulation of tire-marker impact. Dr. Akram Abu-Odeh, an expert at the Center of Excellence in Transportation Computational Mechanics at TTI, made the preliminary model (Figure 14).
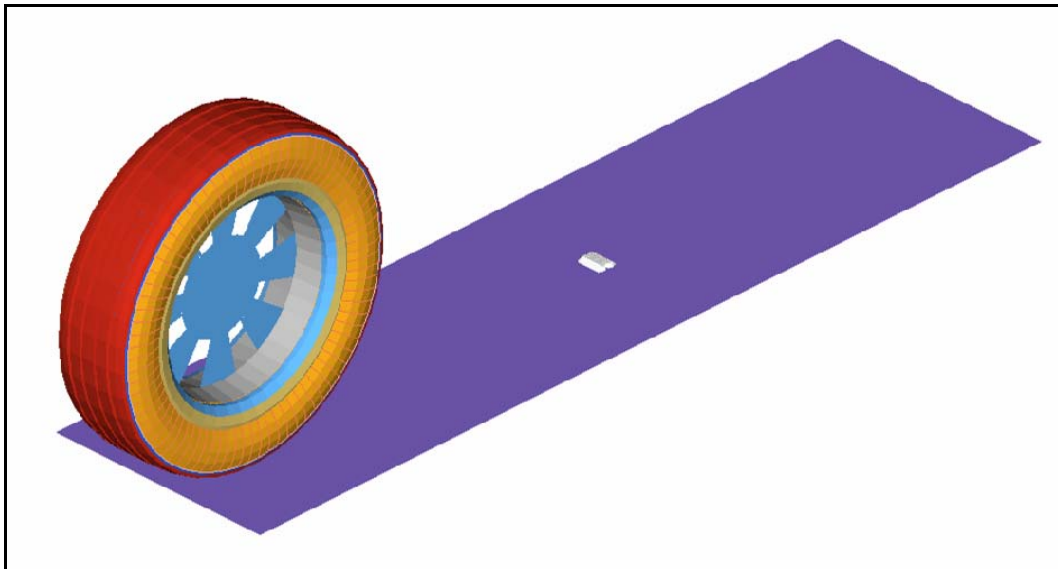
Figure 14. Preliminary Finite Element Model of Tire-Marker Impact.

The model contains three major components: a tire (radius = 20.67 inch), a marker, and the pavement. The tire contains various components like tire tread, rim, shell, steel sidewalls, etc. The marker in the preliminary model was a rigid object and did not have any constitutive material properties. Later versions of this model had finite element models of the RRPMs. The pavement was modeled as a rigid surface in the preliminary model.

The following inputs were defined for the model:

- components—tire, marker, and pavement;
- geometry for components;
- material and section properties;
- loading conditions like tire weight; and
- initial conditions like tire load, velocity, impact angle, and impact location.

The researchers conducted the FEM of the tire-marker impacts from this preliminary model. The FEM of the tire-RRPM impacts was necessary to identify the locations and magnitudes of stresses inside the RRPMs. Two types of RRPM brands were used for the study, which are described as RRPM Type A (Figure 15) and Type B (Figure 16).

The researcher meshed the two RRPM types using Hypermesh. In Hypermesh, a finite element model consists of components called collectors. Every collector is assigned attributes, depending on the kinds of materials (e.g., elastic, plastic, etc.) or sections (e.g., solid, shell, etc.) it has. These attributes are identified by inbuilt templates called 'card images.'
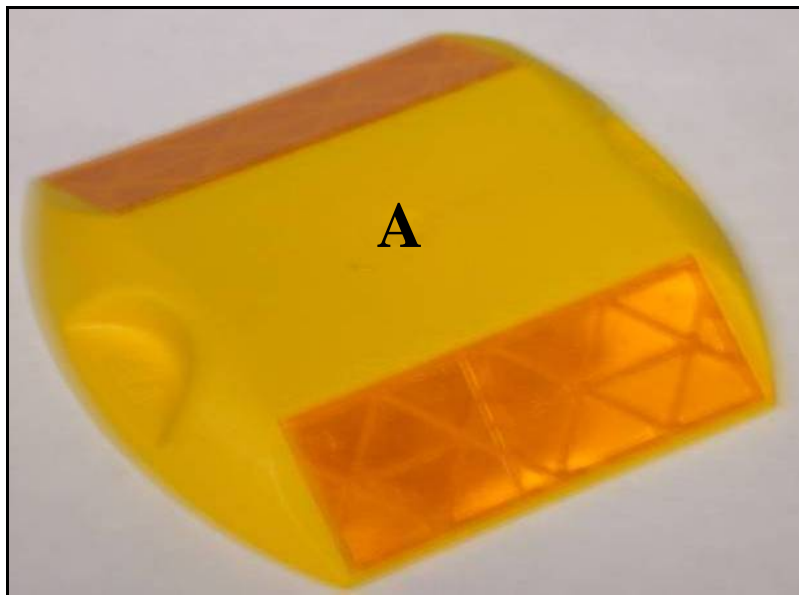
Figure 15. RRPM Type A.
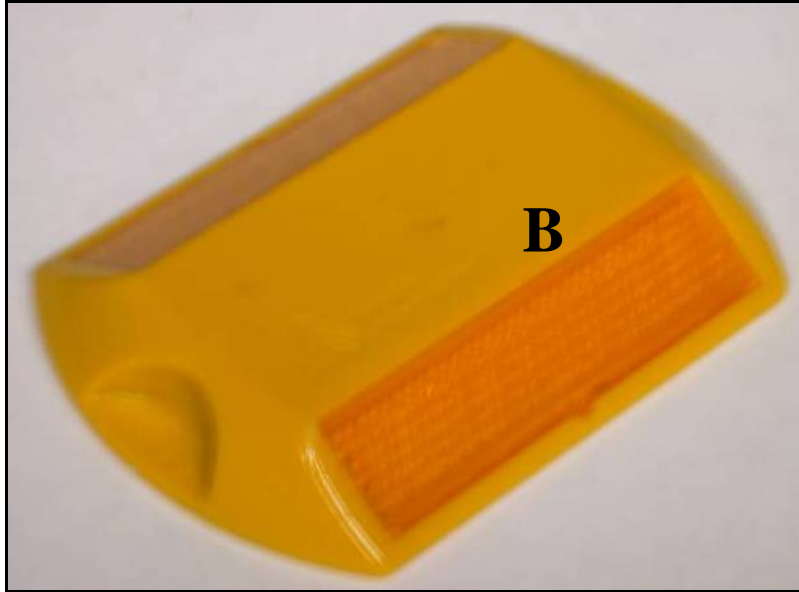
Figure 16. RRPM Type B.

Table 1 lists the card images for the finite element models of the RRPM types. In the table, MAT 24 refers to the material card image 'mat_piecewise_linear_plasticity.' This card image is used to define material properties for the elasto-plastic materials. The minimum properties required for this kind of material are density, Poisson ratio, elastic modulus, and yield stress. In addition, the stress-strain curve can be defined for this kind of material kind. MAT 96 refers to the material card image 'mat_brittle_damage.' This card image is used to identify materials that show brittle damage. The minimum properties required for this material kind are density, Poisson ratio, and elastic modulus. The 'Section_shell' and 'Section_solid' card images define the shell and solid finite element models, respectively. After defining the card images described above, the researchers meshed the geometries of the RRPM types by two-dimensional and three-dimensional finite elements as applicable. Figure 17 and Figure 18 show the finite element meshes for RRPM Types A and B, respectively.

Table 1. Components and Card Images for RRPM Types A and B.

RRPM Type	Component	Material Card Image	Section Card Image
Type A	Body & lens	Elasto-plastic material (MAT 24)	Section_shell
Type B	Body	Elasto-plastic material (MAT 24)	Section_shell
	Lens	Elasto-plastic material (MAT 24)	Section_shell

32
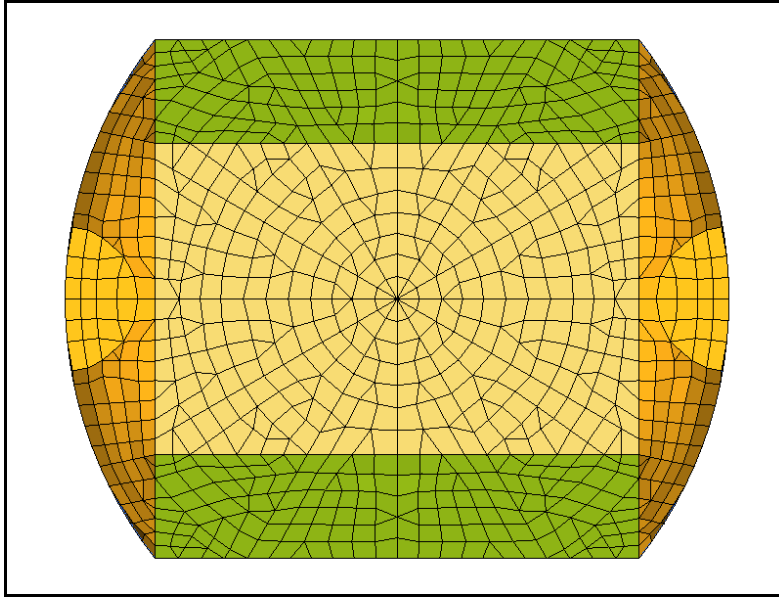
Figure 17. RRPM Type A Mesh.
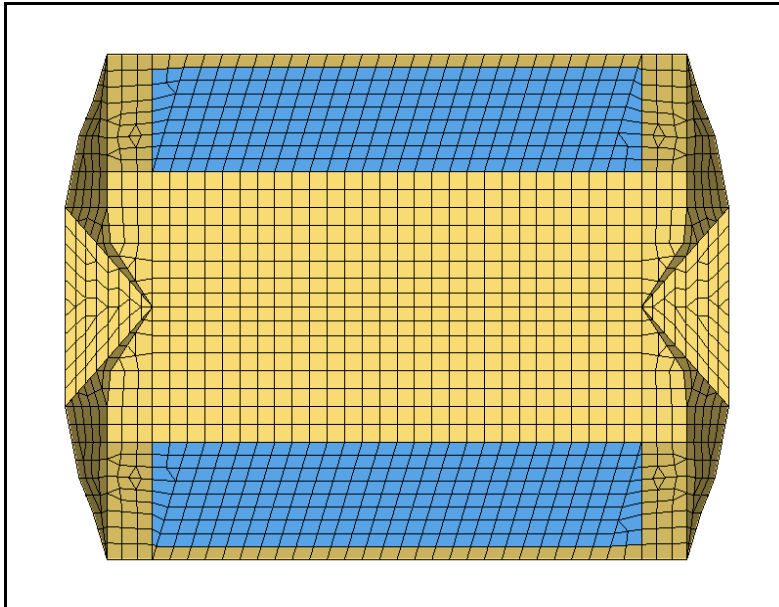
Figure 18. RRPM Type B Mesh.

After meshing, the researchers needed the constitutive chemical composition and material properties of different components of markers like tensile strength, compressive strength, modulus of elasticity, modulus of rigidity, etc. for accurate modeling of tire-marker impacts. Initially researchers intended to perform laboratory tests on some markers to get their chemical composition and material properties. For this purpose, the researchers cut open some markers.

Figure 19 shows how the markers were cut. The idea was to use the components of markers as specimens for getting the constitutive material properties of the markers.

Figure 19. Marker Body Being Cut.

However, from discussions with various experts, the researchers found that such laboratory testing is infeasible or impractical. The components were either too small or needed significant modifications to be converted into test specimens. Hence, information from RRPM manufacturers and literary sources like online databases was taken for the material properties.

Table 2 and Table 3 provide the material properties used in the modeling process. In the tables, 'a' refers to the material properties obtained from the manufacturers and 'b' refers to the properties found from the online databases. Since this information was not based on any laboratory test performed by the researchers, it was considered useful for preliminary purposes only. Calibration was necessary to get accurate estimates of the material properties.

Table 2. Pre-calibration RRPM Type A Material Properties.

Body and Lens (Acrylic)		
Density	1.35E-09	Metric tons/mm^3
Young's modulus	5800	MPa
Poisson ratio	0.35	-
Yield strength	80	MPa

Table 3. Pre-calibration RRPM Type B Material Properties.

Body (Acrylic)		
Density	1.04E-09	Metric tons/mm^3
Young's modulus	2100	MPa
Poisson ratio	0.35	-
Yield strength	44	MPa
Lens (Acrylic)		
Density	1.19E-09	Metric tons/mm^3
Young's modulus	3103	MPa
Poisson ratio	0.11	-
Yield strength	70	MPa

CALIBRATION

Model calibration was necessary to get accurate estimates of constitutive material properties of markers. This step gained more significance for the research since accurate data about the material properties were not available.

The researchers had several plans to calibrate the model. For instance, a load cell could give an estimate of the magnitude of contact forces on markers during the impacts from tires. It is a small cylindrical device, which can measure the global forces in x, y, and z directions applied on it. A marker is placed on it, and then a tire is made to run over it. It would then give the magnitudes of the global forces on the marker, which can be compared to the simulation results. However, the idea was rejected because a load cell only gives the magnitudes of the global forces on the markers and not the stresses or strains inside them.

A better way to calibrate the model would be to get the estimates for stresses and strains inside the RRPMs during the tire-marker impacts and then compare them with simulation results. Strain gauges could be used to measure these strains. From discussions with experts, it was found that estimation of strains using strain gauges in real tire-marker impacts was quite impractical. The impact of a tire over a marker could break the sensitive strain gauges. In addition, there were many external factors in the field that could not be controlled and thus would affect the calibration process.

The researchers decided to calibrate the model using a laboratory set up in a more practical and controlled way. In this way the focus was on calibrating the intrinsic properties of markers while controlling external variables. In addition, the damage to the strain gauges in the laboratory was controlled to a greater extent than in a real-world environment.

A laboratory experimental setup for the calibration was designed similar to that of ASTM D 4280 longitudinal flexural test for testing the markers (described in Chapter 2 under TESTING PRACTICES) (6). Figure 20 and Figure 21 show the experimental setup.

Figure 20. Calibration Test Setup.

Figure 21. Calibration Test Setup (Close View).

Six strain gauges (SG) were used on each marker during the experiment. The strain gauges measured the strains in a predetermined direction at the installed location on the marker. Figure 22 through Figure 25 show the arrangement of strain gauges on the markers. The experiment results provided time plots of the magnitudes of displacement of the top steel bar and strains from the strain gauges.

The researchers then made a finite element model of the laboratory setup (with the same boundary conditions as in the experimental setup). It was used to compare the results from the simulation and experiment and adjust the material properties until the models were calibrated. The modeling was done on Hypermesh, and the simulation was run on LS-DYNA. The modeling process for the RRPM types has been described earlier. The finite element model for the calibration test has steel bars and elastomeric pads in addition to the RRPM models. The card image for the steel bars is MAT 20 (suitable for rigid materials), while the card image for the elastomeric pads is MAT 24 (suitable for elasto-plastic materials).
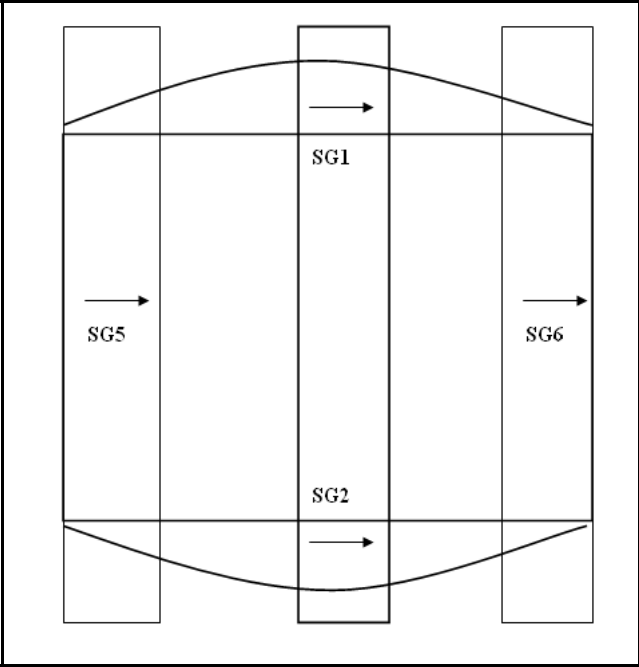
Figure 22. Strain Gauged Marker (Top View).
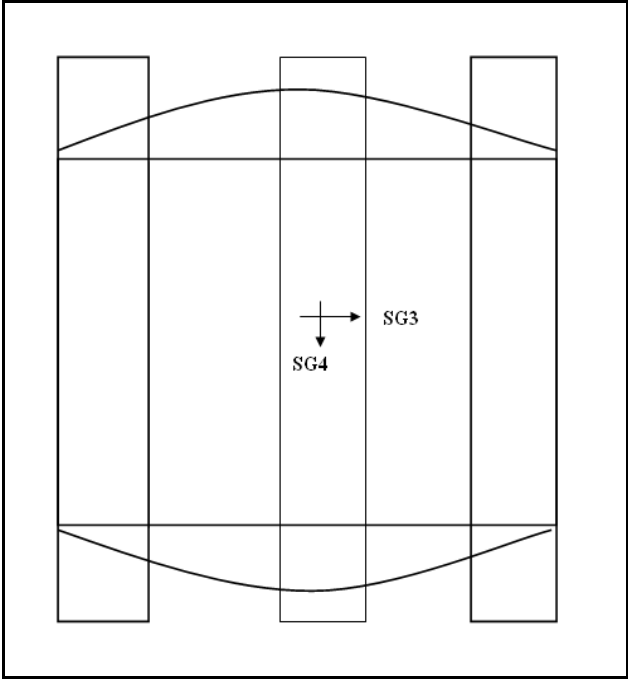
Figure 23. Strain Gauged Marker (Bottom View).
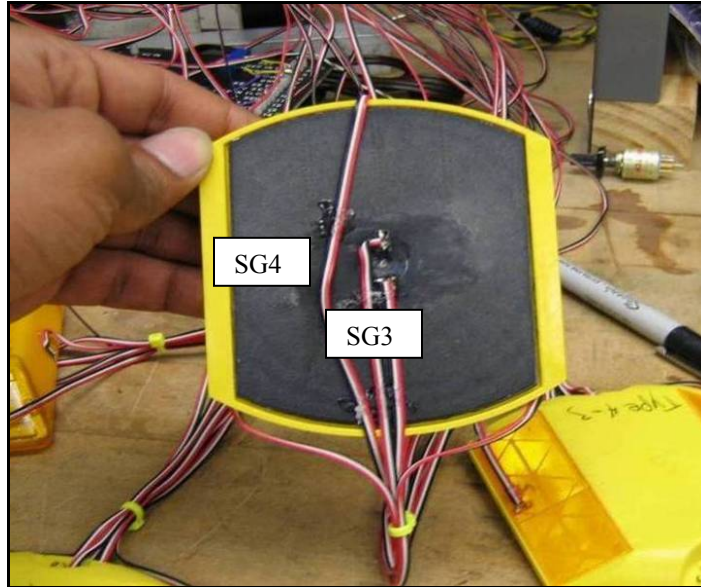
Figure 24. Arrangement for Strain Gauges 3 and 4.
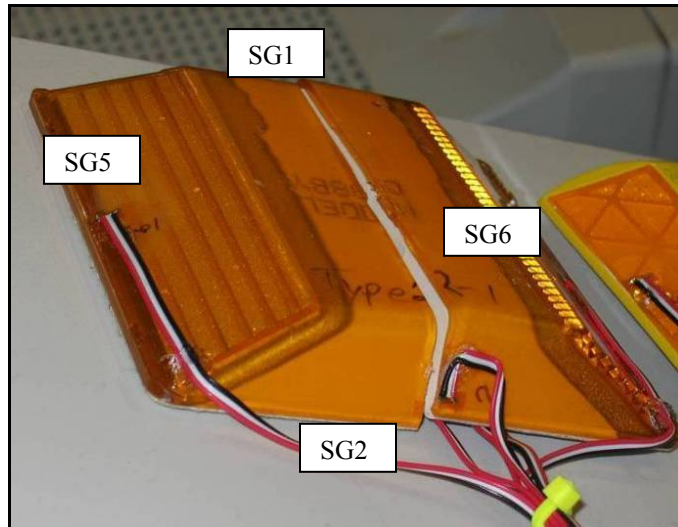
Figure 25. Arrangement for Strain Gauges 1, 2, 5, and 6.

Once the meshing is completed, the next and final step is to assign boundary conditions and define the nature of contacts, if any. A boundary condition was applied at the top steel bar to displace it at a rate of 5.08 mm (0.2 inches) per minute in the downward z direction (vertical direction). The card image for the boundary condition is 'boundary_prescribed_motion_rigid.' This card image is applicable for a node or a set of nodes belonging to a rigid body. Since the top steel bar in the calibration was modeled as rigid, this card image applied well to it. The bottom steel bars were constrained in the z direction (vertical direction). A surface contact between the steel bars (load and mount bars) and the marker model was defined. The card image for the contact was 'automatic_single_surface,' which is used for surface contacts with no orientation. The static and dynamic coefficients of friction between the steel bars and the marker surfaces were kept as 0.15. Figure 26 shows the finite element model of the calibration test for RRPM Type A and the Hypermesh interface.
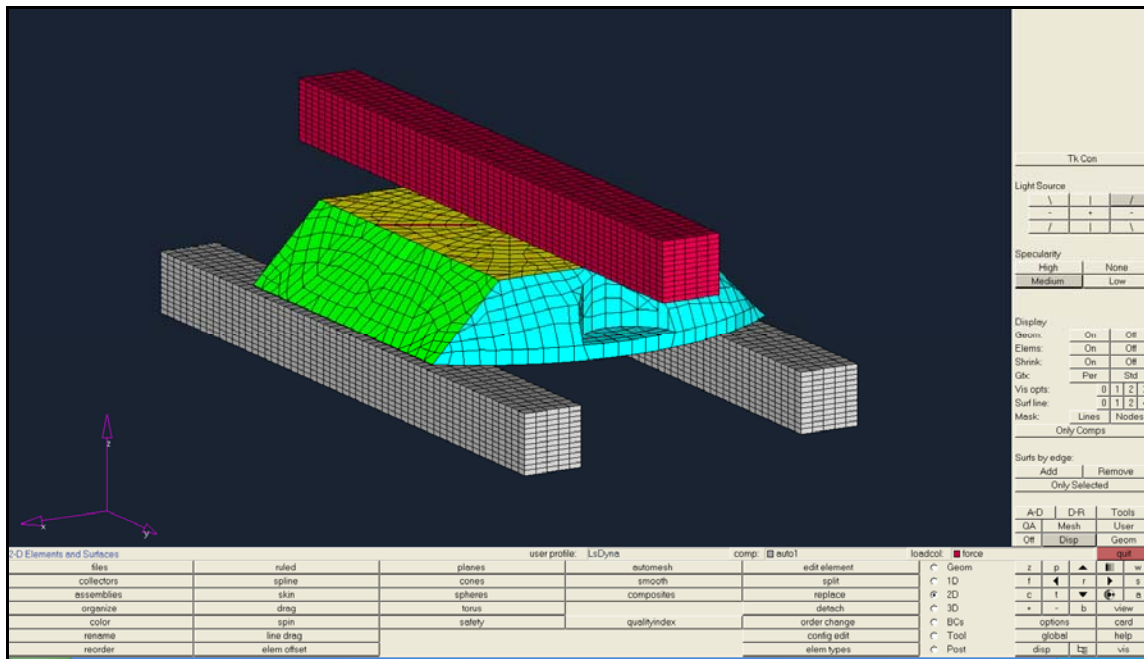
Figure 26. Calibration Test Model for RRPM Type A in Hypermesh Interface (Top Bar Represents Loading Bar and Bottom Bars Represent Mount Bars).

The computer simulation provided the magnitudes of stress and strain inside the markers as the load was applied. These results from the simulations were compared with those from the experiments:

- displacement of the top surface of the marker and
- strains at the locations marked by strain gauges 1-6.

The major criterion for calibration was that experimental and simulation displacements of the top surfaces of the markers should be within 10 percent. The other results (i.e., strain) were primarily to reinforce the calibration.

The only control variables during the calibration process were the intrinsic material properties of the markers. The properties of the steel beam and elastomeric pads were kept constant during the calibration process. Table 4 provides their properties as used in the experiment.

Table 4. Steel Beam and Elastomeric Pad Properties.

Steel Beam		
Density	7.85E-09	Metric tons/mm^3
Young's modulus	205000	MPa
Poisson ratio	0.29	-
Elastomeric Pad		
Density	1.35E-09	Metric tons/mm^3
Young's modulus	1000	MPa
Poisson ratio	0.47	-
Yield strength	50	MPa

The intrinsic material properties of the markers were varied (Table 2 and Table 3) so that the results of the computer simulation were in a reasonable range of results from the laboratory test. Appendix A provides comparisons of results from the simulations and experiments. The solid curves in all the plots show the experimental results, while the dotted curves show the simulation results.

Quantitative analysis was not carried out for comparing the theoretical and experimental strains because the comparisons between the two strains were for reinforcing the major calibration criterion only (as mentioned previously). A visual inspection of the comparisons was

performed instead. Good agreement between the strain magnitudes was achieved if the two curves for the strains were close to each other. There was an average agreement between the two strains if the two curves were at some reasonable distance from each other. A poor agreement was classified when curves were too far from each other.

The results show the following:

- For RRPM Type A, there was a difference of less than 10 percent between displacements of the top surfaces of the marker when simulation results were compared with experimental results (see Appendix A, Figure 111). There was average agreement between the results for strain gauges 3 and 4 (see Appendix A, Figure 113), and good agreement for strain gauges 5 and 6 (see Appendix A, Figure 114). The results did not compare well for strain gauges 1 and 2.

- For RRPM Type B, again there was a difference of less than 10 percent between displacements of the top surfaces of the marker when simulation results were compared with experimental results (see Appendix A, Figure 115). There was good agreement between the results for strain gauges 3 and 4 (see Appendix A, Figure 117), and 5 and 6 (see Appendix A, Figure 118). The results did not compare well for strain gauges 1 and 2 (see Appendix A, Figure 116).

The calibrated models were considered based on the observations listed above. However, the calibration was not a perfect process, as evident from the results. There were a few constraints during the calibration that limited the accuracy of the results:

- It is possible that there was some experimental error, which would have caused the strains in strain gauges 1 and 2 to be far off the simulation strains at the corresponding locations.

- All material properties were based on input from the manufacturers and online material databases. Getting accurate estimates of material properties is necessary for getting the models right, and the inability to obtain these properties limited the accuracy of the calibration.

- The finite element solvers themselves have their limitations, which can reduce the model accuracy. For example, simulating quasistatic loading conditions in LS-DYNA, as in the calibration test simulation, would take a long time. Hence, some compromise with respect to accuracy had to be made to get the results in a

reasonable amount of time. In addition, every model approximates reality, leading to differences with actual conditions.

Table 5 and Table 6 provide the post-calibration material properties for RRPM Types A and B, respectively. The values in parentheses are the pre-calibration material properties.

Table 5. Post-calibration RRPM Type A Material Properties.

Body and Lens		
Density	1.30E-09 (1.35E-09)	Metric tons/mm^3
Young's modulus	3500 (5800)	MPa
Poisson ratio	0.35 (0.35)	-
Yield strength	60 (80)	MPa

Table 6. Post-calibration RRPM Type B Material Properties.

Body		
Density	1.10E-09 (1.04E-09)	Metric tons/mm^3
Young's modulus	1200 (2100)	MPa
Poisson ratio	0.36 (0.35)	-
Yield strength	50 (44)	MPa
Lens		
Density	1.20E-09 (1.19E-09)	Metric tons/mm^3
Young's modulus	3500 (3103)	MPa
Poisson ratio	0.35 (0.11)	-
Yield strength	80 (70)	MPa

FLEXIBLE PAVEMENT MODELING

The basic information of the preliminary tire-marker impact model was provided in the section about preliminary modeling. The preliminary tire-marker impact model is only valid for rigid pavement, which is a constraint to a comprehensive understanding of the tire-marker impact. Therefore, this next section describes how flexible pavement is built in the preliminary model.

As was introduced in the review of the state-of-the-art, flexible pavement is structurally different from rigid pavement, and is usually composed of three layers—surface course, base

course, and subgrade. An optional sub-base layer may be constructed between base course and subgrade. The surface course for flexible pavement mostly uses asphalt concrete, which is harder than the material used in the base course. Subgrade is actually the existing soil, which is the softest among the three layers.

In order to model flexible pavement as accurately as possible, the researchers examined the work of some experts conducting tests on flexible pavements at TTI and acquired some valuable information as well as common data they usually use to model flexible pavement in finite element analysis. The thickness and material properties of an average flexible pavement are summarized in Table 7 according to those TTI researchers. The numbers in parentheses are for flexible pavement on interstate highways with a large percentage of truck traffic. The researchers did a simple sensitivity analysis of the stress results between the average flexible pavement and the flexible pavement on interstate highways. It was found that the thickness and material properties of an average flexible pavement could be used in the model to conduct the research tasks in this project since there was little variation in stress inside the markers between an average asphalt pavement and one for extremely heavy loads.

Table 7. Pavement Profiles and Properties.

Layer Name	Thickness (m)	Mass Density (kg/m^3)	Poisson Ratio	Modulus (MPa)
Surface	0.08 (0.20)*	2322	0.35	3000 (3000)
Base	0.30 (0.30)	2162	0.35	150 (300)
Subgrade	5.00 (5.00)	2001	0.35	50 (10)

*The numbers in parentheses are for flexible pavement on interstate highways with a large percentage of truck traffic.

The material card for the three layers of flexible pavement was chosen to be elastic in the finite element modeling software Hypermesh, although the elastic-plastic card should be more accurate in terms of the material characteristics of flexible pavement. Because modeling elastic-plastic material is much more complex than modeling elastic material and requires comprehensive data input for the flexible pavement, TTI researchers advised against it. Elastic modulus is the key material property that determines the stiffness of the pavement layer and plays a more important role than density and Poisson ratio in finite element modeling. The area of the pavement course should be large enough so that elastic deformation inside the pavement can be produced during the tire-marker impact.

After researchers took all these issues into consideration, they modeled three layers of pavement block to form the typical flexible pavement, according to the profiles and material properties listed in Table 7, to replace the rigid ground that was built in the preliminary model. Hence, the tire-marker impact took place on flexible pavement. The tire-marker impact model on flexible pavement is shown in Figure 27. The tire-marker impact analysis is based on the models of both types of pavement.
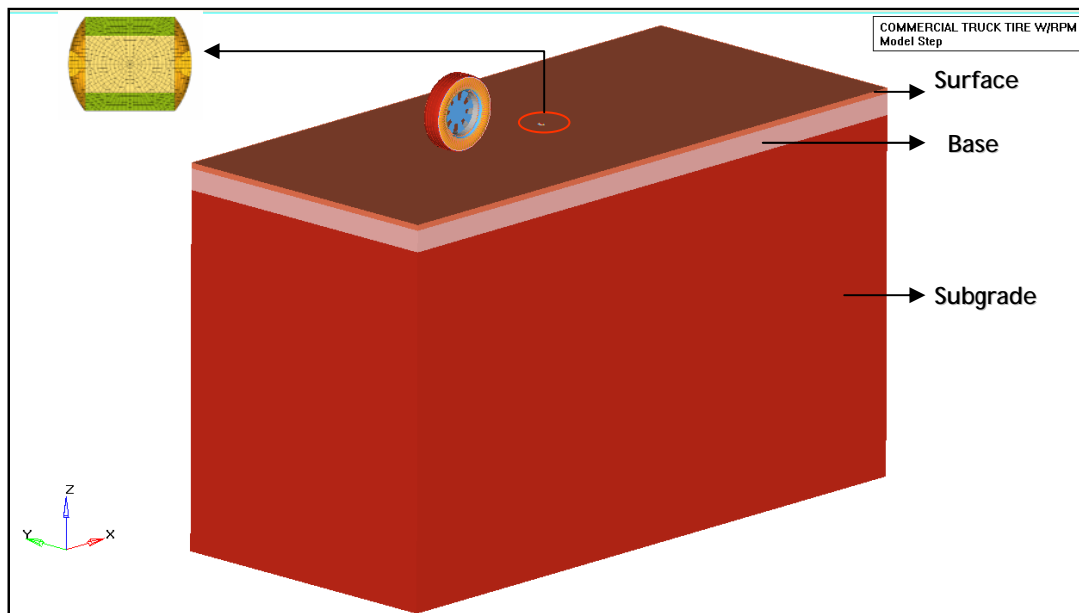
Figure 27. Tire-Marker Impact Model on Flexible Pavement.

TIRE-MARKER IMPACT SIMULATION

Once the calibration and modeling of pavement properties were completed, the markers with refined material properties were integrated with the tire-marker impact model on both types of pavement. The next step was to simulate tire-marker impact with the calibrated models. Stress and interface force inside markers can also be obtained from the simulation of impact. Simulations with different RRPM types were performed with different external factors like tire loads, tire velocities, angles of impact, and locations of impact.

First, the impact in a reference set of external conditions (called base case) was simulated for the three RRPM models. Then the simulations by varying external conditions (each with two other values) were carried out. Table 8 gives values for these variables. One more important

input was the tire inflation pressure, which was kept as 0.7 MPa (100 psi). The simulation provides the magnitudes and locations of critical stress inside a marker when a vehicle tire runs over it. The stress profiles under different conditions (e.g., tire loads, tire velocities, impact angles, and impact locations) were documented and analyzed. The next chapter describes the results of the tire-marker impact simulations and associated analysis.

Table 8. External Factors and Their Scenarios.

External Factors	Base	Value 1	Value 2
Tire load (N)	22,200	13,300	31,100
Tire speed (m/s)	31.3	26.8	35.7
Contact angle (degrees)	0	5	10
Contact location (mm offset from center)	0	25	51

The values of tire loading and tire speed correspond to the values in English units at 3000, 5000, and 7000 lb and 60, 70, and 80 miles per hour (mph), respectively. The reasons for selecting these values are explained next. For tire loading, 5000 lb was chosen as the base value because the federal government limits vehicle weights on interstate highways to a maximum of 20,000 lb for a single axle, averaging 5000 lb for a single truck tire (*40*). Since the load may not be equally distributed among the four tires of an axle, 3000 and 7000 lb were used as the lower and upper values. For tire speed, 70 mph was chosen as the base value due to the speed limit on most interstate highways, and 60 and 80 mph were used as the lower and upper values.

LABORATORY TEST SIMULATION

The analysis of the tire-marker impact is not sufficient for finding a laboratory test that would produce the same kinds of stress inside the markers as during a real tire-marker impact. To accomplish that, it requires simulating different laboratory loading conditions over the markers. The researchers analyzed the principal and Von Mises stress (*41*) profiles inside the markers from simulating these loading conditions and compared them with those produced during the tire-marker impact simulations. This analysis gives insight into the laboratory test required for RRPMs.

The laboratory test simulation consists of two tasks. One is to simulate the existing standard laboratory tests, which are the ASTM compression test and the longitudinal flexural

test. The other is to develop additional laboratory tests that could better simulate the tire-marker impact in some specific scenarios that proved to be critical in this research. The laboratory testing setups are built in Hypermesh and simulated by LS-DYNA. First, various tests were simulated and evaluated based on the tire-marker impact results for rigid pavement, and then the desired tests were selected to further investigate their suitability for the two types of pavements at specific loading rates.

CHAPTER 4. RESULTS AND ANALYSIS OF FINITE ELEMENT MODELING OF RRPMs

The researchers simulated field conditions, i.e., tire-marker impact on both rigid and flexible pavement, after the calibration was completed. They identified the locations and magnitudes of the critical stress inside the markers during the impact. The effects of the variation in external factors on the stress inside the markers during simulation were also evaluated. Afterwards, the tire-marker impact on the two types of pavement was compared. Furthermore, a few laboratory conditions were simulated, including existing ASTM tests and some additionally developed tests that could produce stress profiles inside markers similar to those produced during tire-marker impact simulation. In addition, the interface force and marker profile were evaluated as well.

This chapter provides the results and analysis of these simulations. The chapter is divided into five sections. The first section provides the results of the tire-marker impact simulations for the two RRPM models. The next section details the effects of the external factors (listed in Table 8) on the stress inside the markers, which is followed by the section describing the comparison of impact on the two types of pavement. The following section focuses on the interface force and marker profile. The last section analyzes the laboratory tests.

TIRE-MARKER IMPACT ANALYSIS

The critical part of using FEM to study RRPMs is to analyze the stress produced inside the markers during the simulated tire-marker impact. This section details the Von Mises stress and stress tensor profiles found from the tire-marker impact simulations. For every RRPM model, the Von Mises stress contour in top view and stress tensor plot in isometric view were illustrated. This helps to understand the surface and vertical profiles of the stress.

Stress tensor is a six-vector quantity (a symmetric 3×3 matrix). Von Mises stress reduces it to a scalar number. It is found by combining two-dimensional or three-dimensional stress, whichever is applicable.

It is given by:

$$\sigma_v = \sqrt{\frac{(\sigma_1 - \sigma_2)^2 + (\sigma_2 - \sigma_3)^2 + (\sigma_3 - \sigma_1)^2}{2}},$$

where σ_1, σ_2, and σ_3 are the principal stresses *(41)*. Von Mises stress is compared with the tensile strength of uniaxially loaded material and acts as a yield criterion for ductile materials. Von Mises stress was used for comparison because most of the finite element models for this research are elastic-plastic in which a ductile failure is possible. In addition, it is easy to compare these stresses across all RRPM types and different external factors.

The researchers set up the simulations in such a way that the tire passes over the markers in three stages. Stage 1 simulates the ascendancy of the tire over the retroreflective lens of the markers. Stage 2 simulates the instantaneous stay of the tire on top of the markers. Stage 3 simulates the movement of the tire over the other retroreflective lens of the markers as the tire leaves them. Hence, every stress plot for a tire-marker simulation has three frames that represent the three stages of impact. Moreover, the tire-marker impact on rigid and flexible pavement was analyzed respectively so that they could be compared later in this chapter.

Tire-Marker Impact on Rigid Pavement

RRPM Type A Stress Analysis

Figure 28 and Figure 29 show Von Mises stress plots and stress tensor plots for RRPM Type A on rigid pavement from the tire-marker impact simulation, which consists of all the base external variables, i.e., tire load of a 5000 lb, tire velocity of 70 mph, 0 degree contact angle, and 0 mm (0.0 inch) contact offset. Each frame of the figures represents one stage of the impact according to the number in the upper right corner. A few observations are made as follows:
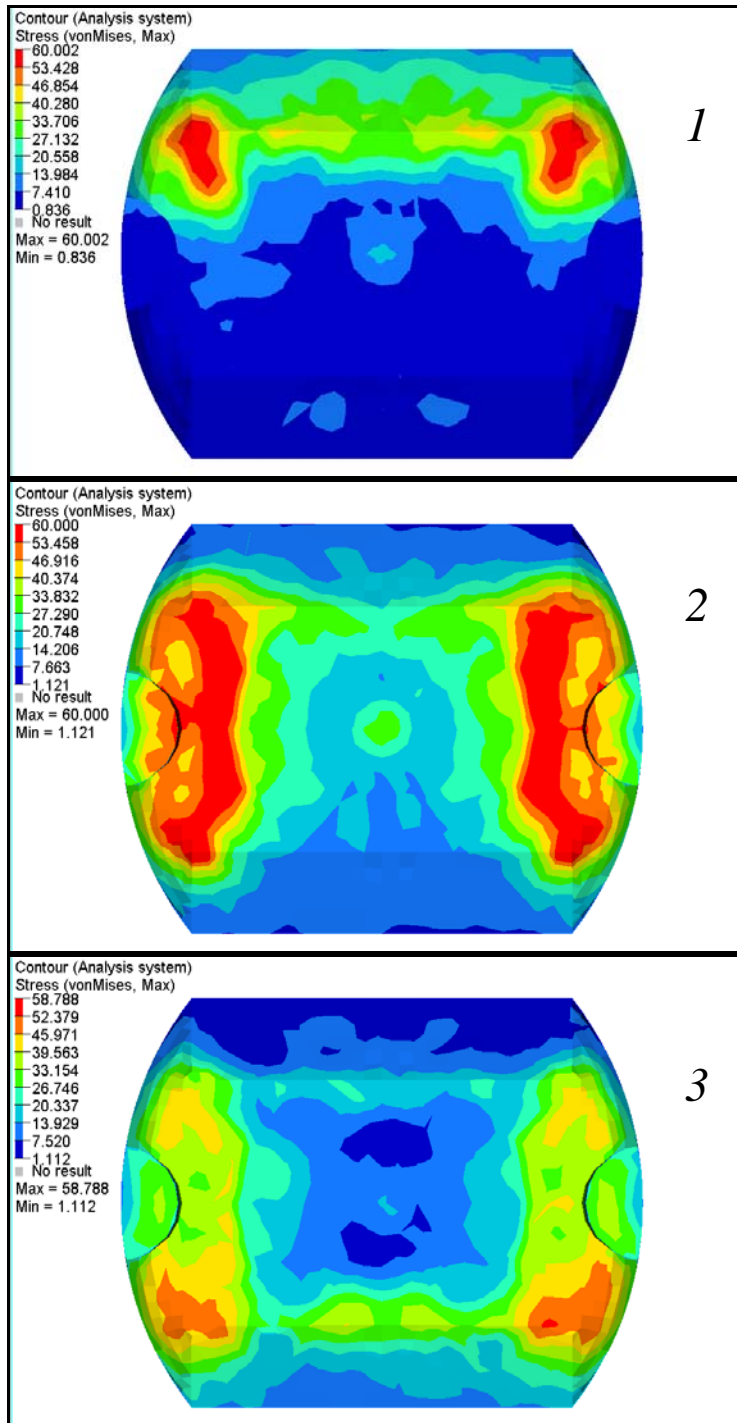
Figure 28. Von Mises Stress Plots for RRPM Type A on Rigid Pavement.
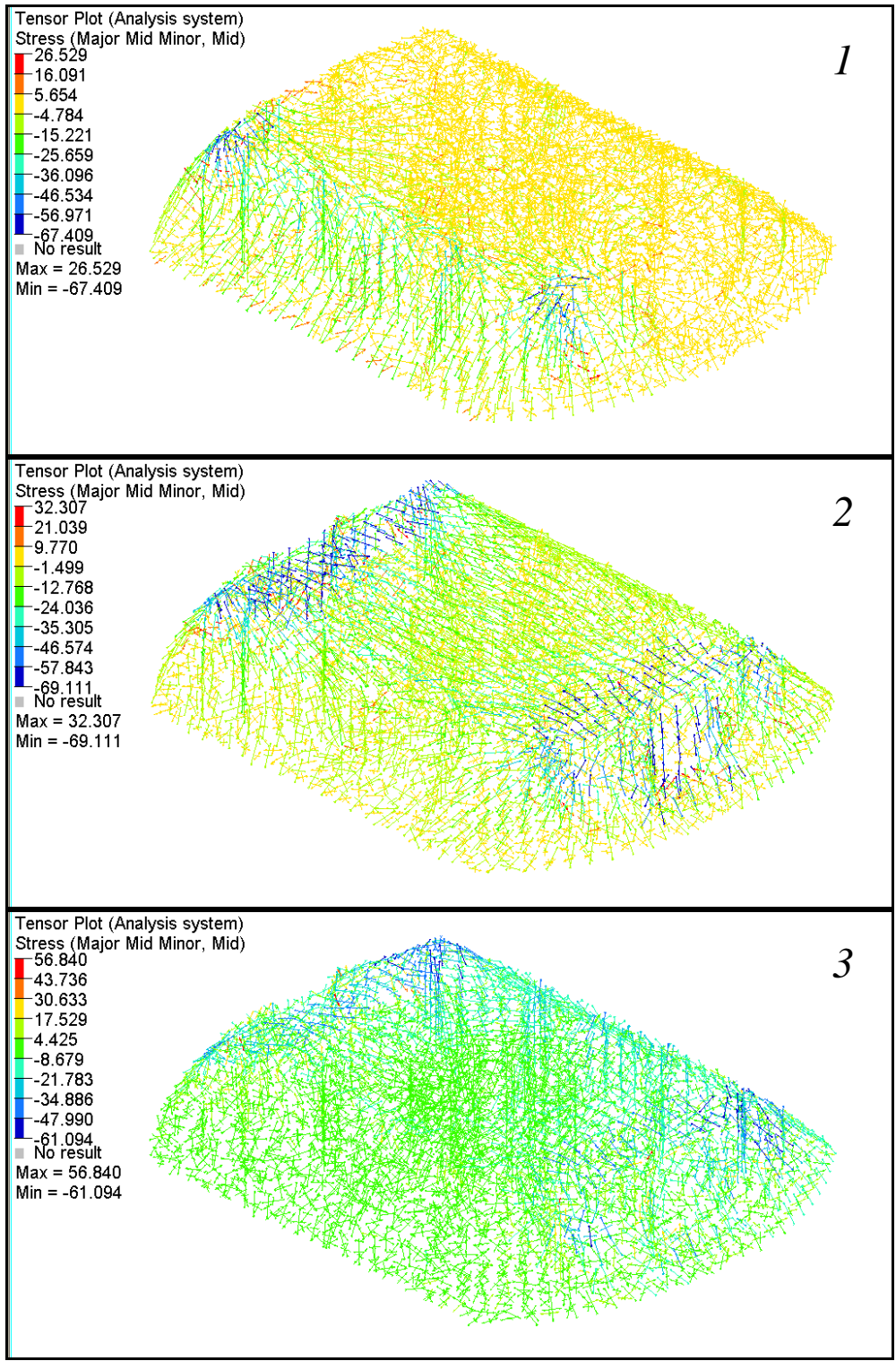
Figure 29. Stress Tensor Plots for RRPM Type A on Rigid Pavement.

- The critical (maximum) Von Mises stress exists at the top edges and non-lens sides of the marker, and its magnitudes are in the range of 58.788 to 60.002 MPa.

- Based on the stress tensor plots, at stages 1 and 3 of impact, tensile stress (marked with positive magnitude) is produced in the opposite side of the marker from where the tire contacts the marker, while compressive stress (marked with negative magnitude) is generated at the top of the lenses and is especially intense at the top edges of the marker. At stage 2, critical compressive stress is seen at the non-lens sides of the top surface as well as the top edges of the marker, while tensile stress is found throughout the body of the marker. The compressive stress is predominant in terms of the magnitude.

RRPM Type B Stress Analysis

Figure 30 and Figure 31 show Von Mises stress plots and stress tensor plots for RRPM Type B on rigid pavement from the tire-marker impact simulation with all the base scenarios of external factors. A few observations are made as follows:

- The critical (maximum) Von Mises stress is produced at the top edges of the marker, and its magnitudes are between 53.455 and 65.932 MPa.

- Based on the stress tensor plots, at stages 1 and 3 of impact, tensile stress is produced in the opposite side of the marker from where the tire contacts the marker, while compressive stress is generated at the top of the lenses and is especially intense at the top edges of the marker. At stage 2 when the tire sits on top of the marker, the compressive stress is seen at the non-lens sides of the top surface and is especially intense at the top edges of the marker, while tensile stress is found throughout the body of the marker. The compressive stress is predominant in terms of the magnitude.
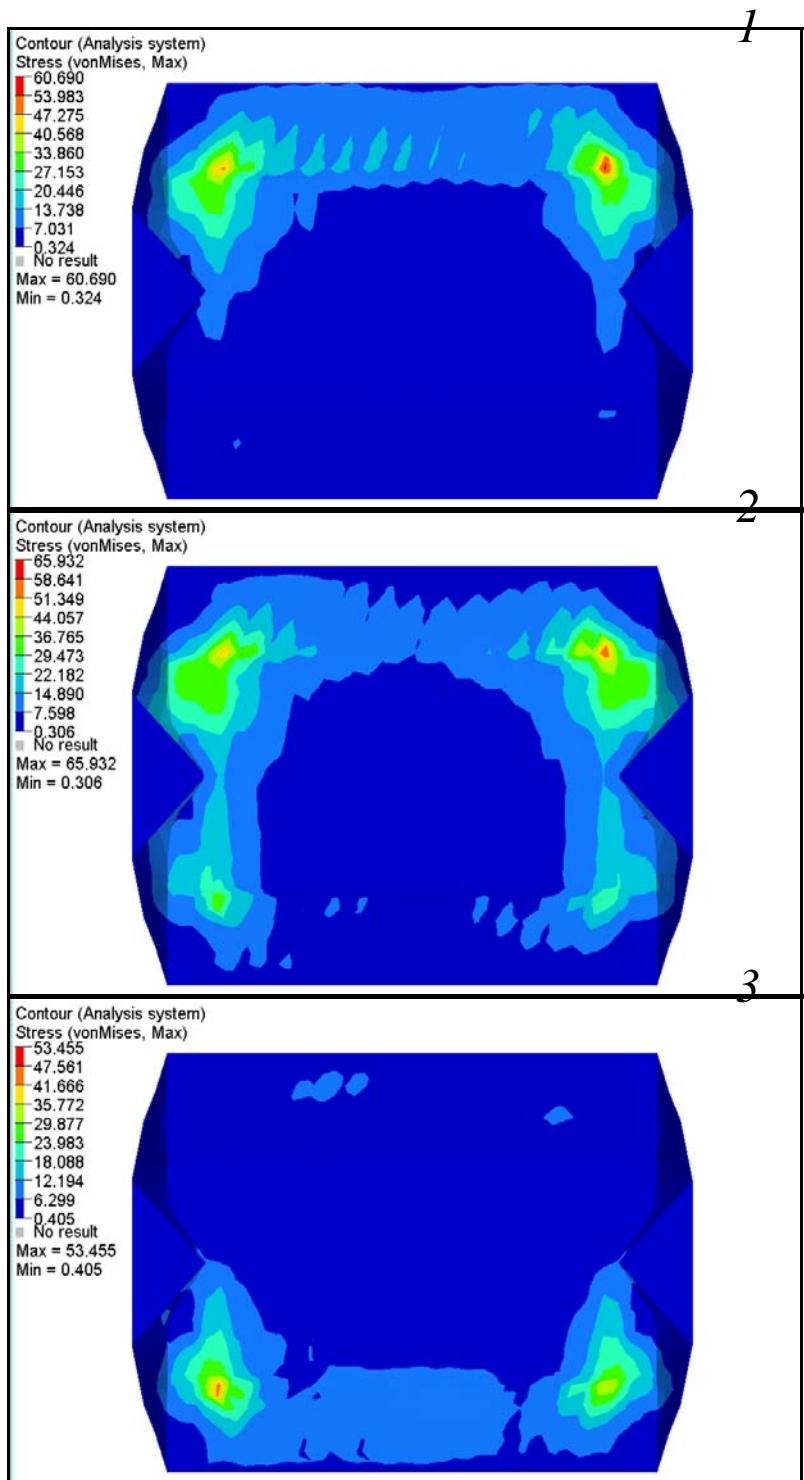
Figure 30. Von Mises Stress Plots for RRPM Type B on Rigid Pavement.
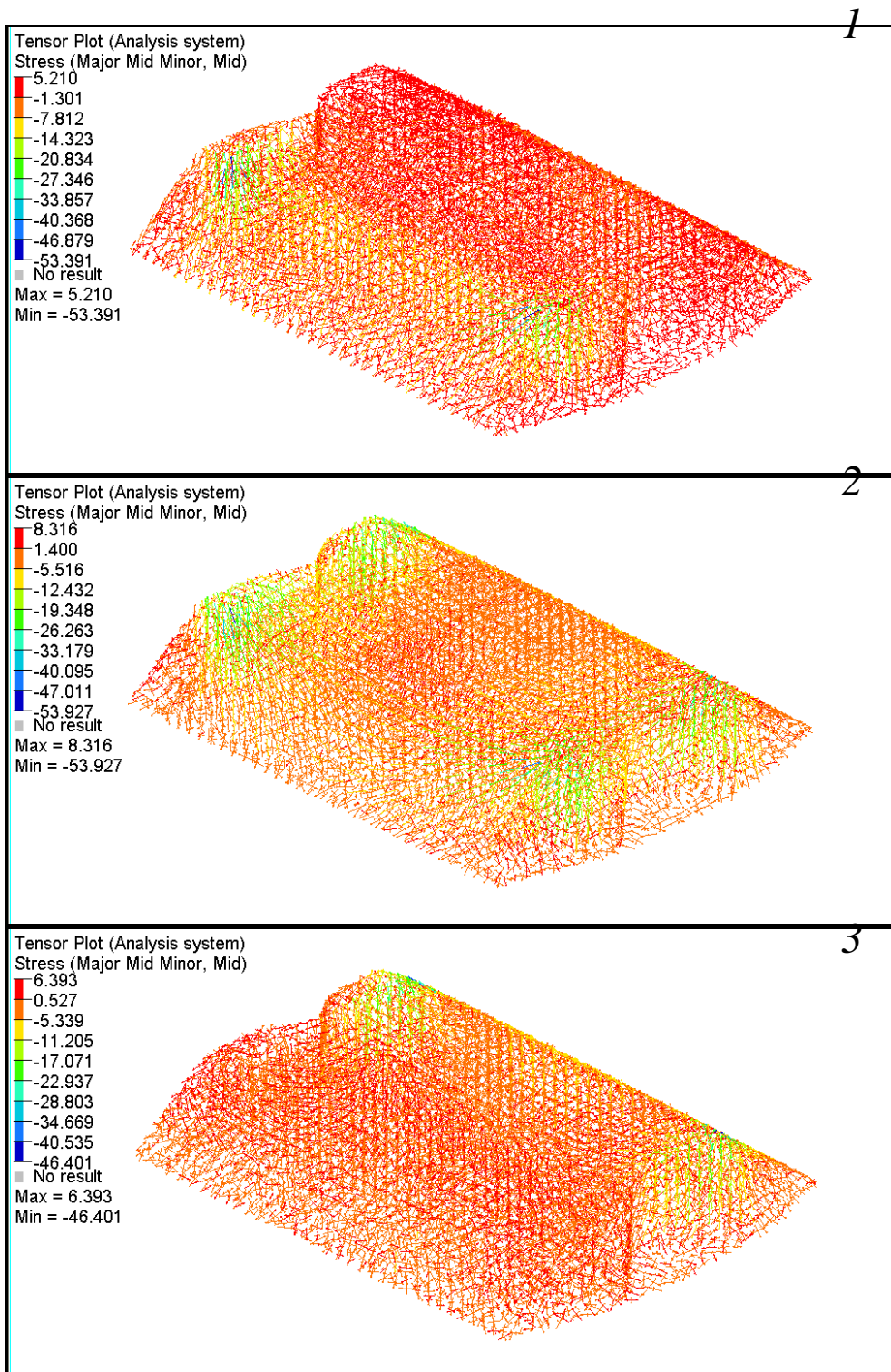
Figure 31. Stress Tensor Plots for RRPM Type B on Rigid Pavement.

Tire-Marker Impact on Flexible Pavement

RRPM Type A Stress Analysis

Figure 32 and Figure 33 show Von Mises stress plots and stress tensor plots for RRPM Type A on flexible pavement from the tire-marker impact simulation with all the base scenarios of external factors. A few observations are made as follows:

- The critical (maximum) Von Mises stress exists at the top edges and non-lens sides of the marker, which is similar to the critical locations for RRPM Type A on rigid pavement. The magnitudes of the critical Von Mises stress are close to 60.000 MPa. Based on the stress tensor plots, at stages 1 and 3 of impact, tensile stress is produced in the opposite side of the marker from where the tire contacts the marker, while compressive stress is generated at the top of the lenses and is especially intense at the top edges of the marker. At stage 2, critical compressive stress is seen at the non-lens sides of the top surface as well as the top edges of the marker, while tensile stress is found throughout the body of the marker. The general distribution of compressive and tensile stress inside the marker is the same as that for RRPM Type A on rigid pavement. The compressive stress is still predominant in terms of the magnitude.

RRPM Type B Stress Analysis

Figure 34 and Figure 35 show Von Mises stress plots and stress tensor plots for RRPM Type B on flexible pavement from the tire-marker impact simulation with all the base scenarios of external factors. A few observations are made:
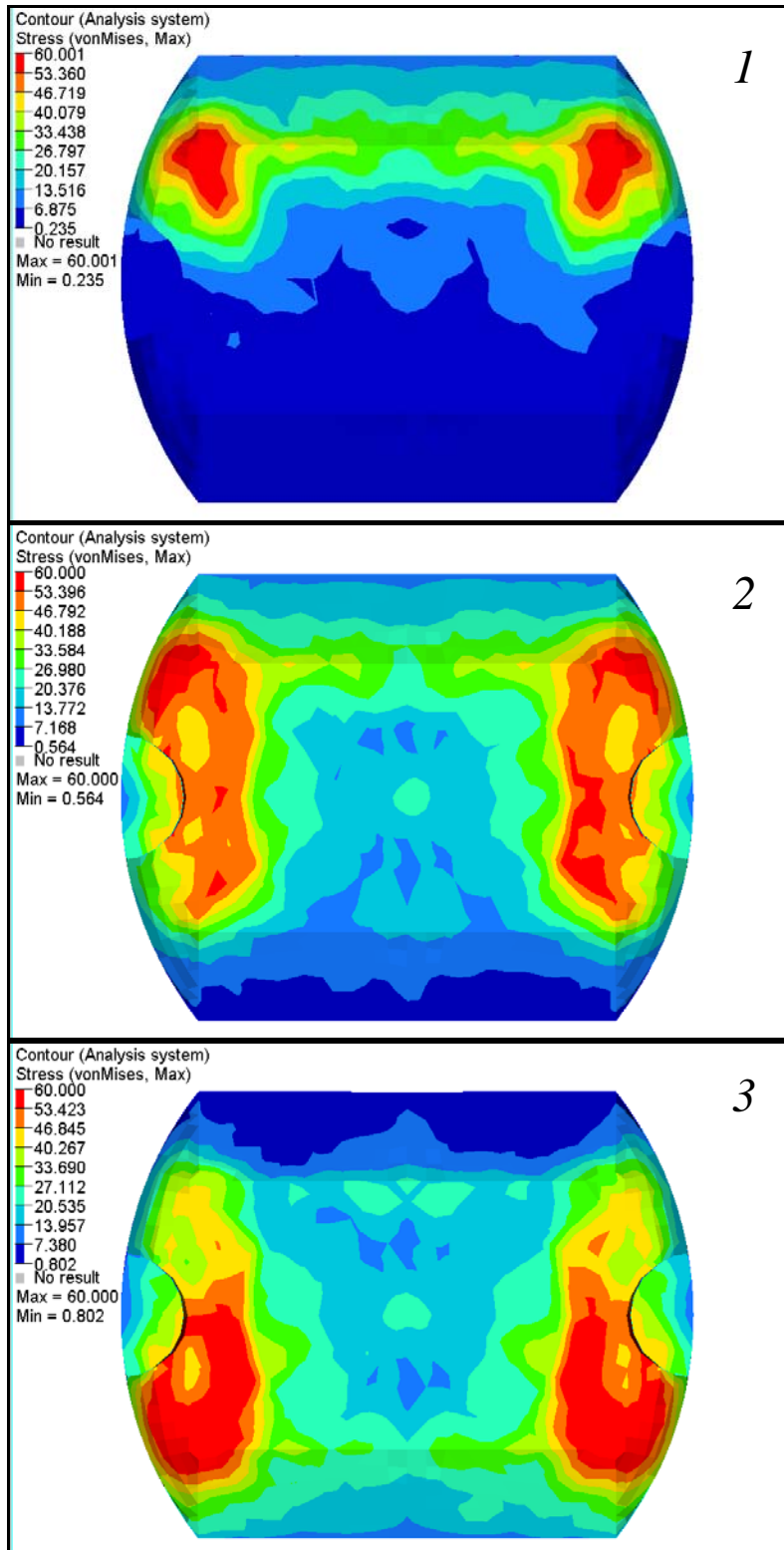
Figure 32. Von Mises Stress Plots for RRPM Type A on Flexible Pavement.
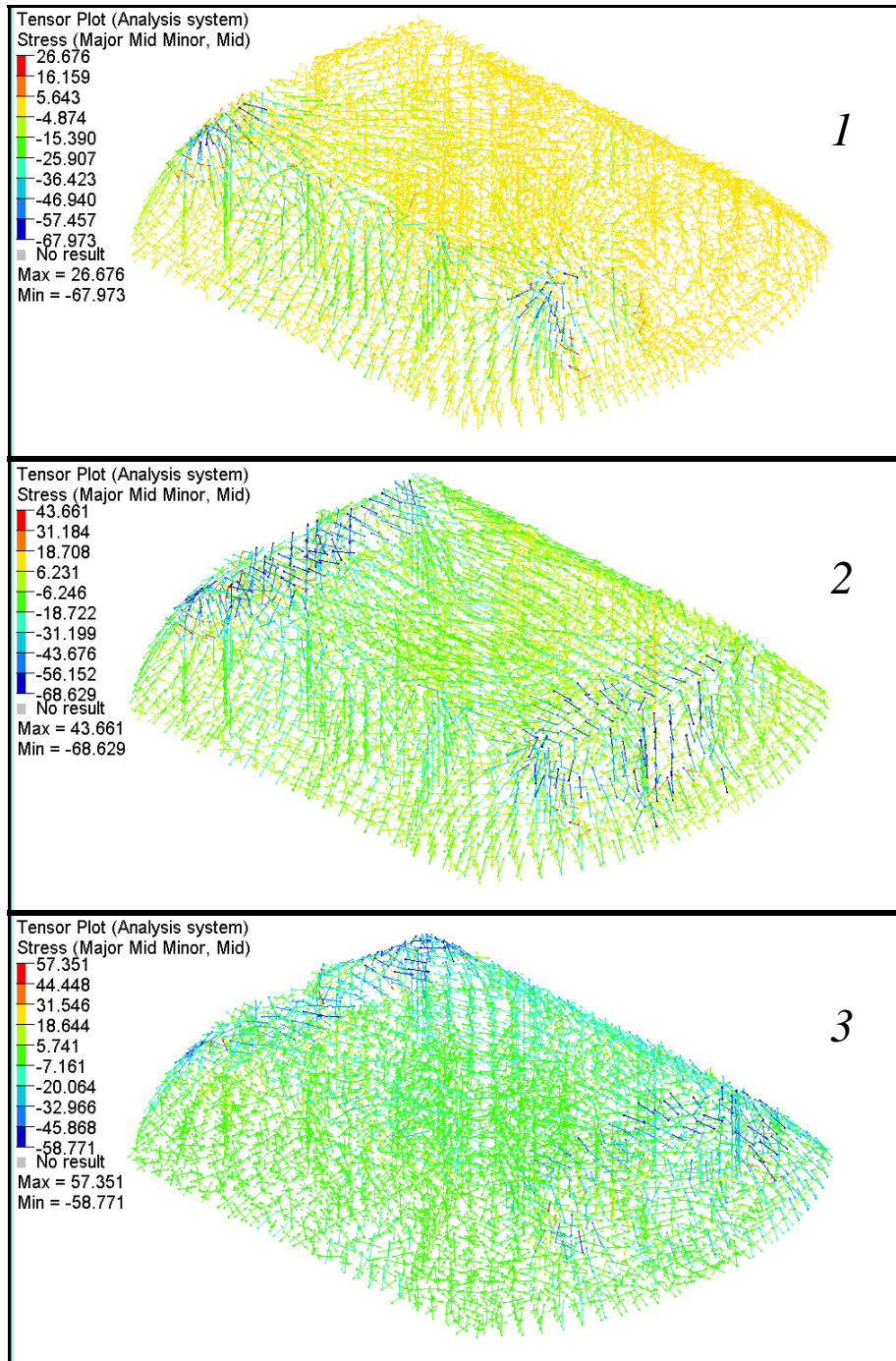
Figure 33. Stress Tensor Plots for RRPM Type A on Flexible Pavement.
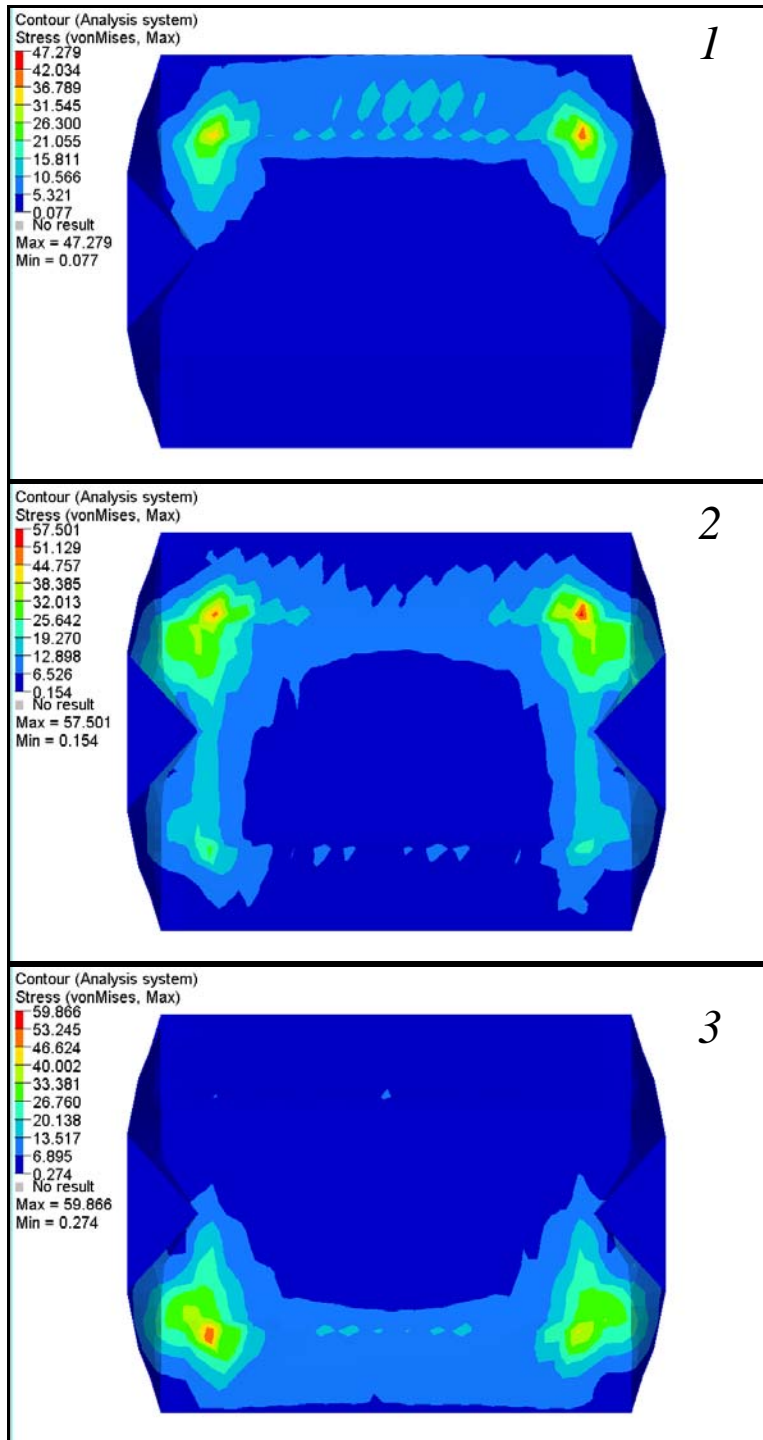
Figure 34. Von Mises Stress Plots for RRPM Type B on Flexible Pavement.
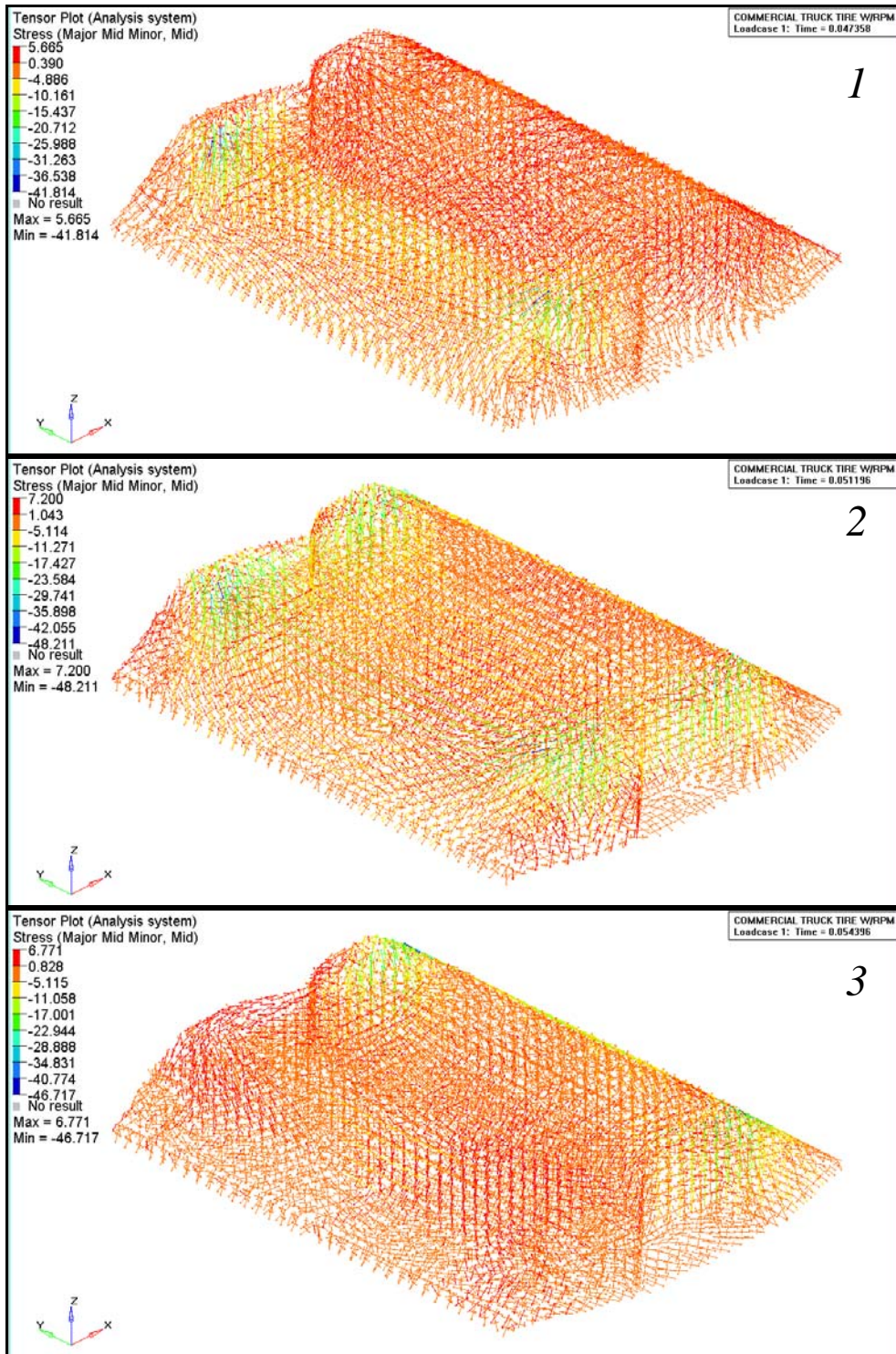
Figure 35. Stress Tensor Plots for RRPM Type B on Flexible Pavement.

- The critical (maximum) Von Mises stress is produced at the top edges of the marker, identical to what is found for RRPM Type B on rigid pavement. The magnitudes of the critical Von Mises stress are in the range of 47.279 to 59.866 MPa.

- Based on the stress tensor plots, at stages 1 and 3 of impact, tensile stress is produced in the opposite side of the marker from where the tire contacts the marker, while compressive stress is generated at the top of the lenses and is especially intense at the top edges of the marker. At stage 2 when the tire sits on top of the marker, the compressive stress is seen at the non-lens sides of the top surface and is especially intense at the top edges of the marker, while tensile stress is found throughout the body of the marker. The general distribution of compressive and tensile stress inside the marker is similar to that on rigid pavement.

EFFECTS OF EXTERNAL FACTORS

First, the researchers examined the effects of external factors—tire loading, tire speed, contact angle, and contact location—on the critical Von Mises stress inside the markers on flexible pavement. Each external factor was studied separately by varying the scenario by one factor while keeping the others constant with base values in the tire-marker impact simulation. In order to better reflect the stress variance over different scenarios of factors, elastic modulus was increased for the material of Type A because it reaches yield strength at each stage of the simulated tire-marker impact, making it difficult to distinguish the stress variance. Type B does not have this problem, so nothing was modified for it. Figure 36 and Figure 37 show the trend of the critical Von Mises stress over different scenarios of each external factor for Types A and B, respectively. These figures are based on the stress results from the different scenarios of simulation that resulted from each variation.

Based on the trend plots for the two markers, it was found that the tire loading and contact location have consistent effects on the critical Von Mises stress during the impact on flexible pavement. In addition, contact angle has some effect on the stress for Type A, but such effect is inconsistent for Type B. Tire speed does not have a consistent effect on the critical Von Mises stress for both types of markers. Later, the same study for rigid pavement was carried out,

and the results were inconsistent with those for flexible pavement. Therefore, loading and contact location should be considered important factors when developing a laboratory test.

Loading: Consistent effect

Location: Consistent effect

Speed: No effect

Angle: Some effect
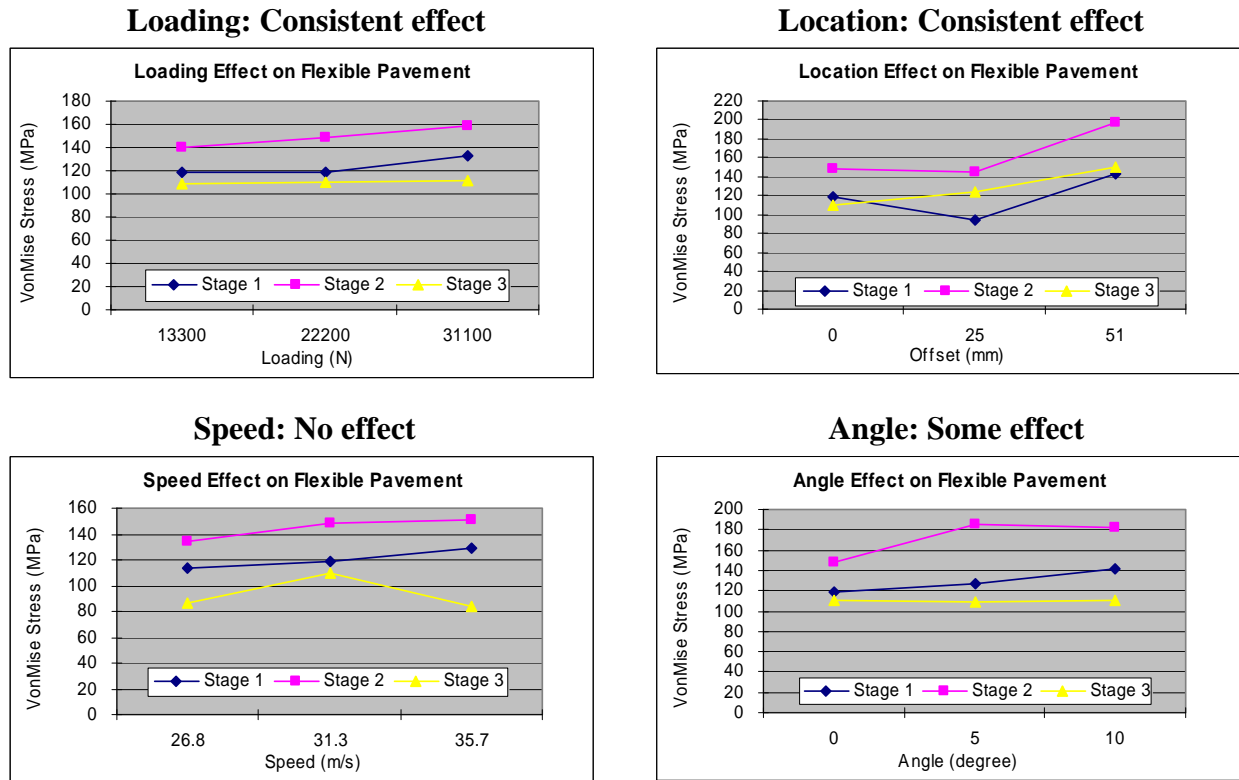
Figure 36. Effects of External Factors on Critical Von Mises Stress for RRPM Type A on Flexible Pavement.

COMPARISON OF TIRE-MARKER IMPACT ON TWO TYPES OF PAVEMENTS

The critical locations and magnitudes of Von Mises, compressive, and tensile stresses were compared between tire-marker impact on rigid and flexible pavement. The elastic modulus for the material of Type A was increased for the same reason explained in the last section. Based on the Von Mises stress plots that resulted from the tire-marker impact simulation, the critical locations of Von Mises stress inside the markers are almost identical between the two types of pavement in that they are all located at the top edges of the markers. However, in terms of the magnitude of critical Von Mises stress at those locations, it is about 10 percent larger on rigid pavement than on flexible pavement. Figure 38 shows the comparison of the average magnitudes of critical Von Mises stress for Types A and B.
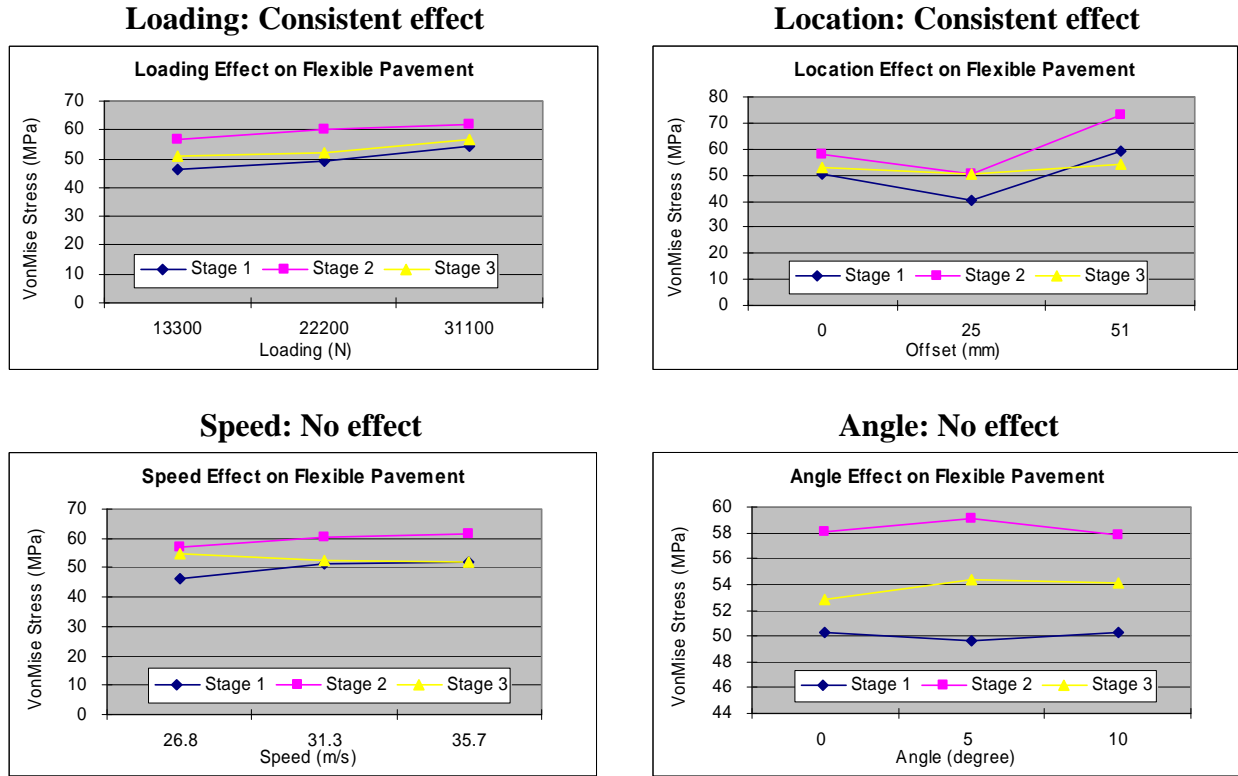
Figure 37. Effects of External Factors on Critical Von Mises Stress for RRPM Type B on Flexible Pavement.
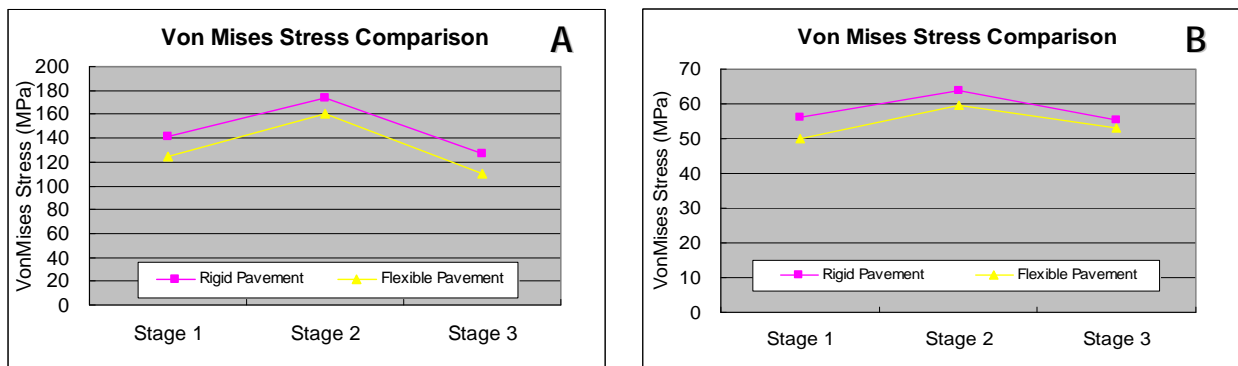
Figure 38. Comparison of Critical Von Mises Stress for RRPM Types A and B.

After researchers examined the stress tensor plots, they found that the critical locations of compressive stress inside the markers are the same on two types of pavement, and both are at the top edges of the markers, but the average magnitude of compressive stress at those critical locations is about 11 percent larger on rigid pavement than on flexible pavement. Figure 39 shows the comparison of the average magnitudes of critical compressive stress over the three stages of the impact based on the simulations for both types of markers.
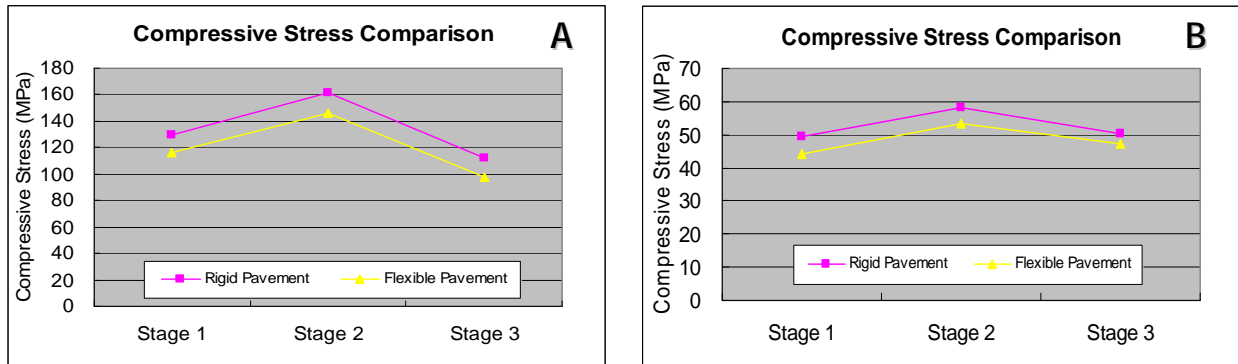
Figure 39. Comparison of Critical Compressive Stress for RRPM Types A and B.

As for tensile stress, it is generally distributed in the same way on both types of pavement. However, for RRPM Type A, the patterns of the critical tensile stress are different between the two types of pavement. But for RRPM Type B, the patterns of the critical tensile stress look somewhat similar. For Type A, the critical tensile stress tensors scatter inside the marker on rigid pavement, while on flexible pavement they are generated from the mid-bottom of the marker and go upward with a consistent angle. The average magnitudes of the critical tensile stress are not significantly different between rigid and flexible pavement for both types of markers during stages 1 and 2 of the impact. However, the critical tensile stress during stage 3 of the impact on flexible pavement is significantly larger than that on rigid pavement. Nevertheless, such difference is very small for Type B. Figure 40 shows the comparison of the average magnitudes of the critical tensile stress over the three stages of the impact based on the simulations for Types A and B. Figure 41 and Figure 42 show the patterns of the critical tensile stress inside the markers on rigid and flexible pavements for Types A and B, respectively.
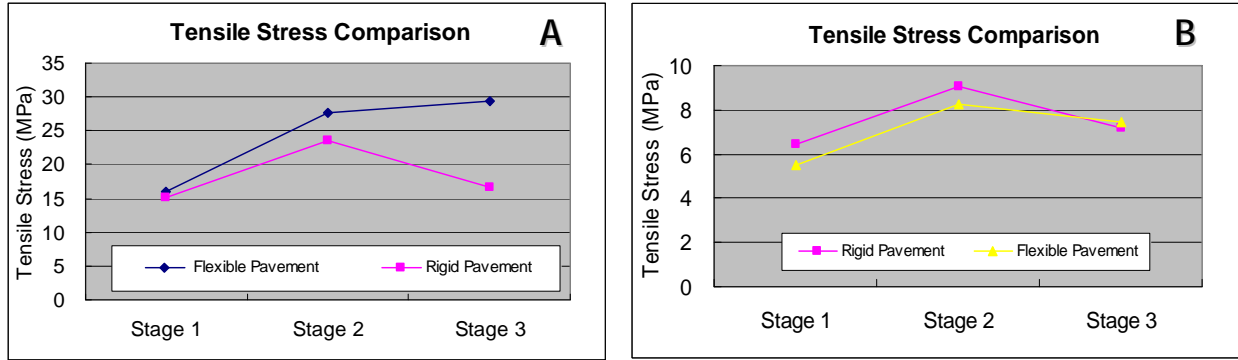
Figure 40. Comparison of Critical Tensile Stress for RRPM Types A and B.

Based on the results discussed above, it is evident that the magnitude of the critical compressive stress at the top edges of the markers during the tire-marker impact tends to be larger on rigid pavement than on flexible pavement. Such results are expected since the field study shows that RRPMs on rigid pavement have more severe damage at the top edges, upper lens, and non-lens sides, which is caused by compressive stress, than those on flexible pavement at the same test deck.

On the other hand, the critical tensile stress scatters in the body of the markers during the impact on rigid pavement, while it is produced from the mid-bottom of the markers on flexible pavement. Furthermore, the magnitude of the critical tensile stress during stage 3 of the impact on flexible pavement is larger than that on rigid pavement, as was shown with both types of markers, although such difference was considered to be insignificant for Type B. In fact, the tensile stress for Type B is relatively small in magnitude, which might be a reason for the slight difference between the two types of pavement. Overall, it supports the field observation at the test decks on flexible pavement that some RRPMs have fractures across the mid-bottom of the markers, which results from the critical tensile stress, and such structural damage was rarely observed at any test deck on rigid pavement.

The finding that there are different magnitudes of critical compressive and tensile stress inside the markers for rigid and flexible pavement indicates the need to evaluate the loading rate used in laboratory tests for RRPMs installed on the two types of pavement. Furthermore, a laboratory test focusing on tensile stress is necessary for RRPMs on both types of pavement, but it is more critical to RRPMs on flexible pavement, while a test that is good at testing compressive stress should be important to RRPMs on both types of pavement.

Tensor Plot (Analysis system)
Stress (Major Mid Minor, Mid)

20.808
8.690
-3.428
-15.545
-27.663
-39.780
-51.898
-64.015
-76.133
-88.251
No result
Max = 20.808
Min = -88.251

Tire-marker impact on rigid pavement

Tensor Plot (Analysis system)
Stress (Major Mid Minor, Mid)

30.121
18.110
6.099
-5.912
-17.922
-29.933
-41.944
-53.955
-65.965
-77.976
No result
Max = 30.121
Min = -77.976

Tire-marker impact on flexible pavement
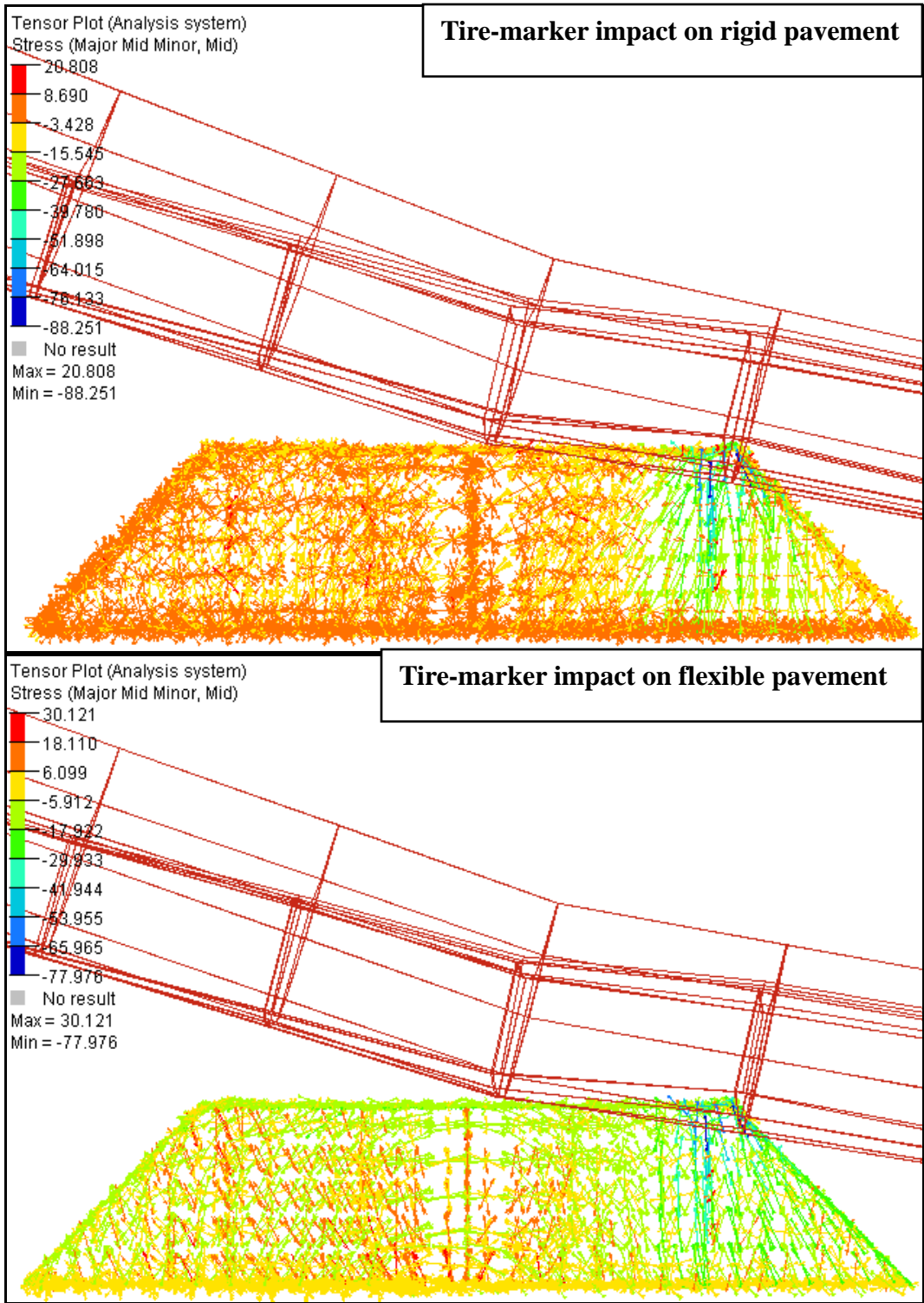
Figure 41. Comparison of Tensile Stress Patterns for RRPM Type A.
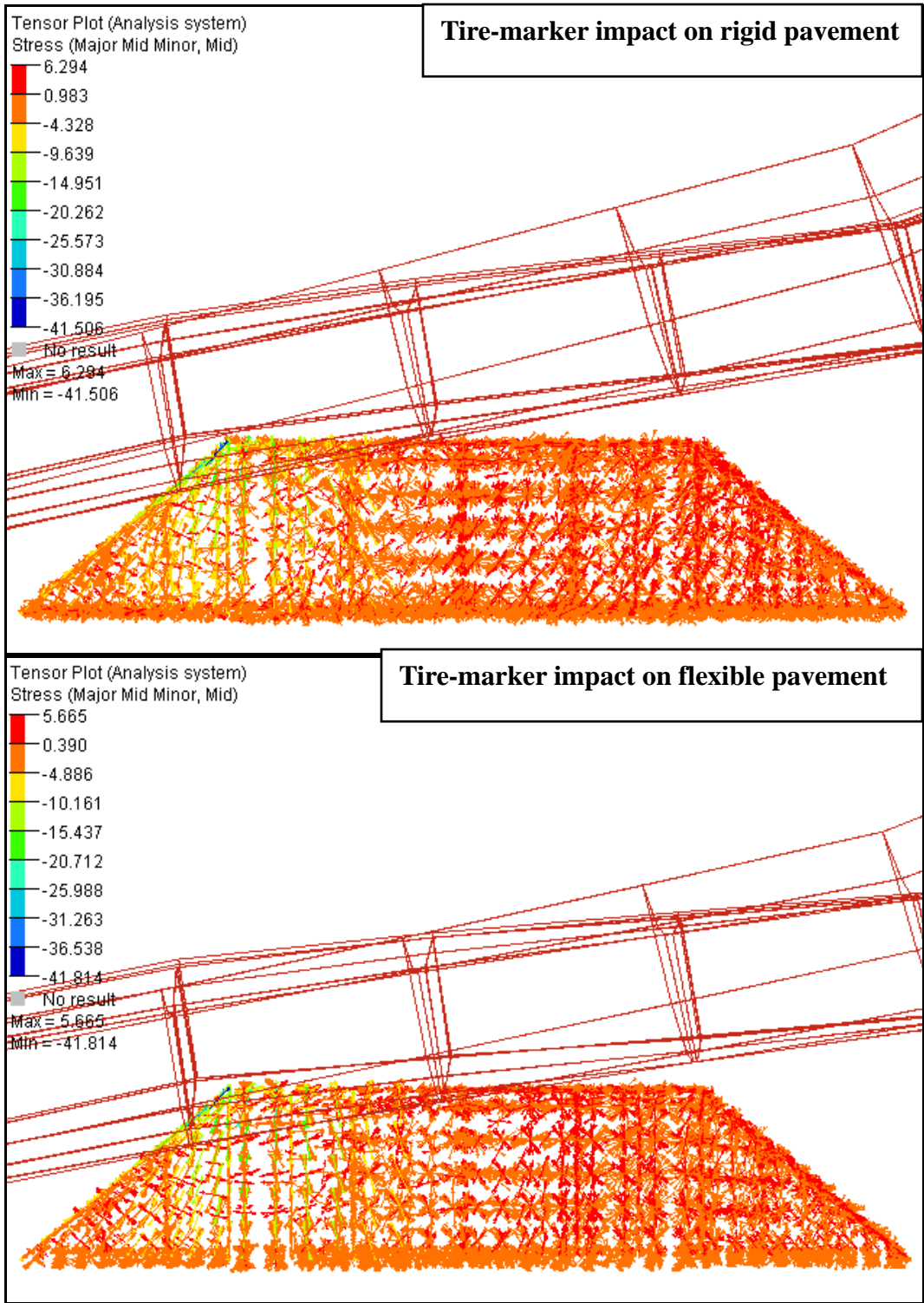
Figure 42. Comparison of Tensile Stress Patterns for RRPM Type B.

INTERFACE FORCES AND MARKER PROFILE

Interface Force Comparison

This research compares the interface forces between rigid and flexible pavement. The interface force refers to the force produced between the marker base and the pavement surface during the tire-marker impact. There are two types of interface force (defined by the direction of the force): shear interface force and perpendicular interface force. Both can be obtained from the tire-marker impact simulation. The shear force has been considered critical to the retention of RRPMs on the road. The results of this comparison were used to investigate the requirements of adhesive materials on different surface types. This is meaningful because different bonding materials are currently used in the field for different types of pavement.

Forty-five scenarios of tire-marker impact simulation were set up and run on both types of pavement. They were combined with all the scenarios of external factors except for the scenarios having contact angle and offset at the same time. After researchers obtained all the results of peak forces in x (shear) and z (perpendicular) direction, they used the sample means to examine the relationship between the peak interface forces on rigid and flexible pavement. The average peak interface forces on the two types of pavement are shown in Table 9.

Table 9. Comparison of Interface Forces (Newtons) between Two Types of Pavement.

	Interface Forces (RRPM A)			Interface Forces (RRPM B)		
Average Peak Force (N)	**x(+)**	**x(-)**	**z**	**x(+)**	**x(-)**	**z**
Rigid pavement	4656	2550	20536	3117	1753	19976
Flexible pavement	4244	1718	18886	2821	1438	18530

The results summarized in Table 9 indicate that the positive shear force and the perpendicular force are about 10 percent larger on rigid pavement, and the negative shear force (opposite of the direction of vehicle movement) on rigid pavement is 20 to 50 percent higher. Statistical tests also indicate those differences are statistically significant. In addition to this comparison, the trend of the interface forces over the entire impact process on both types of pavement was plotted from the base scenario simulation for Types A and B, which are shown in Figure 43 and Figure 44, respectively. It is evident that the interface forces between markers and

pavement surface on rigid pavement are noticeably larger than those on flexible pavement. Furthermore, the researchers believe that RRPMs on flexible pavement undergo less shear interface force than those on rigid pavement, as can be explained by the fact that RRPMs on flexible pavement sink into the pavement over a period of time. This finding is supported by the field study that was conducted in which more RRPMs had been found to be removed by traffic on rigid pavement than on flexible pavement over time at the same test deck. Therefore, extra attention should be given to the adhesive materials during the RRPM installation process. The use of stronger binding material to install RRPMs on rigid pavement, especially at places where traffic volume or truck percentage is high, should be considered. This conclusion supports the finding from the field observation that RRPMs on rigid pavement using bitumen adhesive have a higher rate of marker loss compared to those with epoxy adhesive. This difference of marker loss rate between the two adhesive types is probably due to the inferior shear force resistant capability of bitumen adhesive.

Marker Profile Study

The profile of RRPMs has been known to affect marker durability. So, the researchers studied the effect of marker profile on the stress inside markers using the existing tire-marker impact model. The marker profile here is defined as the height, lens slope, length, and width of a marker. The profile of the finite element marker models was varied to find out how they affect the magnitudes of the critical Von Mises stress inside the markers during the simulated tire-marker impact.

Because the mesh of an individual marker is based on the whole geometry of the marker, a re-mesh is required whenever the shape of a marker is changed, which is very time consuming. So, researchers decided to use another approach, which is varying the scale of the marker in the directions of x, y, and z in a coordinate system, to get the same effect of changing the profile of a marker while reducing the time burden to conduct the study. The only limitation is that the approach cannot be used to study the marker height and lens slope separately because the scale variation in z direction will change the height and lens slope simultaneously. The compromise nevertheless did not affect the results the researchers expected to achieve. For the sake of simplicity, the study is conducted only on rigid pavement.
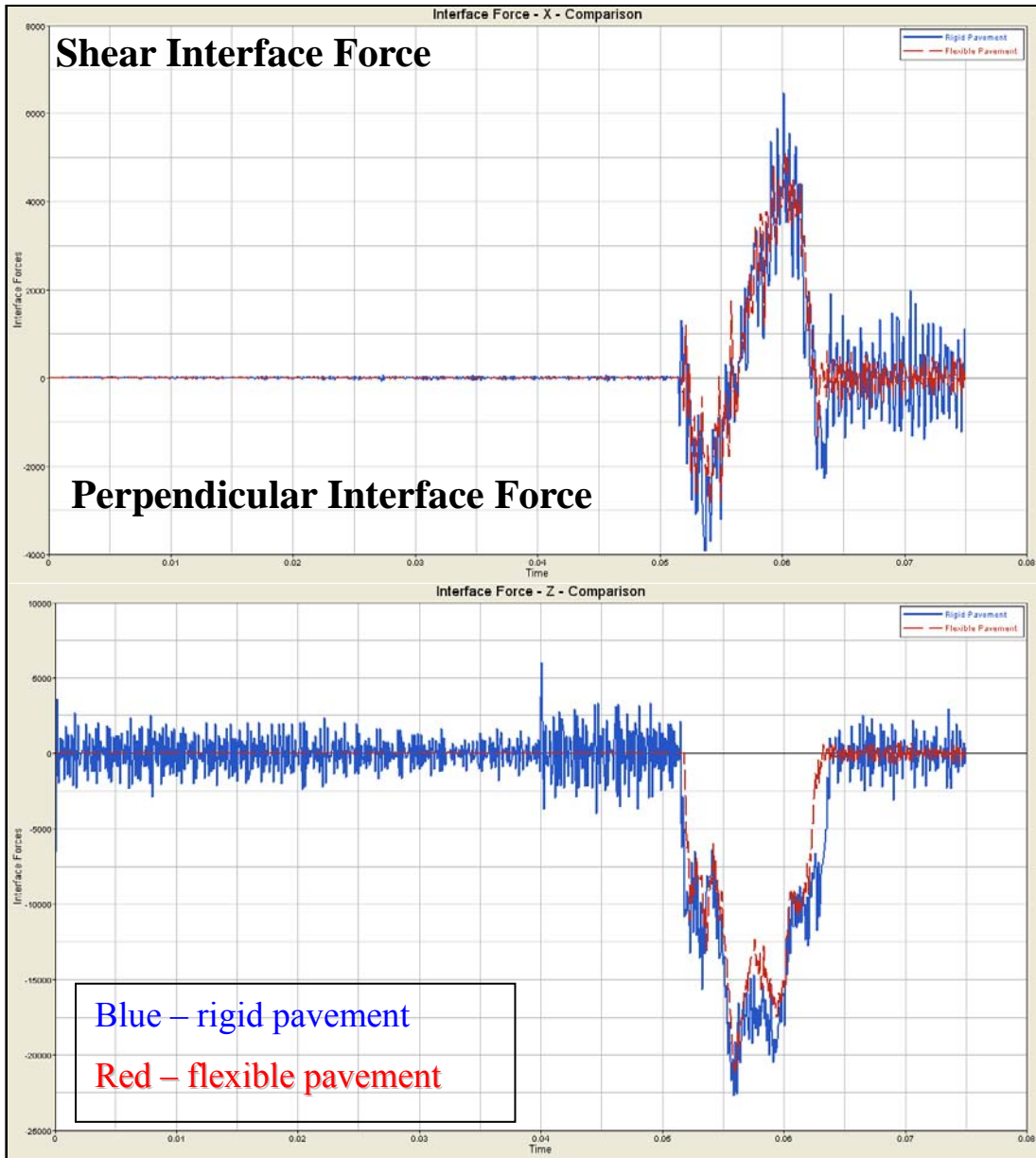
Figure 43. Comparison of the Magnitudes of Interface Forces between Two Types of Pavement for RRPM Type A.
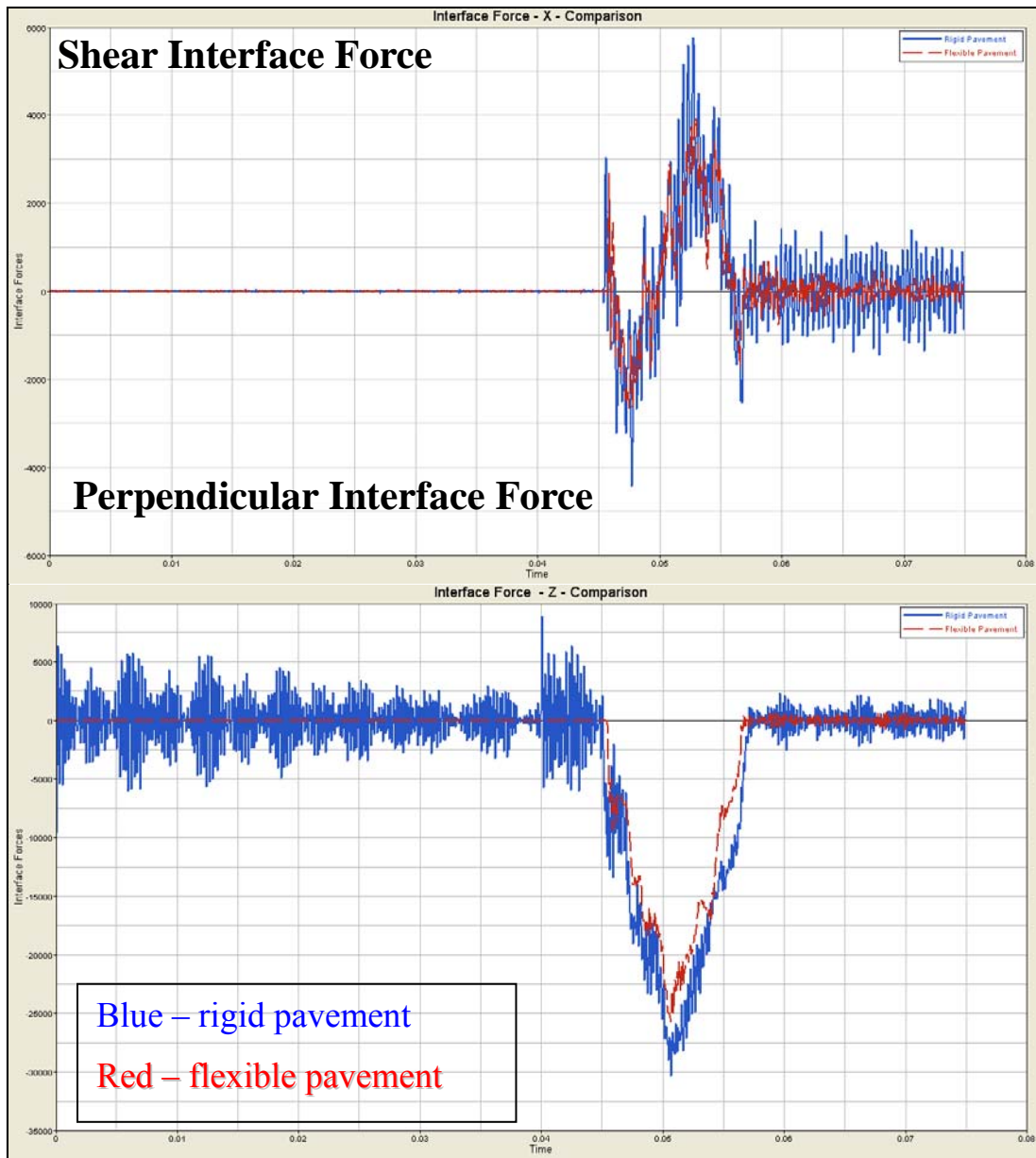
Figure 44. Comparison of the Magnitudes of Interface Forces between Two Types of Pavement for RRPM Type B.

The coordinate system of x, y, and z that the marker model uses is shown in Figure 45. By varying the scale of the marker in z, x, and y direction, different profiles for the two marker models were obtained. All the marker profiles meet the minimum height of 10 mm (0.4 inch) required by the *MUTCD*. Table 10 and Table 11 show the profiles of Types A and B commensurate with the scales.

71
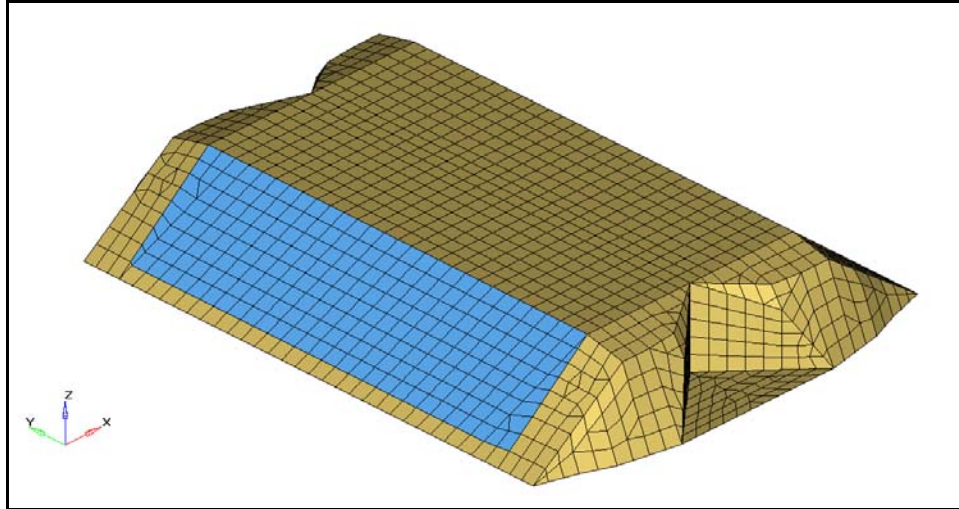
Figure 45. RRPM Type B in X, Y, and Z Coordinate System.

Table 10. RRPM Type A Profiles (Unit: Millimeters).

RRPM A		Height	Length	Width			Slope
Direction	Scale	(z)	(x)	(y)	Upper x	Upper y	(Degree)
	0.8	12.2	74.997	96	45	70	39
	0.9	13.725	74.997	96	45	70	42
	1	15.25	74.997	96	45	70	45
	1.1	16.775	74.997	96	45	70	48
Z	1.2	18.3	74.997	96	45	70	51
	0.8	15.25	59.9976	96	36	70	52
	0.9	15.25	67.4973	96	40.5	70	48
	1	15.25	74.997	96	45	70	45
	1.1	15.25	82.4967	96	49.5	70	43
X	1.2	15.25	89.9964	96	54	70	40
	0.8	15.25	74.997	76.8	45	56	45
	0.9	15.25	74.997	86.4	45	63	45
	1	15.25	74.997	96	45	70	45
	1.1	15.25	74.997	105.6	45	77	45
Y	1.2	15.25	74.997	115.2	45	84	45

Table 11. RRPM Type B Profiles (Unit: Millimeters).

RRPM B		Height	Length	Width			
Direction	Scale	(z)	(x)	(y)	Upper x	Upper y	Slope
	0.8	10.8	71	95	38	83	33
	0.9	12.15	71	95	38	83	36
	1	13.5	71	95	38	83	39
	1.1	14.85	71	95	38	83	42
Z	1.2	16.2	71	95	38	83	44
	0.8	13.5	56.8	95	30.4	83	46
	0.9	13.5	63.9	95	34.2	83	42
	1	13.5	71	95	38	83	39
	1.1	13.5	78.1	95	41.8	83	37
X	1.2	13.5	85.2	95	45.6	83	34
	0.8	13.5	71	76	38	66.4	39
	0.9	13.5	71	85.5	38	74.7	39
	1	13.5	71	95	38	83	39
	1.1	13.5	71	104.5	38	91.3	39
Y	1.2	13.5	71	114	38	99.6	39

After running the base tire-marker impact simulation on rigid pavement with different scenarios of marker profile, the researchers produced the maximum Von Mises stress generated at the top edges of the markers for each profile scenario. The researchers investigated the effects of marker height combined with lens slope (z direction scale), marker length combined with lens slope (x direction scale), and marker width (y direction scale) on the critical Von Mises stress. Figure 46 and Figure 47 show the effects for Types A and B, respectively.

Based on the plots, the variation of marker scale in z direction has the most consistent effect on the stress inside the markers during the tire-marker impact. As the marker scale in z direction increases, the maximum Von Mises stress increases consistently for both types of markers, indicating that the increase of marker height and lens slope will result in more stress inside the markers during the tire-marker impact. No consistent effect was found in terms of the variation of marker scale in x direction (marker length and lens slope) for both types of markers. As for the scale in y direction (marker width), the result from Type A shows that increasing the width of the marker will cause more stress inside the marker, which is not reflected in the result for Type B. Generally, the marker height and lens slope are more critical to the durability of markers, and from this perspective it is better to have RRPMs designed with a height and lens slope as small as possible. A minimum marker height is required by the *MUTCD*, but the lens

slope can be small to some extent since new technology allows a lens with a small slope to provide adequate retroreflectivity to drivers.
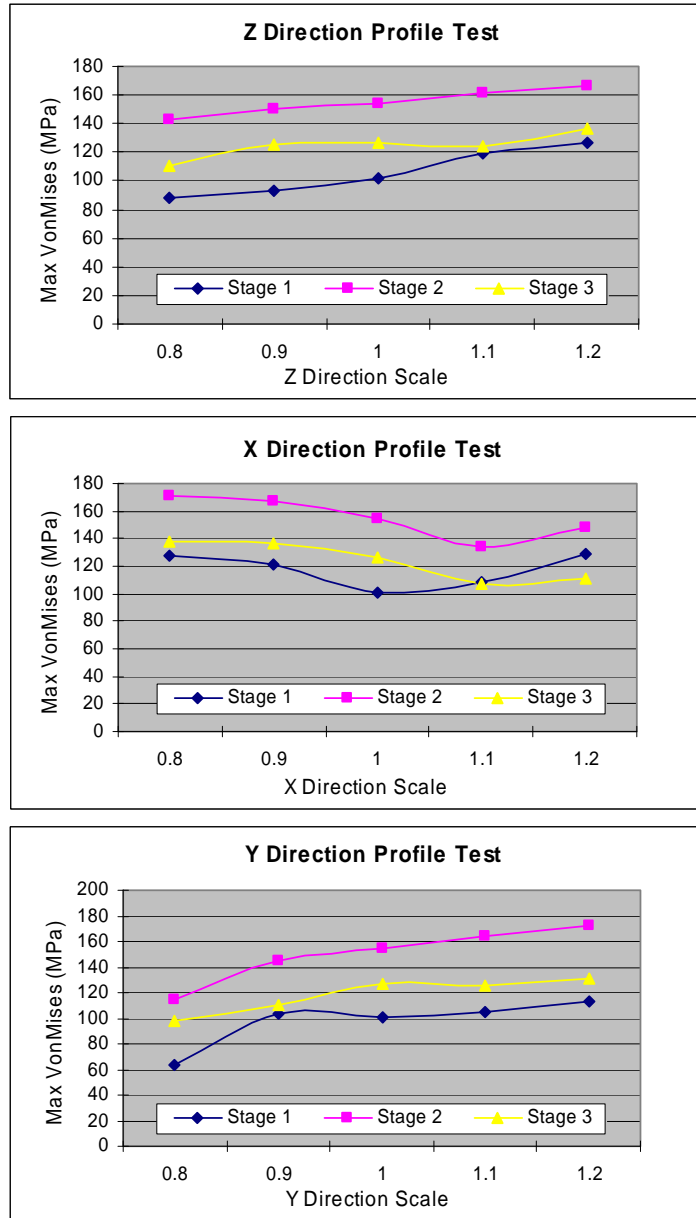
Figure 46. Effects of Profile Scale on Critical Von Mises Stress for RRPM Type A.

Z Direction Profile Test

X Direction Profile Test

Y Direction Profile Test
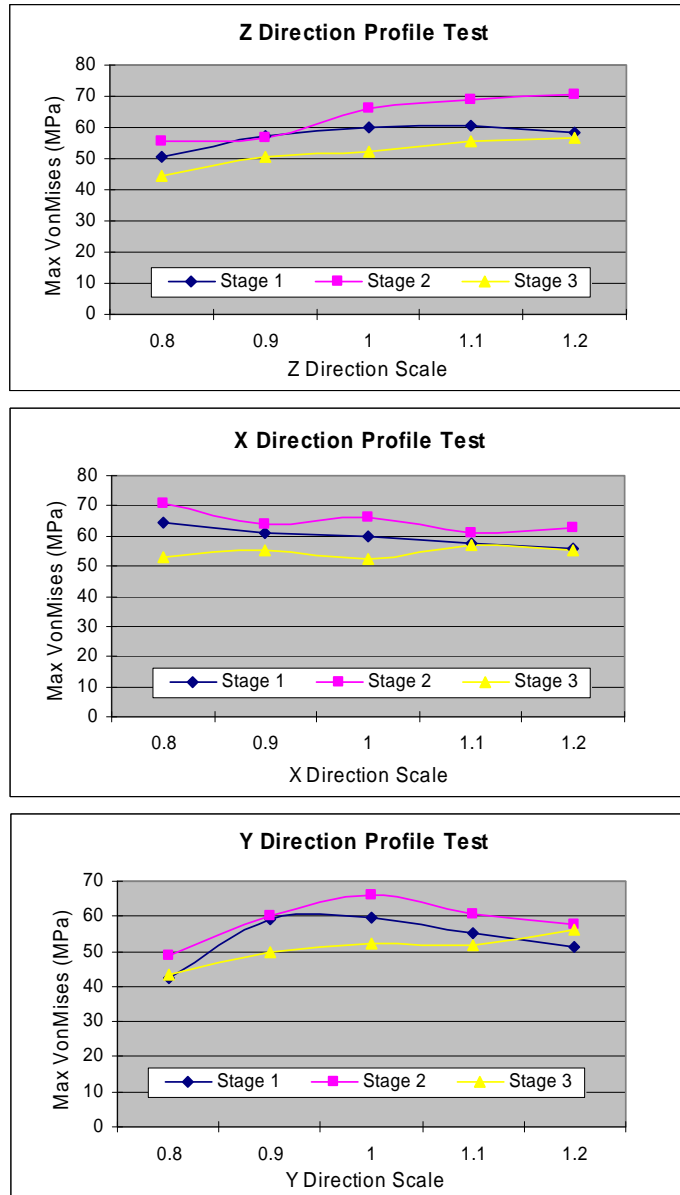
**Figure 47. Effects of Profile Scale on the Critical
Von Mises Stress for RRPM Type B.**

LABORATORY TEST EVALUATION

The main objective of this research project is to recommend laboratory testing procedures
that would simulate the real tire-marker impact. The simulation of tire-marker impact helped in
getting estimates of stresses that RRPMs encounter during the impact in the field. The
researchers sought to simulate a few loading conditions that could produce similar stresses. This

section first discusses the results of a few laboratory tests that were simulated to replicate the tire-marker impact on rigid pavement. Next, it details the further evaluation of selected laboratory tests in consideration of loading rate and both pavement types.

The stress tensor plots of the two markers are illustrated in the tire-marker impact analysis. Every frame shows the distribution of the principal stresses σ_1, σ_2, and σ_3 inside the markers. Based on these plots, the researchers identified and designed laboratory testing procedures that could produce stresses inside the markers similar to that produced by the tire-marker impact. The researchers then modeled and simulated these testing procedures using the finite element tools (Hypermesh for modeling and LS-DYNA for simulation). In all the laboratory simulations, post-calibrated material properties for the markers were used. The properties for the steel loading bars or the plates were kept the same as those used in the calibration. Researchers did not include elastomeric pads in the model (as in calibration) to keep the modeling simple. They assumed that this would not make a large difference to the simulation results because of their experience in the calibration process, where they had run simulations with and without the elastomeric pads and did not find a significant difference in the stress distribution between the two scenarios.

The researchers considered a laboratory test to be a good test if it accurately replicated any one of the three stages of the tire-marker impacts. Thus, a laboratory test simulation should produce a similar kind of stress inside the markers as produced during any of the three stages of the tire-marker impact. Additionally, it should produce similar magnitudes of stress. The following paragraphs describe the loading conditions and results from the laboratory test simulations.

Initial Evaluation

The initial evaluation of laboratory tests was conducted only against the tire-marker impact on rigid pavement. The researchers analyzed each laboratory test simulation in two aspects. A good test should do well for both aspects, which are described as follows:

1. First, the stress tensor plots were obtained for the markers for each laboratory test simulation and compared qualitatively (locations and magnitudes of the tensile and compressive stresses) in the three stages of the tire-marker impact simulation.

2. The magnitudes of Von Mises stress were compared at some locations of elements inside the markers from the tire-marker impact and the laboratory test simulations. The researchers chose those elements that could have critical stresses based on the results from the tire-marker impact simulation. The locations for the elements inside RRPM Type A are illustrated in Figure 48, and they are similar for RRPM Type B. The laboratory test and the tire-marker impact simulations would compare well if the percentage differences in the magnitudes of Von Mises stress between the two are small for all the chosen elements. Additionally, a low variation in the percentage differences among the elements would be ideal because it means that the laboratory test simulation and the tire-marker impact simulation would produce similar stress profiles.
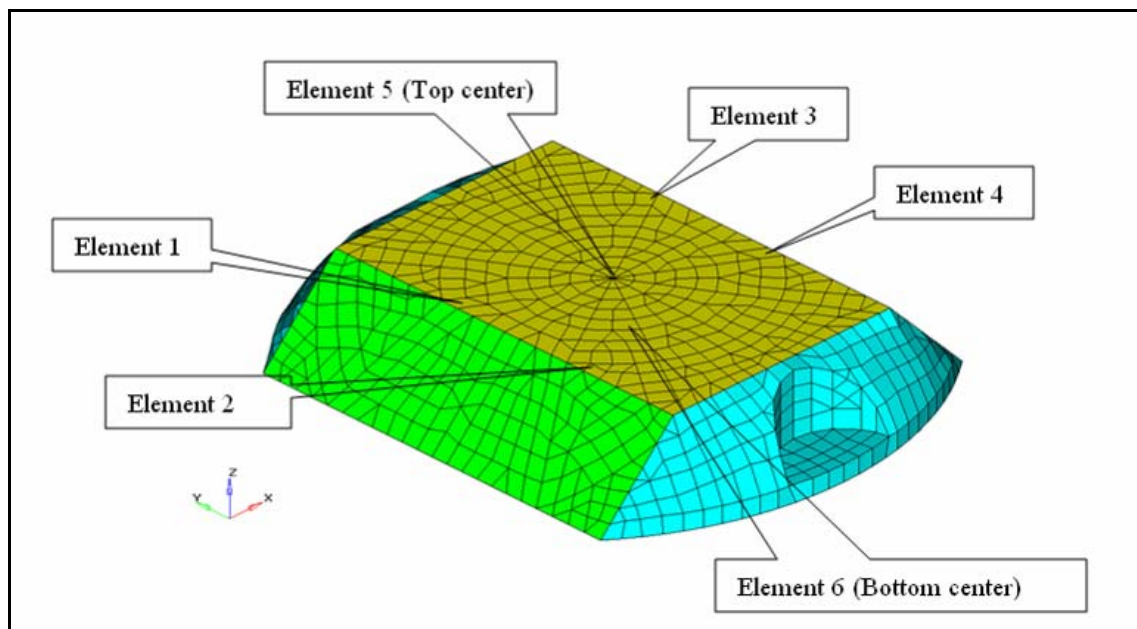
Figure 48. Locations of Finite Elements 1-6 Chosen for Comparison between Tire-Marker Impacts and Laboratory Test Simulations (for RRPM Type A).

ASTM Compression Test

The researchers modeled the ASTM compression test (*6*) described in ASTM standard D4280. The rate of loading was kept at 2.54 mm (0.1 inch) per minute as stated in the ASTM

77

standard. Elastomeric pads were not included between the steel plates and the markers. Figure 49 shows a finite element model of the test.
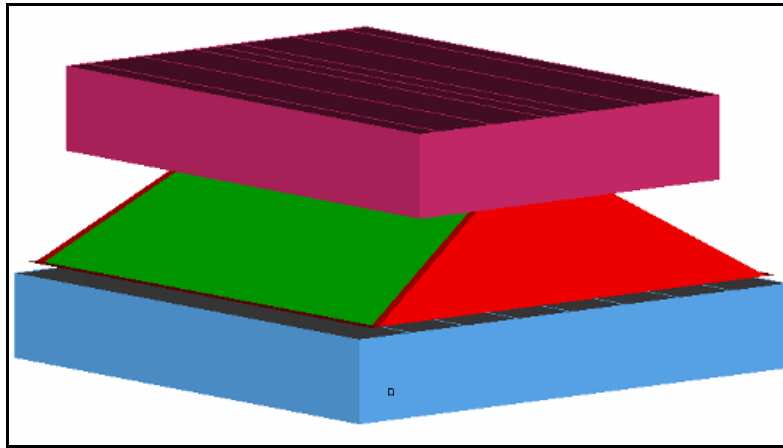
Figure 49. Finite Element Model of ASTM Compression Test.

Figure 50 shows the stress tensor plots for RRPM Types A and B. The stress distributions from these simulations were similar to those found during stage 2 of the tire-marker impact simulation. There was major compressive stress on the edge contacts of the top surface at the retroreflective sides, as found during stage 2.

Figure 51 shows percentage differences between the maximum Von Mises stresses (in finite elements 1-6) from the ASTM compression test and the three stages of the base tire-marker impact simulation. It should be noted that the percentage differences have been truncated to ±100 percent in Figure 51. This method was followed in all the figures representing such analyses (including Appendix B). This was done to eliminate very high percentage differences and to make it easier to analyze the variations among elements. Also note that a positive difference meant the laboratory test produced higher stresses than the tire-marker impact.

As seen from Figure 51, the Von Mises stresses were comparable between the laboratory simulation and stage 2 of the tire-marker impact for elements 1-4. The percentage differences were in the ranges of –45 to –53 percent for RRPM Type A and –54 to –76 percent for RRPM Type B. For elements 5 and 6 of all the RRPM types, the percentage differences were greater. For other stages, the percentage differences were very high and varied to a large extent.

78
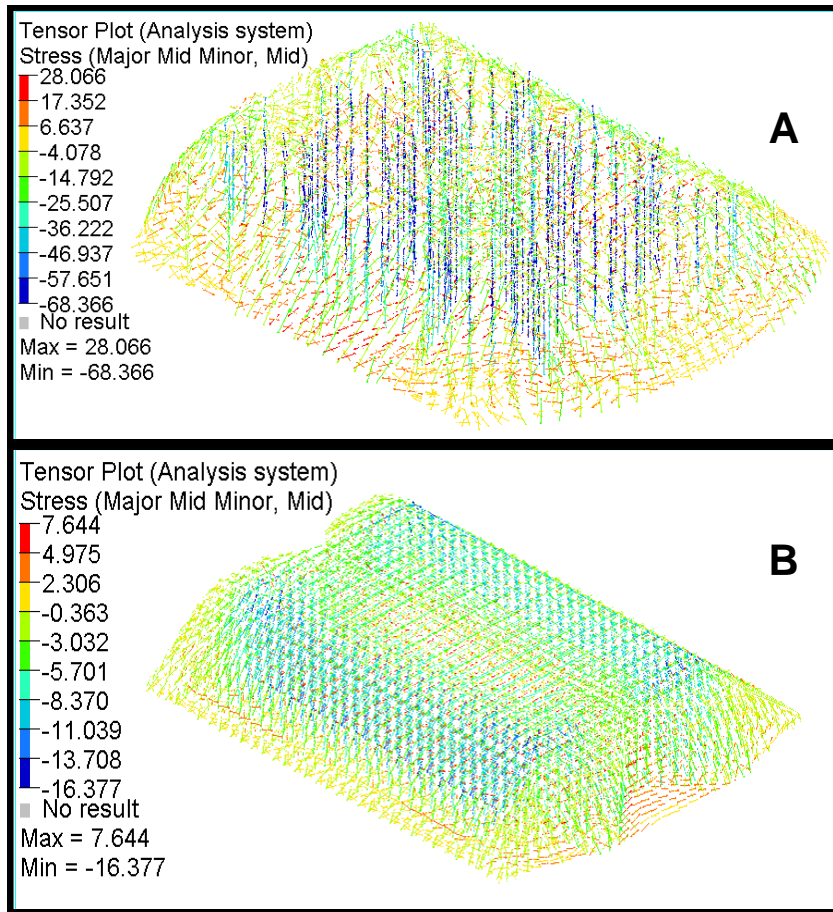
**Figure 50. Stress Tensor Plots (in Megapascals) for RRPM
Types A and B (ASTM Compression Test).**

ASTM Longitudinal Flexural Test

The researchers modeled the ASTM longitudinal flexural test (*6*) described in ASTM standard D4280. The rate of loading was kept at 5.08 mm (0.2 inch) per minute as stated in the ASTM standard. However, there were no elastomeric pads. The same experiment had been used for the calibration part of the research. Figure 26 shows the finite element model of the test.
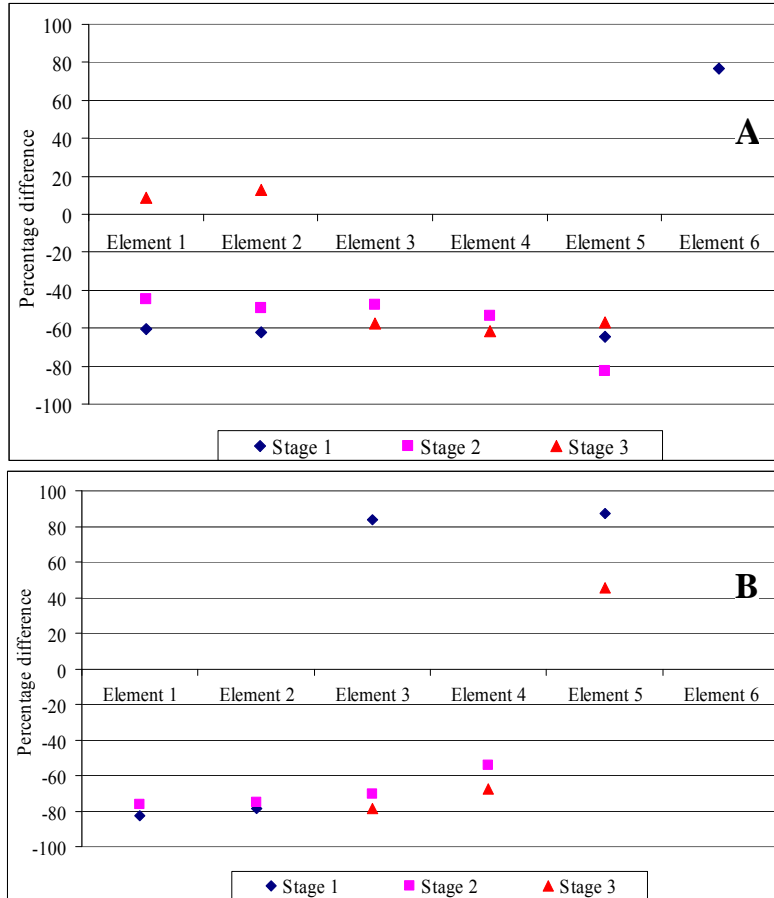
**Figure 51. Percentage Differences between Maximum Von Mises Stresses
from Three Stages of Base Tire-Marker Impact Simulation and ASTM
Compression Test Simulation in Finite Elements 1-6 (RRPM Types A and B).**

Figure 52 shows the stress tensor plots for RRPM Types A and B. The simulation caused compression at the areas around the marker where the loading bar was placed. It caused major tension at the bottom of the marker. The maximum compressive and tensile stresses are comparable, which did not happen during any stage of the tire-marker impact simulation.

Figure 53 shows percentage differences between maximum Von Mises stresses (in finite elements 1-6) from the ASTM flexural test and the three stages of the base tire-marker impact simulation. The Von Mises stresses were comparable between the laboratory simulation and stage 2, especially for elements 1-4. For other stages, the percentage differences were higher and varied to a large extent among the elements.
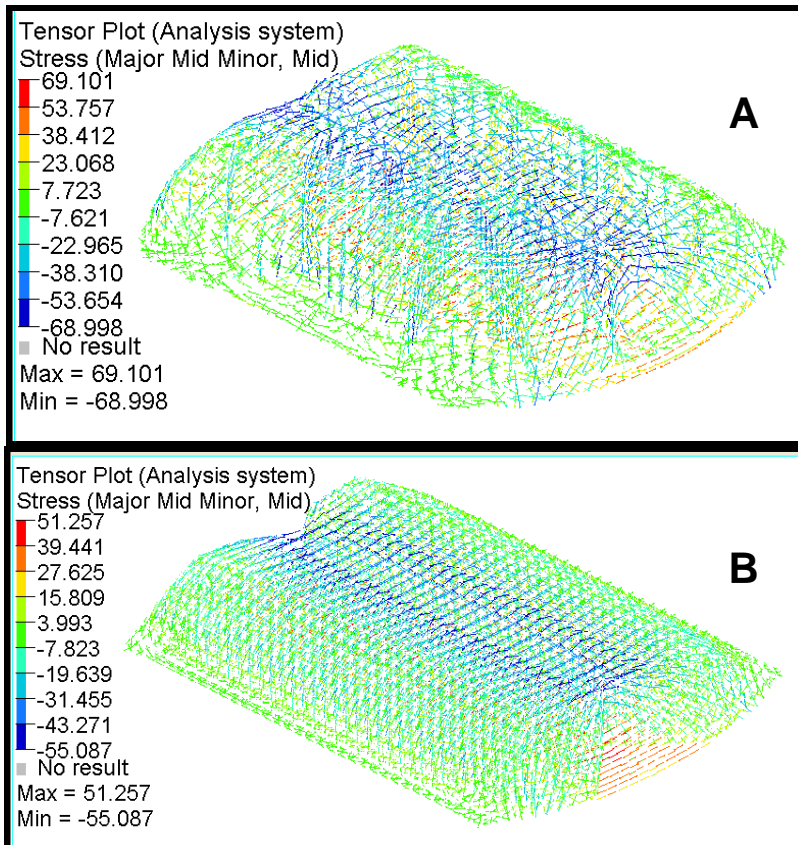
**Figure 52. Stress Tensor Plots (in Megapascals) for RRPM
Types A and B (ASTM Flexural Test).**

Cylindrical Compression Test

The researchers designed, modeled, and simulated a variation of the ASTM compression test. Instead of having two steel plates at the top and bottom of the marker, this test model had two hollow cylinders. The cylinder at the top had an outer diameter of 38.1 mm (1.5 inches) and a thickness of 3.175 mm (0.125 inches). The cylinder at the bottom had an outer diameter of 63.5 mm (2.5 inches) and a thickness of 3.175 mm (0.125 inch). The top and bottom cylinders had such dimensions that the top one could fit into the bottom one. The loading rate was kept at 2.54 mm (0.1 inch) as in the ASTM compression test. Figure 54 shows the finite element model of this test.
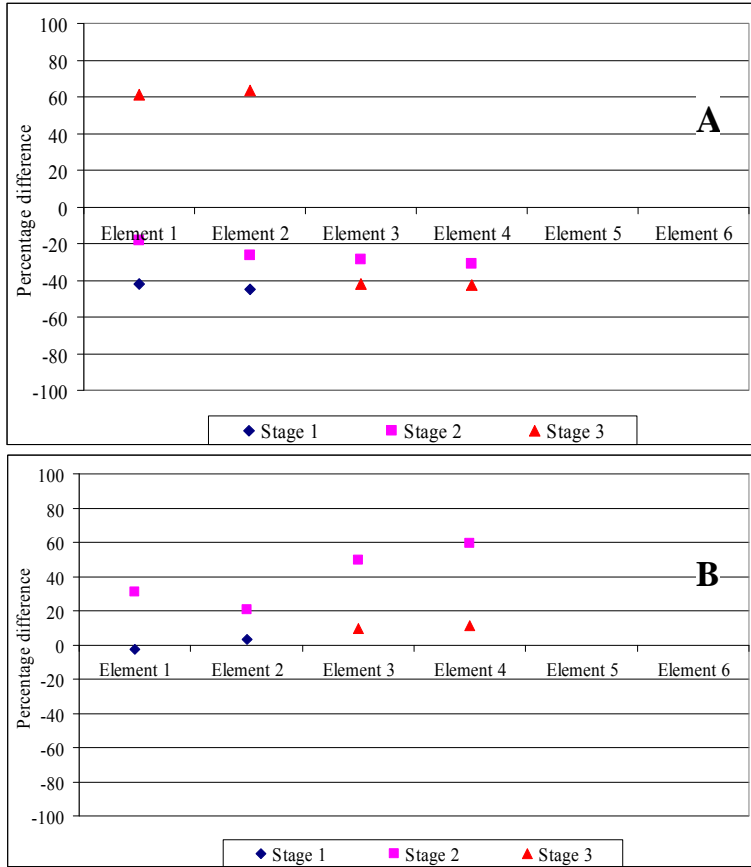
Figure 53. Percentage Differences between Maximum Von Mises Stresses from Three Stages of Base Tire-Marker Impact Simulation and ASTM Flexural Test Simulation in Finite Elements 1-6 (RRPM Types A and B).
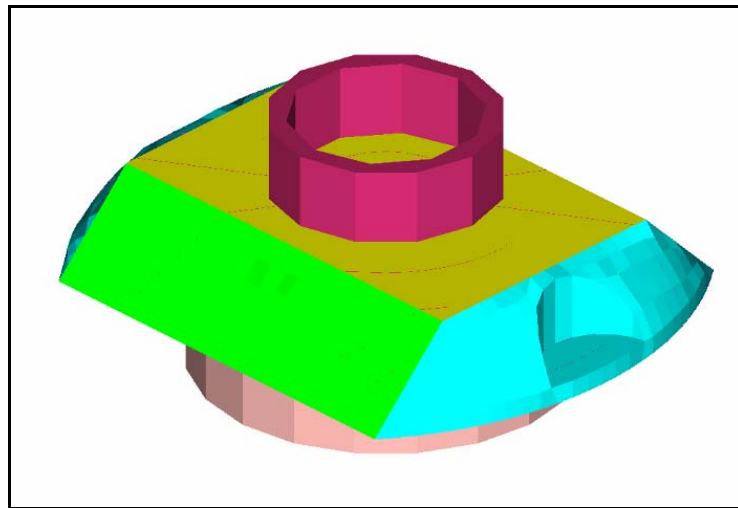
Figure 54. Finite Element Model of Cylindrical Compression Test.

Figure 55 shows stress tensor plots from the test simulations for RRPM Types A and B. From the figures it is seen that there are large compressive stresses around the top cylinder and large tensile stresses at the bottom of the marker (mostly around the bottom cylinder's contacts with the marker). The locations and magnitudes of the principal stresses from this test are similar to stage 2 of the tire-marker impact simulation.

Figure 55. Stress Tensor Plots (in Megapascals) for RRPM Types A and B (Cylindrical Compression Test).

Figure 56 shows the percentage differences between maximum Von Mises stresses (in finite elements 1-6) from the cylindrical compression test and the three stages of the base tire-marker impact simulation. The Von Mises stresses in elements 1-4 were comparable with stage 2 of the tire-marker impact simulation for RRPM Types A and B. The percentage differences varied from –79 to –82 MPa and from –43 to –66 MPa for RRPM Types A and B, respectively. The percentage differences varied a great deal for elements 1-4 for the other stages. They were higher for elements 5-6 for all stages (see Appendix B).

83
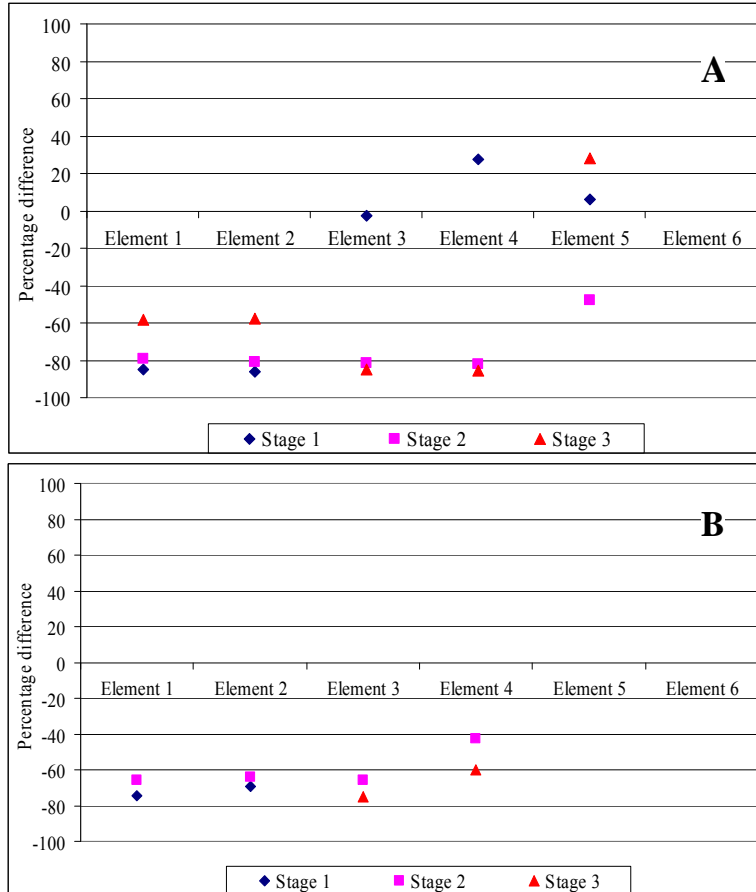
Figure 56. Percentage Differences between Maximum Von Mises Stresses from Three Stages of Base Tire-Marker Impact Simulation and Cylindrical Compression Test Simulation in Finite Elements 1-6 (RRPM Types A and B).

Offset Compression Test (Lower Loading Rate)

The researchers designed, modeled, and simulated a new test and called it the offset compression test. It was similar to the ASTM compression test except that there was no loading steel plate. Instead, there was a steel bar (12.7 mm [0.5 inch] wide and as long as the marker), which was placed along one of the retroreflective edges of the marker. This was done in an attempt to produce compression in one of retroreflective sides of the marker and tension in other parts of the marker. There were no elastomeric pads as in the ASTM test. The rate of loading was kept at 2.54 mm (0.1 inch) per minute as in the ASTM test. Figure 57 shows the finite element model of the test.
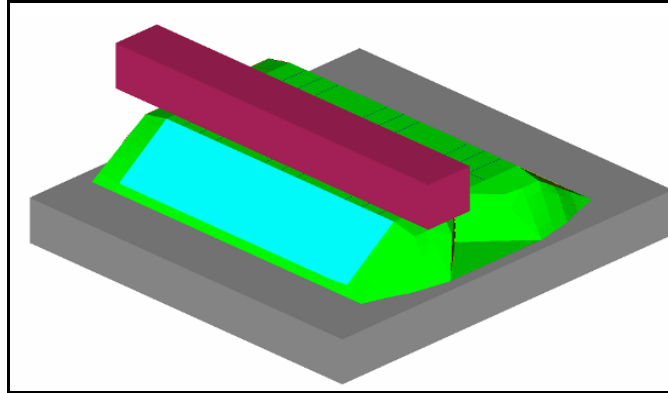
Figure 57. Finite Element Model of Offset Compression Test.

Figure 58 shows the stress tensor plots for RRPM Types A and B. The simulation caused major compression in areas around the location on the marker where the loading bar was placed and in the retroreflective surface. It caused tension in other areas although the magnitudes of the tensile stresses were not large, especially in RRPM Type B.
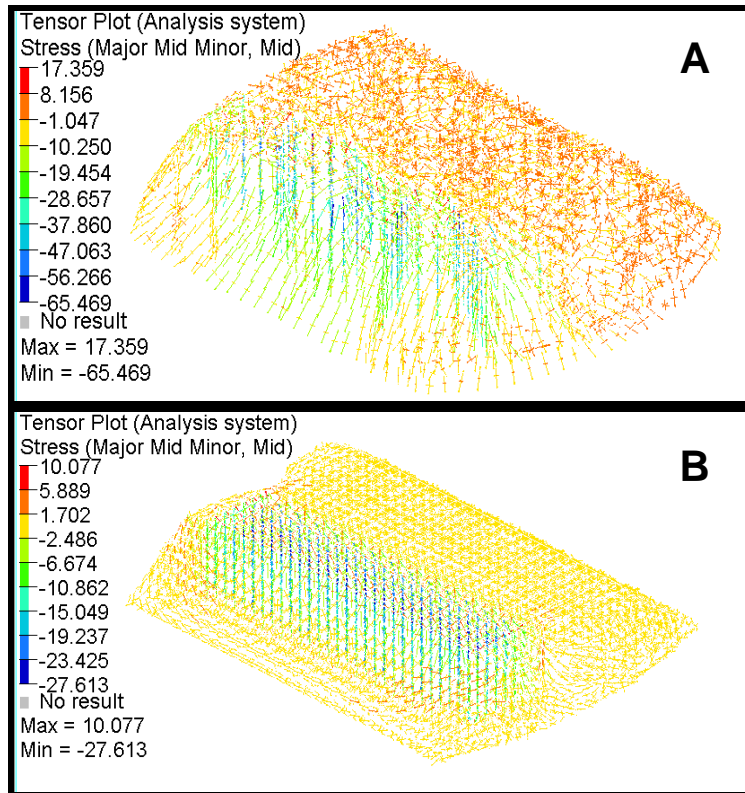
**Figure 58. Stress Tensor Plots (in Megapascals) for RRPM
Types A and B (Offset Compression Test, Lower Loading Rate).**

Figure 59 shows the percentage differences between maximum Von Mises stresses (in finite elements 1-6) from the offset compression test (lower loading rate) and the three stages of the base tire-marker impact simulation. For all the RRPM types, the differences were less between the test simulation and stages 1 and 2 of the tire-marker impact simulation. For stage 1, the percent differences in elements 1-4 varied from –50 to –66 percent for RRPM Type A and –61 to –87 percent for RRPM Type B. For stage 2, the percent differences in elements 1-4 varied from –52 to –93 percent for RRPM Type A and –52 to –97 percent for RRPM Type B. The Von Mises stresses did not favor comparably for stage 3.

Another variation of this test could be to apply the load in such a way that the edge of the loading bar parallel to the retroreflective side protrudes beyond the edge line of the retroreflective side (say by 2.54 mm [0.1 inch]).

One of the challenges while developing this test was to constrain the marker in such a way that it does not tip off when loading is applied. This is because the loading is applied at an offset from the centerline of the marker and would cause a moment about the centerline. Hence, an arrangement is needed that can nullify the moment.

Offset Compression Test (Higher Loading Rate)

The researchers modeled and simulated a slightly different version of the previous test. This time the load was applied at a rate of 5.08 mm (0.2 inch) per minute. This was done to compare the stress magnitudes for different loading rates.

Figure 60 shows the stress tensor plots for RRPM Types A and B. The stress locations were the same as in the previous test. However, this test caused larger stresses, especially in RRPM Type B, which has a larger tensile stress (18.732 MPa as compared to 10.077 MPa in the previous test) and a larger compressive stress (–53.978 MPa as compared to -27.613 MPa in the previous test). The results imply that the rate of loading could make a difference to the stress magnitudes in the markers.
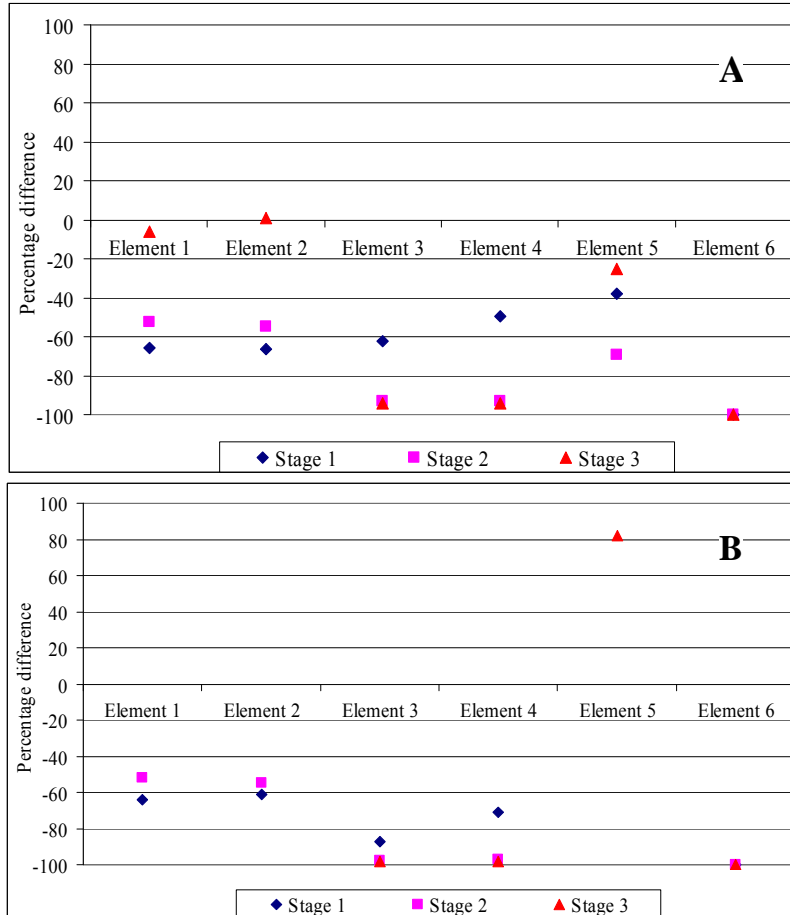
Figure 59. Percentage Differences between Maximum Von Mises Stresses from Three Stages of Base Tire-Marker Impact Simulation and Offset Compression Test (Lower Loading Rate) Simulation in Finite Elements 1-6 (RRPM Types A and B).

Figure 61 shows the percentage differences between maximum Von Mises stresses (in finite elements 1-6) from the offset compression test (higher loading rate) and the three stages of the base tire-marker impact simulation. As in the case of the previous test, the differences are less in elements 1-4 for stages 1 and 2 of the tire-marker impact simulation.
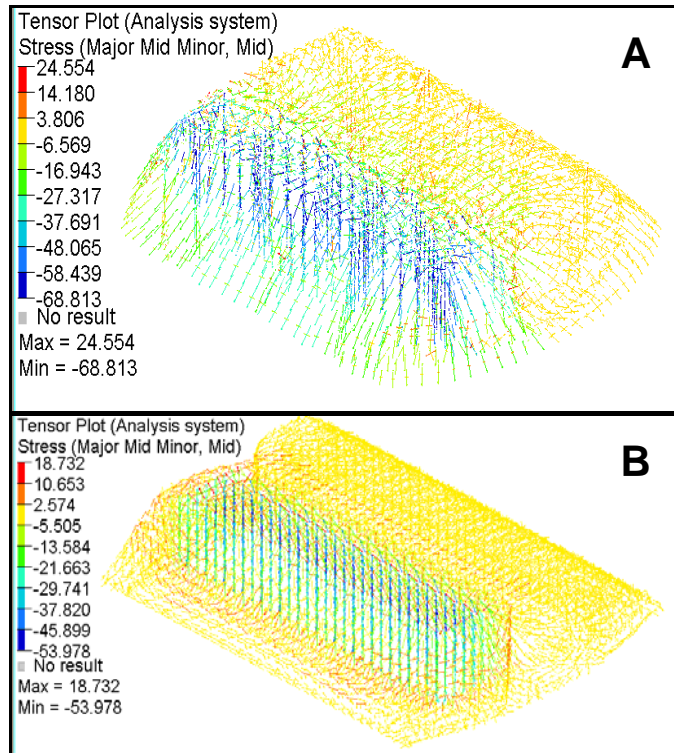
**Figure 60. Stress Tensor Plots (in Megapascals) for
RRPM Types A and B (Offset Compression Test,
Higher Loading Rate).**

Reversed ASTM Longitudinal Flexural Test

The researchers designed, modeled, and simulated one more laboratory procedure (Figure 62). This was similar to the ASTM longitudinal flexural test. The only difference was that there were two loading steel bars at the top and just one at the bottom. The top steel bars were kept as far apart as possible in a direction perpendicular to the traffic direction of the marker without protruding beyond the top of the marker. The bottom bar was placed at the center of the marker perpendicular to the traffic direction. The loading rate was 5.08 mm (0.2 inch) per minute as in the ASTM flexural test. There were no elastomeric pads as in the ASTM test.
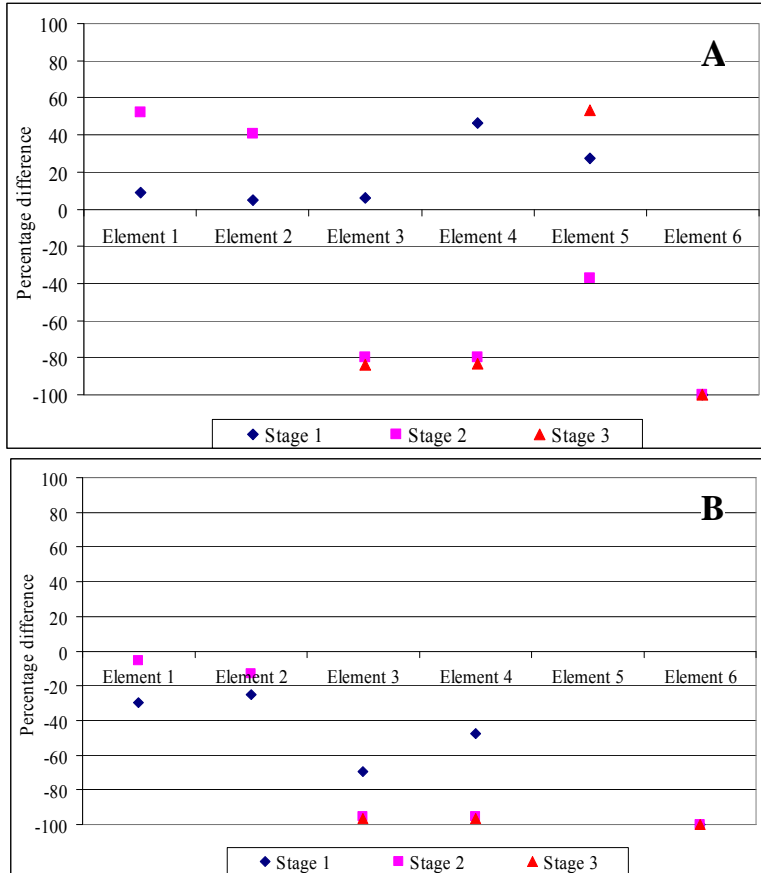
Figure 61. Percentage Differences between Maximum Von Mises Stresses from Three Stages of Base Tire-Marker Impact Simulation and Offset Compression Test (Higher Loading Rate) Simulation in Finite Elements 1-6 (RRPM Types A and B).
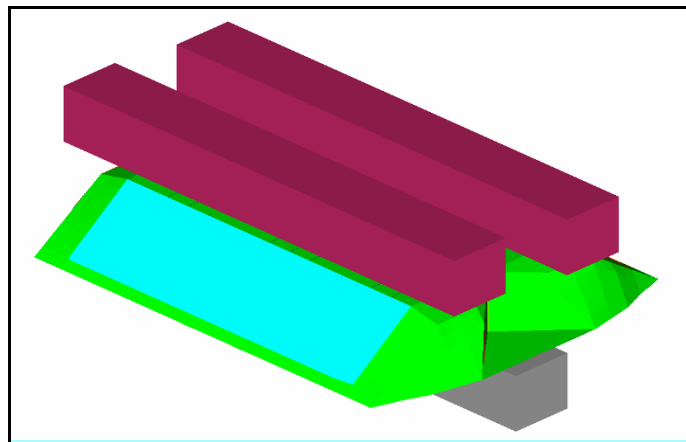
Figure 62. Finite Element Model of Reversed ASTM Flexural Test.

Figure 63 shows stress tensor plots for RRPM Types A and B. RRPM Type A had large compressive stresses at the top, while the RRPM Type B also had the same compressive stresses, although lower in magnitude. There were major tensile stresses at the center top surface of RRPM Type A. The maximum tensile stresses were comparable to the maximum compressive stresses.
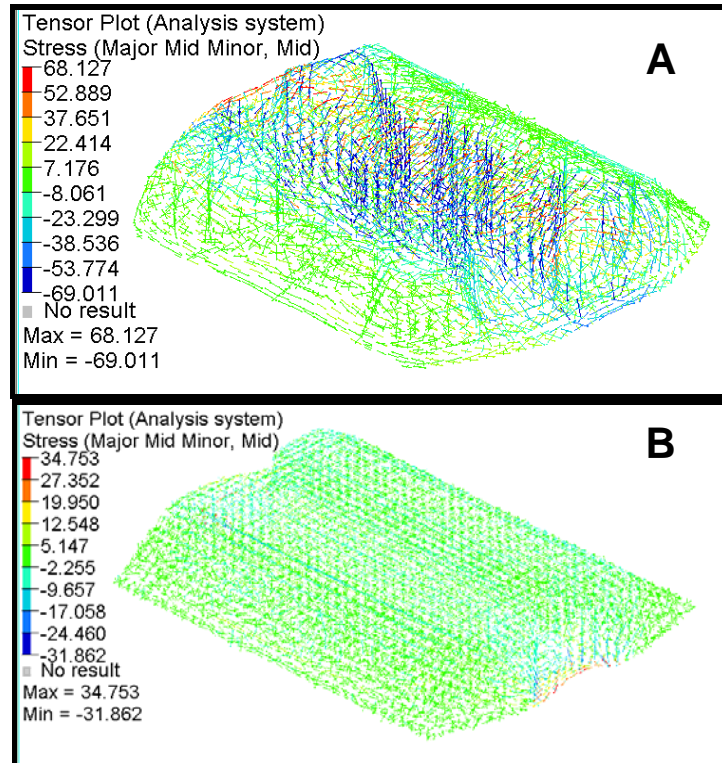
Figure 63. Stress Tensor Plots (in Megapascals) for RRPM
Types A and B (Reversed ASTM Flexure Test).

Figure 64 shows the percentage differences between maximum Von Mises stresses (in finite elements 1-6) from the reversed ASTM flexural test and the three stages of the base tire-marker impact simulation. The differences varied much among the elements for stages 1 and 3. For stage 2, however, the percentage differences did not vary much. The percent differences in elements 1-4 for this stage were from –23 to –33 percent for RRPM Type A and –47 to –67 percent for RRPM Type B. The percent differences varied a great deal for elements 5-6 for all three stages of impact.
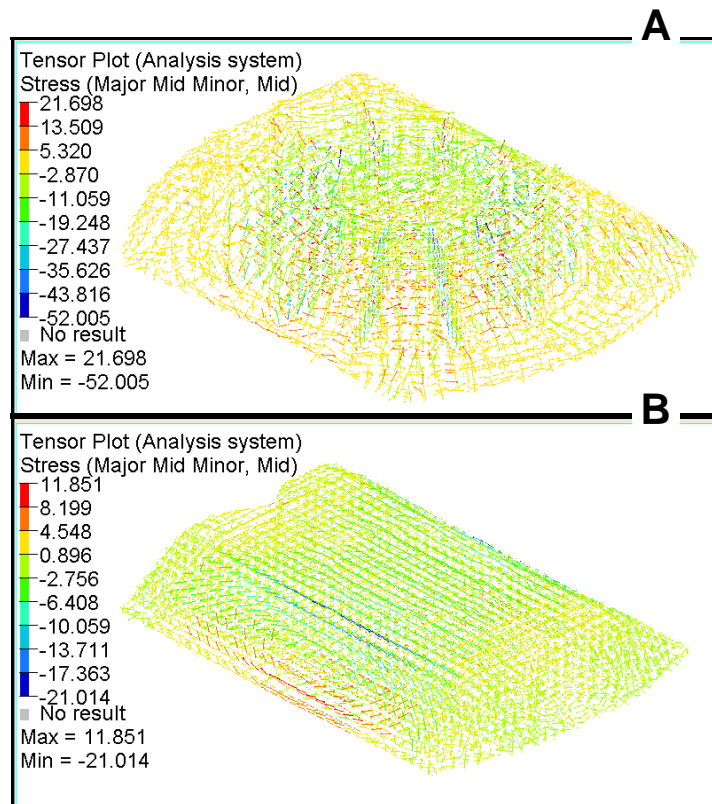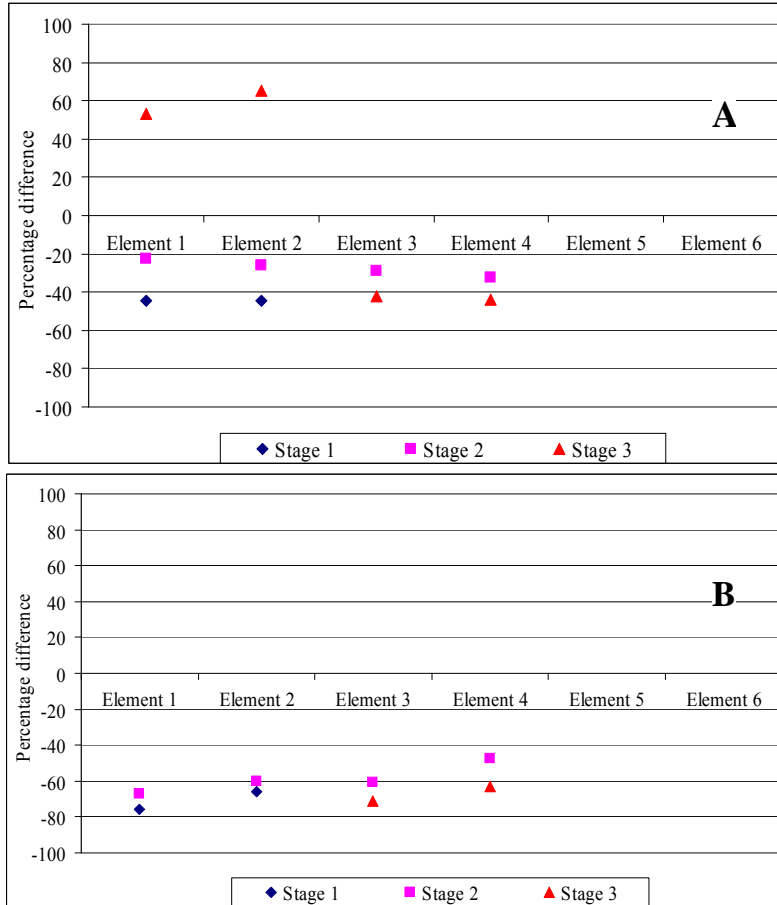
Figure 64. Percentage Differences between Maximum Von Mises Stresses from Three Stages of Base Tire-Marker Impact Simulation and Reversed ASTM Flexural Test Simulation in Finite Elements 1-6 (RRPM Types A and B).

Laboratory Tests Comparison

Previous analysis was used to compare the Von Mises stresses from different laboratory testing simulations with the three stages of tire-marker impact simulation, to compare the effectiveness of the six laboratory testing simulations. Appendix B provides comparisons of the six laboratory test simulation results. (The points in the plots are connected by dotted curves, which are not appropriate as the data are discrete and not continuous; however, this is done to better illustrate the comparisons.) The figures in Appendix B are another representation of the analysis that the researchers carried out earlier. However, comparing all the laboratory tests together makes it easy to visualize the bigger picture.

From Figure 119 and Figure 120 in Appendix B, it is clear that the ASTM compression test, the cylindrical compression test, and both the offset compression tests replicate stage 2 of the tire-marker impact well. This is because for these tests, the percentage differences in Von Mises stresses were lower in the chosen finite elements (except 5 and 6) of both RRPM types. The percent differences also did not vary much. The offset compression test simulates stage 1 of the tire-marker impact better than others do (see Figure 121 and Figure 122 in Appendix B). In the offset compression test, a higher loading rate makes a difference to the percentage differences. Figure 123 and Figure 124 in Appendix B show clearly that none of the laboratory test simulations simulate stage 3 of the tire-marker impact simulation since there is a great deal of variation among the elements for all the tests.

To better identify which laboratory test better simulated the tire-marker impact, the percentage differences for all the tests are compiled in one single table. Table 12 shows this compilation and contains percent differences in Von Mises stresses between the laboratory test simulations and the three stages of the tire-marker impact simulations for all the possible cases. The yellow-colored cells in the chart represent the percentage differences lying between 0 and +100. The peach-colored cells represent the percentage differences lying between –100 and 0. Table 12 also has the average of the percentage differences for every stage individually and across all the stages combined. The blue-colored cells in the Table represent the averages of percent differences between –50 and 50.

Each laboratory test was compared with every stage (1-3) of the tire-marker impact simulation. Stages 1, 2, and 3 of the tire-marker impact simulation were considered to be separate activities; therefore, laboratory tests that could simulate any of these stages were chosen. The researchers defined a few objective criteria to identify a good test:

1. The percentage differences across all the elements should be either positive or negative when comparing a laboratory test and any stage of the tire-marker impact simulation.

2. The percentage differences should lie within ±100 percent.

3. The average percentage differences for any stage of the laboratory test should be within ±50 percent.

Table 12. Percentage Differences in Von Mises Stresses from Laboratory Test Simulations and Tire-Marker Impact in Elements (E) 1-6 for All Possible Cases.

RRPM Type	Laboratory test	Stage 1						Stage 2						Stage 3						Average (stage 1)	Average (stage 2)	Average (stage 3)	Average (across three stages)
		E1	E2	E3	E4	E5	E6	E1	E2	E3	E4	E5	E6	E1	E2	E3	E4	E5	E6				
RRPM Type A	ASTM compression test	-61	-62	178	233	-64	77	-45	-49	-48	-53	-82	209	9	13	-57	-61	-57	132	50	-11	-4	12
	ASTM flexural test	-42	-45	279	394	476	731	-19	-27	-29	-31	184	1355	61	63	-42	-43	595	991	299	239	271	270
	Cylindrical compression test	-85	-86	-3	27	6	103	-79	-81	-82	-82	-48	255	-58	-58	-85	-85	28	166	-6	-19	-15	-14
	Offset compression test (lower loading rate)	-66	-66	-62	-50	-38	-100	-52	-55	-93	-93	-69	-100	-6	1	-94	-94	-25	-100	-64	-77	-53	-65
	Offset compression test (higher loading rate)	9	5	6	46	27	-100	52	40	-80	-80	-37	-100	201	212	-84	-83	54	-100	-1	-34	33	-1
	Reversed ASTM flexural test	-45	-44	277	383	476	731	-23	-26	-29	-33	184	1355	53	65	-42	-44	595	991	296	238	270	268
RRPM Type B	ASTM compression test	-82	-78	84	405	87	306	-76	-75	-70	-54	108	267	182	244	-78	-68	45	394	120	16	120	85
	ASTM flexural test	-3	3	830	1650	1068	2476	31	20	50	59	1198	2226	1452	1545	9	12	807	3035	1004	597	1143	915
	Cylindrical compression test	-75	-69	114	529	187	344	-66	-64	-66	-43	218	301	305	393	-75	-60	123	440	172	47	188	135
	Offset compression test (lower loading rate)	-64	-61	-87	-71	134	-100	-52	-55	-98	-97	160	-100	473	517	-98	-98	82	-100	-42	-40	129	16
	Offset compression test (higher loading rate)	-30	-25	-70	-48	362	-100	-6	-13	-95	-95	413	-100	1019	1093	-96	-97	259	-100	15	17	346	126
	Reversed ASTM flexural test	-75	-66	144	476	188	393	-67	-60	-61	-47	220	346	291	447	-71	-63	124	500	177	55	205	145

From Table 12, it is evident that the tests selected could not satisfy the above criteria. Hence, the researchers lowered the criteria from elements 1-6 to elements 1-4. This was done because the percentage differences for elements 5 and 6 were too high and, thus, unreasonable for some cases (as seen in Table 12). Table 13 shows the percentage differences and their averages without considering elements 5 and 6. After dropping elements 5 and 6 from the analysis, new results were analyzed to obtain a list of the tests that satisfied the criteria defined above. These results are given in Table 14.

Hence, the analysis was limited to the laboratory tests listed in Table 14. The findings as listed in Table 14 are to be validated with the qualitative analysis of principal stresses as completed for all the laboratory tests. It was mentioned that the offset compression test (both loading rates) simulated stage 1 of the tire-marker impact simulation only and the ASTM compression test simulated stage 2 of the tire-marker impact only. Since the ASTM flexural test produces major tensile stresses at the bottom center of the marker, it did not simulate any stage of the tire-marker impact. Similarly, since the reversed flexural test produced major tensile stresses at the top center of the marker, it did not simulate any stage of the tire-marker impact.

Considering both the qualitative and quantitative analyses that were carried out for comparing the six laboratory tests in their effectiveness to simulate the tire-marker impacts, it was found that the offset compression test (higher loading rate) is a good test for simulating stage 1 of the tire-marker impact. The researchers also found the ASTM compression test to be a good test for simulating stage 2 of the tire-marker impact. They did not find any test to replicate stage 3 of the tire-marker impact but hypothesized that a variation of the offset compression test, in which the loading bar is kept along the other retroreflective side's top edge of the marker, would replicate stage 3 of the tire-marker impact.

Table 13. Percentage Differences in Von Mises Stresses from Laboratory Test Simulations and Tire-Marker Impact in Elements 1-4 for All Possible Cases.

RRPM Type	Laboratory test	Stage 1				Stage 2				Stage 3				Average (stage 1)	Average (stage 2)	Average (stage 3)	Average (across three stages)
		E1	E2	E3	E4	E1	E2	E3	E4	E1	E2	E3	E4				
RRPM Type A	ASTM compression test	-61	-62	178	233	-45	-49	-48	-53	9	13	-57	-61	72	-49	-24	0
	ASTM flexural test	-42	-45	279	394	-19	-27	-29	-31	61	63	-42	-43	146	-26	10	43
	Cylindrical compression test	-85	-86	-3	27	-79	-81	-82	-82	-58	-58	-85	-85	-36	-81	-72	-63
	Offset compression test (lower)	-66	-66	-62	-50	-52	-55	-93	-93	-6	1	-94	-94	-61	-73	-48	-61
	Offset compression test (higher)	9	5	6	46	52	40	-80	-80	201	212	-84	-83	17	-17	62	20
	Reversed ASTM flexural test	-45	-44	277	383	-23	-26	-29	-33	53	65	-42	-44	143	-27	8	41
RRPM Type B	ASTM compression test	-82	-78	84	405	-76	-75	-70	-54	182	244	-78	-68	82	-69	70	28
	ASTM flexural test	-3	3	830	1650	31	20	50	59	1452	1545	9	12	620	40	755	472
	Cylindrical compression test	-75	-69	114	529	-66	-64	-66	-43	305	393	-75	-60	125	-60	141	69
	Offset compression test (lower)	-64	-61	-87	-71	-52	-55	-98	-97	473	517	-98	-98	-71	-75	198	17
	Offset compression test (higher)	-30	-25	-70	-48	-6	-13	-95	-95	1019	1093	-96	-97	-43	-52	480	128
	Reversed ASTM flexural test	-75	-66	144	476	-67	-60	-61	-47	291	447	-71	-63	120	-59	151	71

Table 14. Short Listed Laboratory Tests.

RRPM Type	Tire-Marker Impact Simulation		
	Stage 1	Stage 2	Stage 3
A	Offset compression test (higher loading rate)	ASTM compression test	Not applicable
		ASTM flexural test	
		Reversed ASTM flexural test	
B	Offset compression test (higher loading rate)	ASTM flexural test	Not applicable

It should be mentioned here that these results would be more applicable for the tire-marker impacts on the rigid (concrete) pavement than on the flexible (asphalt) pavement. The researchers would not draw conclusions for these laboratory tests, especially the existing ASTM compression and flexural tests, until further evaluation of laboratory tests against tire-marker impact simulation on both types of pavement is conducted. Next, the four laboratory tests were further evaluated. Two of the laboratory tests are the ASTM compression test and longitudinal flexural test, and the other two are the offset (compression) test and location offset test. The offset test has been proved to be a good laboratory test that simulates stages 1 and 3 of tire-marker impact on rigid pavement, while the location offset test was developed to account for the tire-marker impact with offset from the center of the marker, which has been demonstrated to have more impact on markers.

Further Evaluation

In further evaluation, the researchers exclusively concentrated on comparing the tensor plots of compressive and tensile stress inside the markers in the laboratory test simulation against the tire-marker impact simulation to see whether the simulated laboratory tests can generate stress in a pattern and magnitude similar to the simulated tire-marker impact. The stress tensor plots are believed to be more specific in describing the stress distribution and more precise in correlating to the tire-marker impact on both types of pavement. So, the criteria of selecting a qualified laboratory testing procedure rely on the capability of a test to produce the critical stress at the same place inside the markers and to produce a similar pattern of critical stress at an appropriate loading rate to approximate the magnitude of the critical stress (within 50 percent) generated from the designated tire-marker impact.

Specifically, different laboratory tests have different weights of importance in terms of compressive and tensile stress. Compressive stress should attract more attention in the ASTM compression test against the tire-marker impact simulation, while tensile stress should be a more critical measurement in the ASTM longitudinal flexural test. It was considered reasonable to weigh a measure of effectiveness over another according to the nature of a laboratory test, and no single test is expected to replicate the tire-marker impact completely based on the initial evaluation. Overall, compressive stress is an important measurement for tire-marker impact on

both types of pavement because it is predominant inside markers during the impact in terms of the magnitude, and tensile stress might be more critical to the impact on flexible pavement, as was demonstrated by the unique damage type, which was previously described and will be further elaborated upon in Chapter 5.

In addition, the tire-marker impact simulations that were compared with the laboratory test simulation consist of the external factors with specific values. Base values were used for the external factors that had been proved to be insignificant to the impact, while the largest values were used for the external factors that had been demonstrated to have effects on the impact. In this way, the laboratory tests can be examined to their limit for evaluating the field performance of RRPMs. Different loading rates were exercised in the laboratory tests to determine the one that generates the critical stress that has the closest magnitude (within the 50 percent range) in comparison to the tire-marker impact. The researchers endeavored to differentiate the loading rates for RRPMs to be installed on different types of pavement.

ASTM Compression Test

The ASTM compression test was simulated and evaluated quantitatively against stage 2 of the tire-marker impact simulation with tire loading of 31,100 N and tire speed of 31.3 m/s, and without contact angle and offset. The simulated setup of the test is shown in Figure 65.

Based on the tensor plots of compressive stress, the ASTM compression test is able to produce maximum compressive stress at the four corners of the upper surface of the marker, similar to the critical location of compressive stress generated by the tire-marker impact. As long as the magnitudes of compressive stress are close between the test and tire-marker impact, the ASTM compression test is good at testing the compressive stresses inside the markers during the tire-marker impact. The tensor plots of the stresses inside the markers for the test with a loading rate of 4.0 mm/minute (0.157 inch/minute) are shown in Figure 66 for Types A and B.
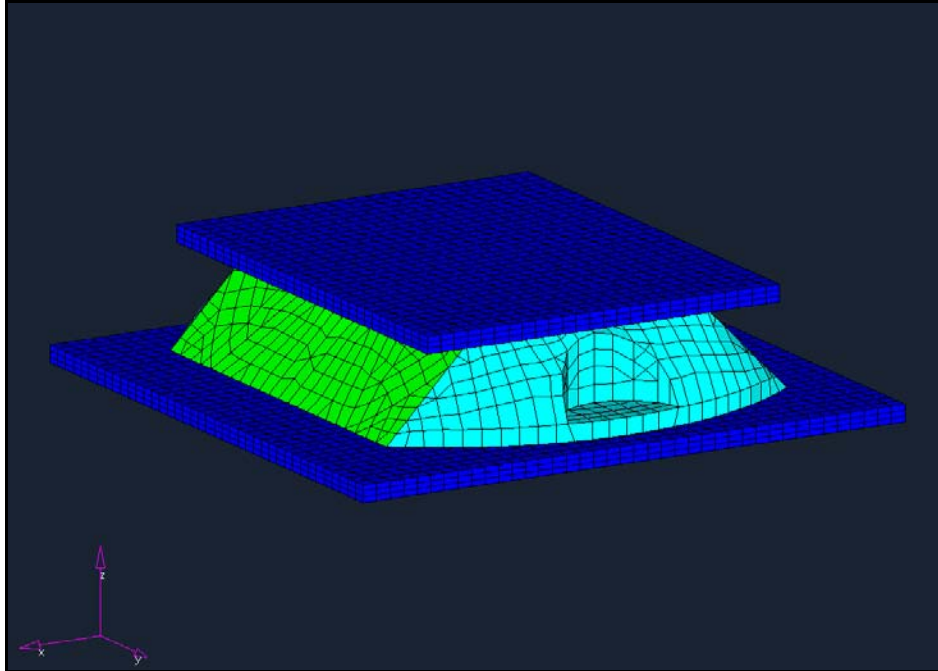
Figure 65. Simulated ASTM Compression Test.

Different loading rates were tried for the test. The magnitudes of the critical compressive and tensile stress in accordance with the loading rates of the test as well as those from the designated tire-marker impact simulation are presented in Table 15. Only compressive stress was evaluated to determine the appropriate loading rate. Based on the criteria of selecting a loading rate, the loading rates of 3.0 mm/minute (0.118 inch/minute) and 4.0 mm/minute (0.157 inch/minute) were selected for the ASTM compression test for RRPMs to be installed on flexible and rigid pavement, respectively.

Table 15. Evaluation of ASTM Compression Test in Different Loading Rates.

Laboratory Test		ASTM Compression Test				Tire-Marker Impact	
Loading Rate (mm/minute)		**2.5**	**3.0**	**4.0**	**5.0**	**Flexible**	**Rigid**
Compressive stress (MPa)	RRPM Type A	105.183	129.785	176.042	184.736	124.131	150.201
	RRPM Type B	55.258	57.749	63.632	64.936	56.954	63.558
Tensile stress (MPa)	RRPM Type A	25.88	30.811	37.39	45.738	32.598	25.141
	RRPM Type B	13.187	16.886	22.587	33.111	8.098	9.049
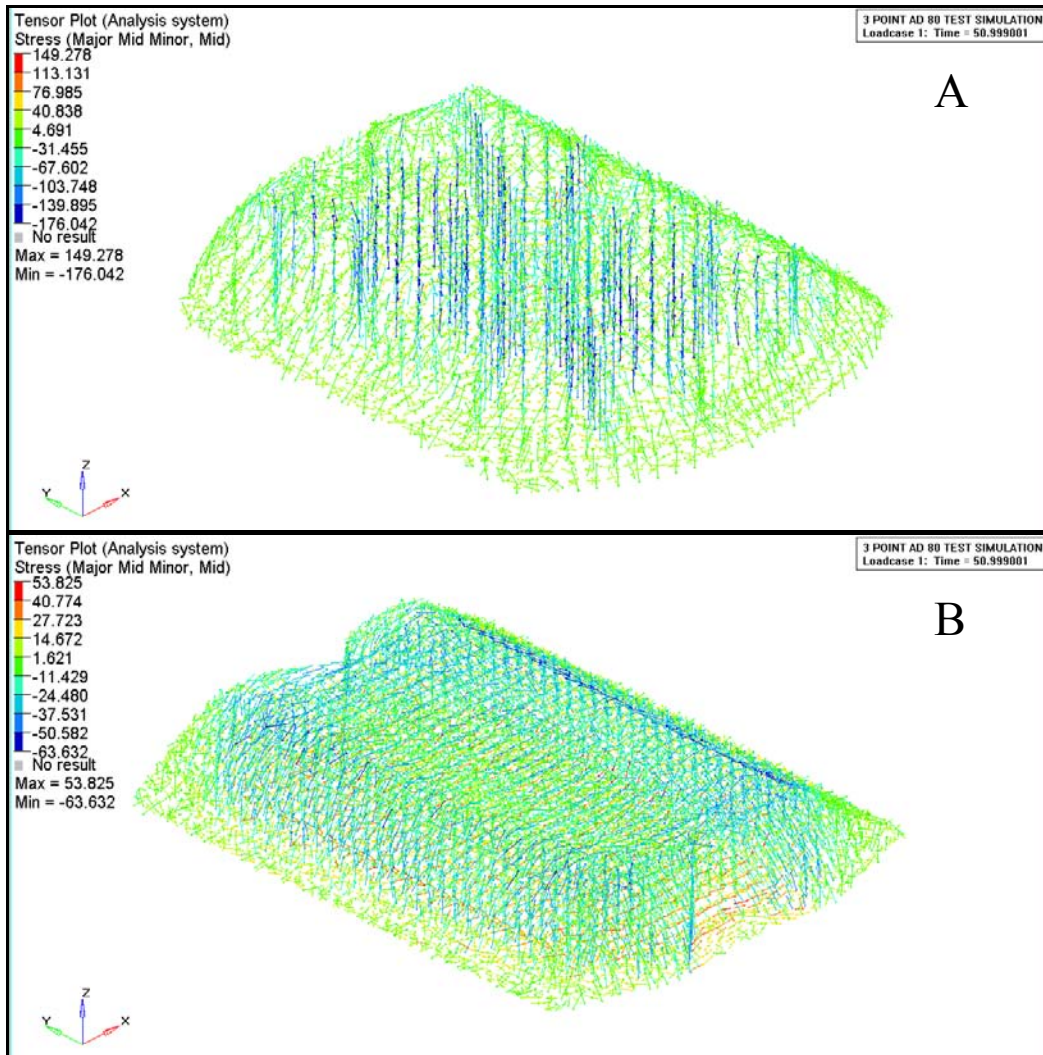
Figure 66. Stress Tensor Plots for RRPM Types A and B in ASTM Compression Test.

ASTM Longitudinal Flexural Test

The ASTM longitudinal flexural test was simulated and evaluated quantitatively against stage 2 or 3 of the tire-marker impact simulation with tire loading of 31,100 N and tire speed of 31.3 m/s, and without contact angle and offset. The simulated setup of the test is shown in Figure 67.
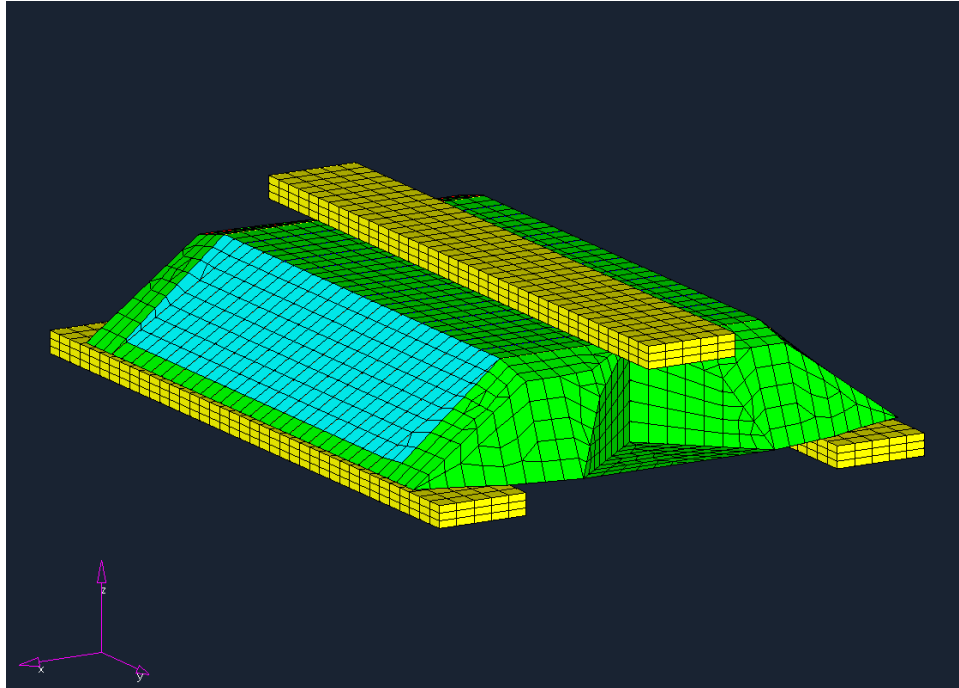
Figure 67. Simulated ASTM Longitudinal Flexural Test.

The test generates a similar pattern of tensile stress inside the markers compared to that produced during the entire process of the tire-marker impact on flexible pavement. A significant group of tensile stress is generated from the marker base approaching upward inside the marker, which is considered critical in this study. The side view of the stress tensor plots for Types A and B in the ASTM longitudinal flexural test with a loading rate of 2.5 mm/minute (0.098 inch/minute) is shown in Figure 68.

After executing different loading rates, a loading rate of 2.5 mm/minute (0.098 inch/minute) was selected for the ASTM longitudinal flexural test for RRPMs to be installed on both types of pavement since a loading rate of 5.0 mm/minute (0.197 inch/minute) might be too large for the RRPMs. The magnitudes of the critical tensile and compressive stress, the corresponding loading rates of the test, and the critical stress from the designated tire-marker impact simulation are presented in Table 16. Only tensile stress was evaluated to determine the suitable loading rate.

100
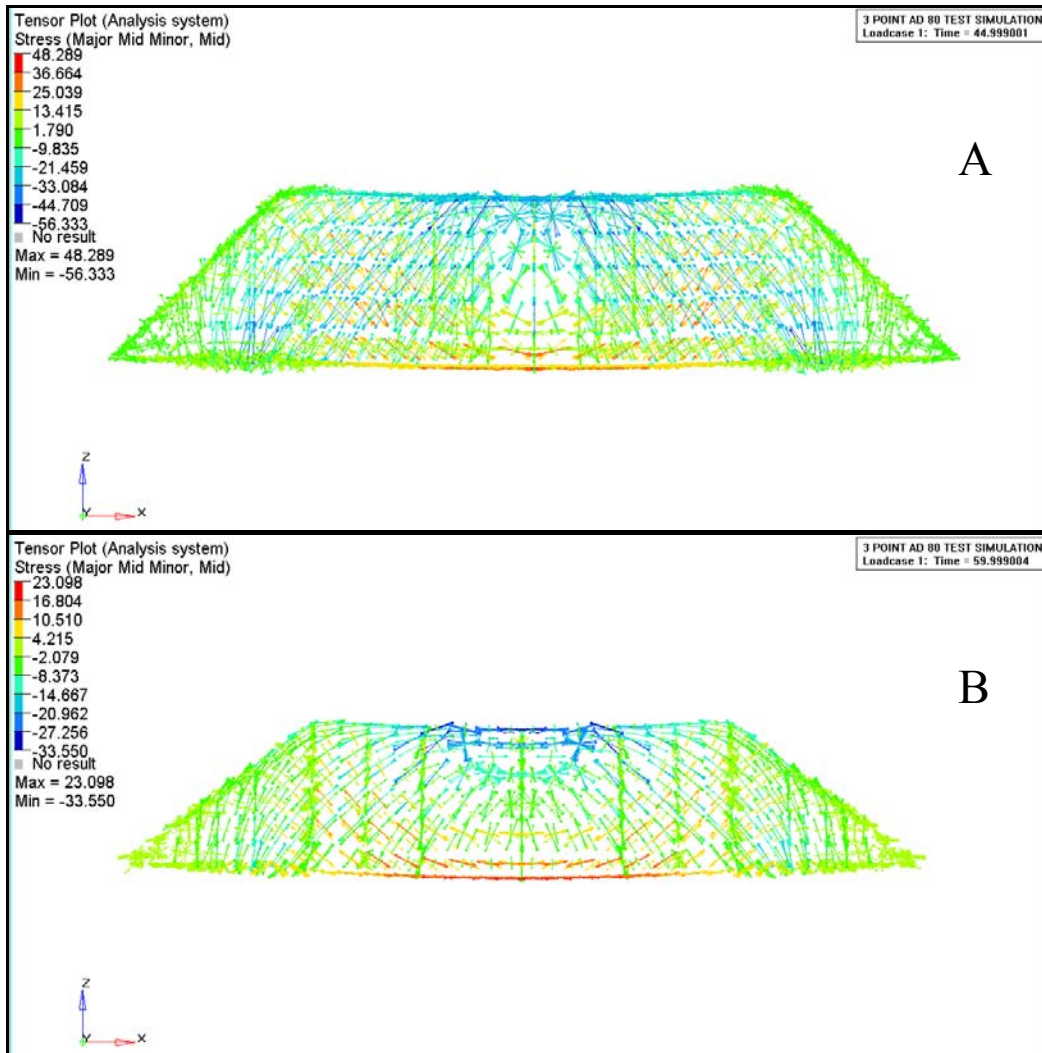
**Figure 68. Side View of Stress Tensor Plots for RRPM Types A and B
in ASTM Longitudinal Flexural Test.**

Table 16. Evaluation of ASTM Longitudinal Flexural Test in Different Loading Rates.

Laboratory Test		ASTM Longitudinal Flexural Test		Tire-Marker Impact	
Loading Rate (mm/minute)		2.5	5.0	Flexible	Rigid
Tensile stress (MPa)	RRPM Type A	36.664	87.441	32.598	25.141
	RRPM Type B	16.804	35.21	8.098	9.049
Compressive stress (MPa)	RRPM Type A	84.323	166.926	124.131	150.201
	RRPM Type B	33.55	55.088	56.954	63.558

Offset Test

The researchers re-evaluated the offset test against stage 1 or 3 of the tire-marker impact simulation with tire loading of 31,100 N and tire speed of 31.3 m/s, and without contact angle and offset. The simulated setup of the test is shown in Figure 69.
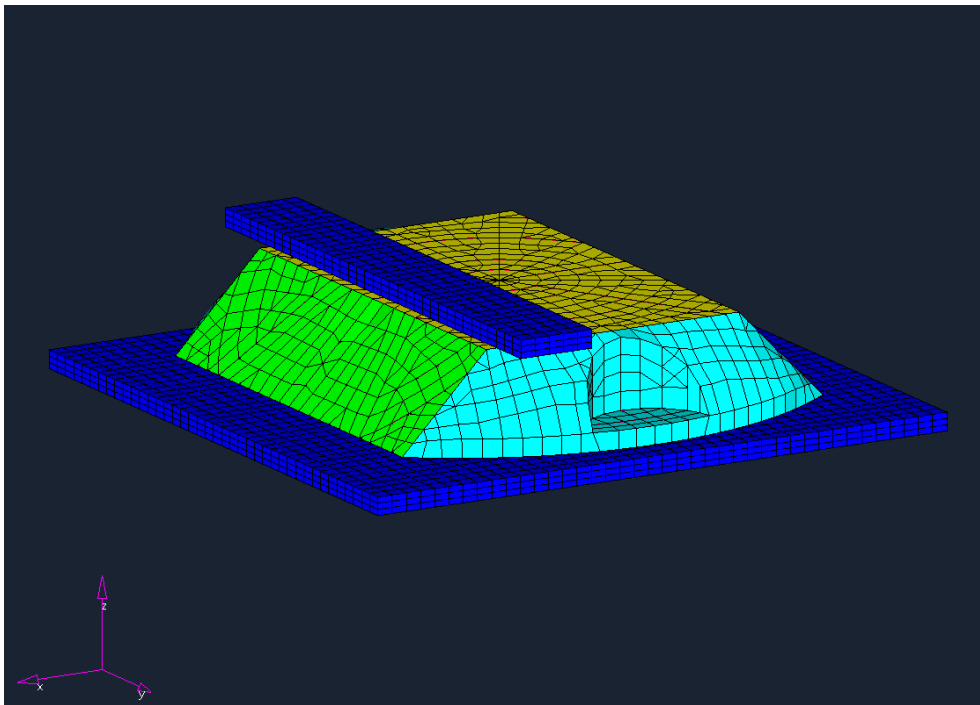
Figure 69. Simulated Offset Test.

Based on the tensor plots of compressive and tensile stresses inside the markers, the test is able to replicate stage 1 or 3 of tire-marker impact. Maximum compressive stress is generated at the two upper corners of the marker where the steel bar contacts the marker while a significant amount of tensile stress is produced in the rest of the marker. Figures 70 and 71 show an isolated and a side view of the tensor plots of the stresses inside marker Types A and B during the test at a loading rate of 4.0 mm/minute (0.157 inch/minute), respectively.
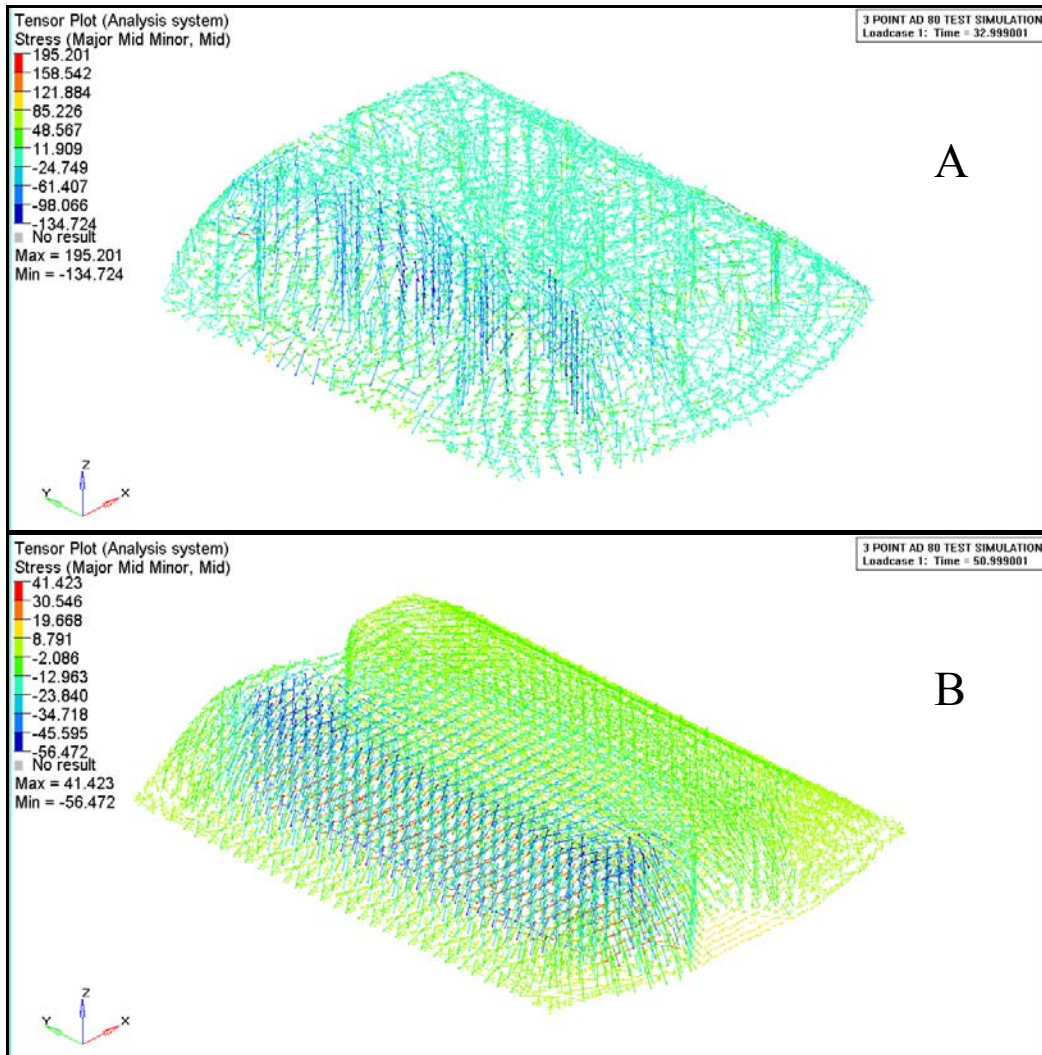
Figure 70. Stress Tensor Plots for RRPM Types A and B in Offset Test.

By varying the loading rate in the test, both the critical compressive stress and tensile stress were compared with those generated from the designated tire-marker impact. The comparison is shown in Table 17. Based on the evaluation criteria, a loading rate of 4.0 mm/minute (0.157 inch/minute) best satisfies the criteria for both compressive and tensile stress and thus is selected as the loading rate for the offset test for RRPMs to be installed on both types of pavement.
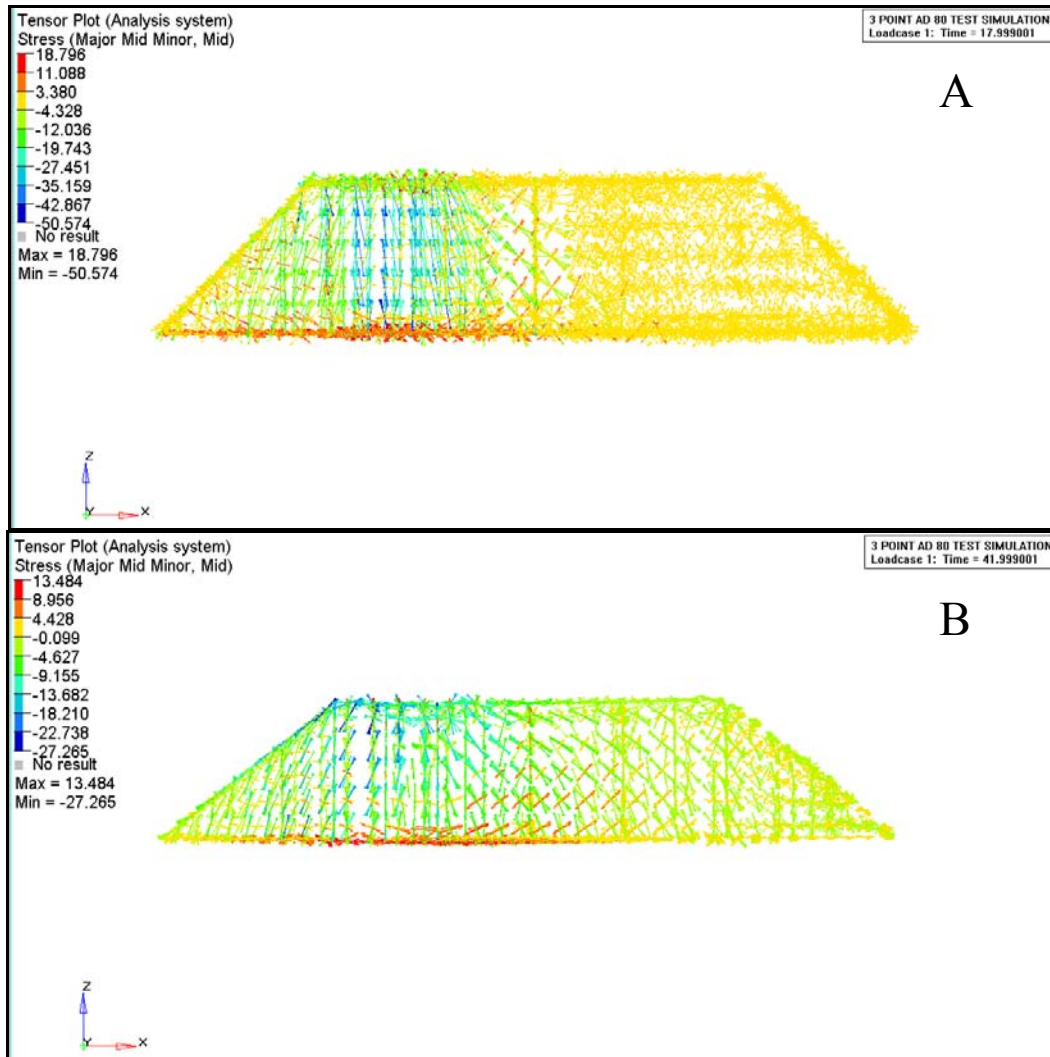
Figure 71. Side View of Stress Tensor Plots for RRPM Types A and B in Offset Test.

Table 17. Evaluation of Offset Test at Different Loading Rates.

Laboratory Test		Offset Test			Tire-Marker Impact	
Loading Rate (mm/minute)		**3.0**	**4.0**	**5.0**	**Flexible**	**Rigid**
Compressive stress (MPa)	RRPM Type A	65.082	134.724	146.935	111.878	131.998
	RRPM Type B	33.106	56.472	62.807	51.151	55.064
Tensile stress (MPa)	RRPM Type A	12.853	34.707	50.621	32.598	18.618
	RRPM Type B	10.788	17.563	22.204	7.454	7.247

Location Offset Test

The location offset test was designed to deal with the high compressive stress generated from the tire-marker impact scenario in which a tire hits the marker with offset rather than right in the middle. So, the test was evaluated against stage 2 of the tire-marker impact simulation with tire loading of 31,100 N, tire speed of 31.3 m/s, and contact offset of 51 mm (2 inch) and without contact angle. The simulated setup of the test is shown in Figure 72.
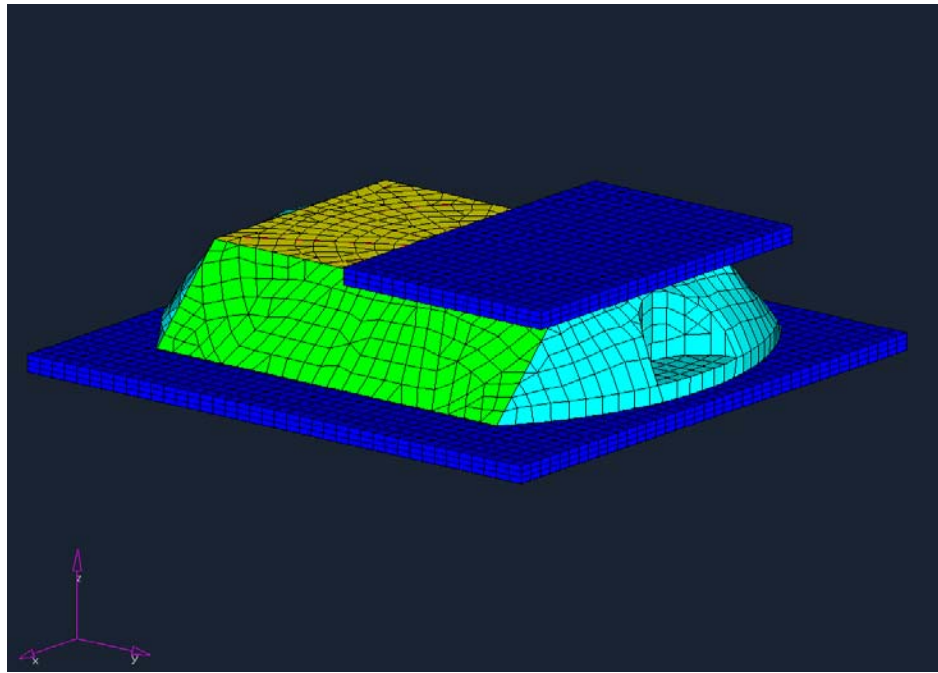
Figure 72. Simulated Location Offset Test.

The test produces critical compressive stress at the same two top edges of the marker where maximum compressive stress is produced as a tire sits on top of the marker with offset, indicating it is a potentially good test for the designed purpose. The tensor plots of stress inside the markers during the test at a loading rate of 4.0 mm/minute (0.157 inch/minute) are shown in Figure 73.
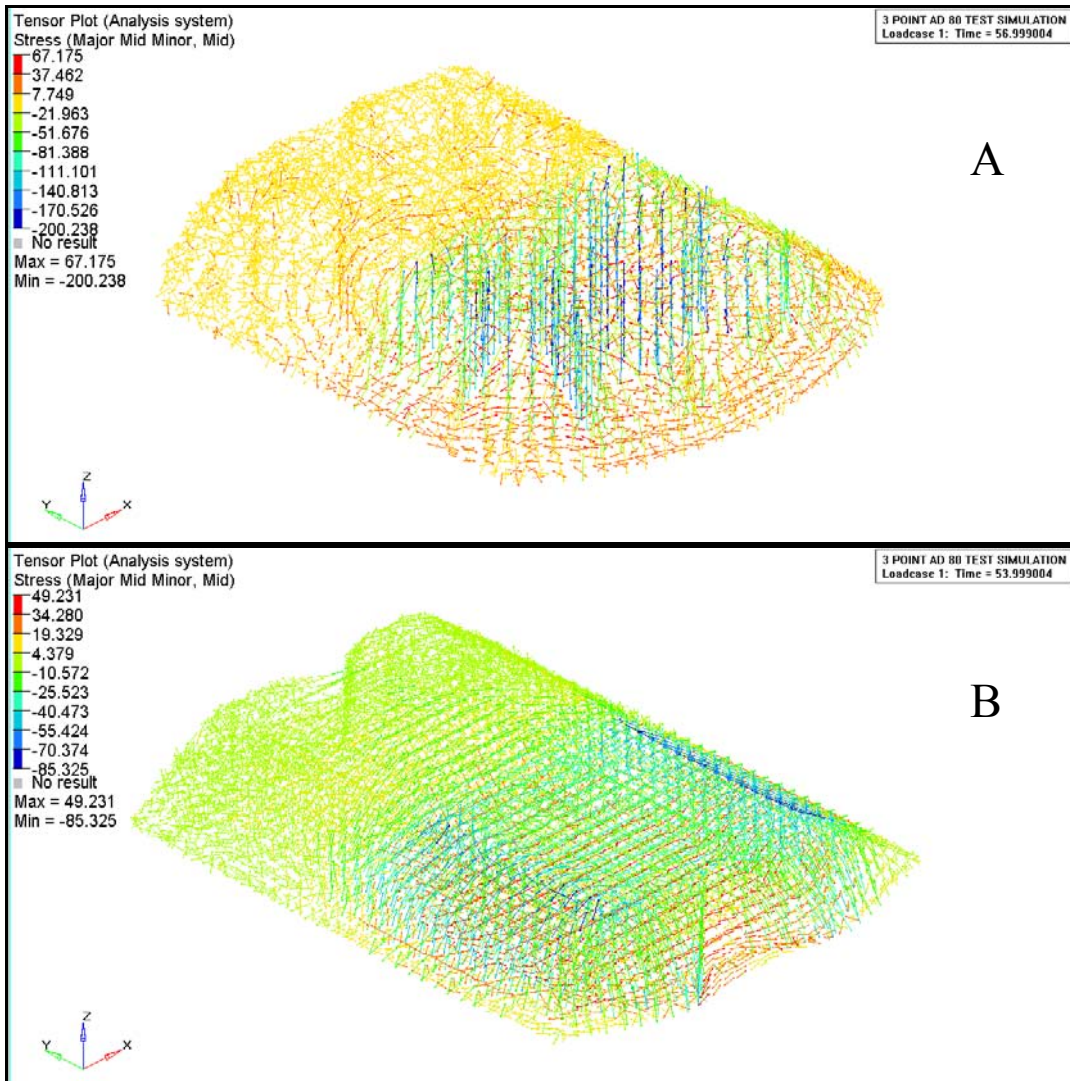
Figure 73. Stress Tensor Plots for RRPM Types A and B in Location Offset Test.

The magnitudes of the critical compressive and tensile stress commensurate with the loading rates of the test as well as those from the designated tire-marker impact simulation are presented in Table 18. Only compressive stress was evaluated to determine the appropriate loading rate. The results demonstrate that the loading rates of 4.0 (0.157 inch/minute) and 5.0 mm/minute (0.197 inch/minute) should be used in the location offset test to examine the performance of RRPMs on flexible and rigid pavement, respectively.

Table 18. Evaluation of Location Offset Test in Different Loading Rates.

Laboratory Test		Location Offset Test			Tire-Marker Impact	
Loading Rate (mm/minute)		3.0	4.0	5.0	Flexible	Rigid
Compressive stress (MPa)	RRPM Type A	117.917	200.238	223.765	186.384	222.884
	RRPM Type B	68.302	85.325	88.149	75.82	86.464
Tensile stress (MPa)	RRPM Type A	29.104	37.462	40.562	33.959	26.249
	RRPM Type B	15.277	23.858	28.677	10.262	10.595

Laboratory Test Summary

Based on the evaluation of the four laboratory tests, the researchers believe that each of them is capable of replicating the tire-marker impact in certain perspectives, but none of them is able to replicate the tire-marker impact comprehensively. Therefore, these tests should be used together to test the performance of RRPMs in the field. Specifically, the ASTM compression test is good at replicating stage 2 of the tire-marker impact in terms of compressive stress. The ASTM longitudinal flexural test is capable of replicating all three stages of the impact in terms of tensile stress. The offset test is able to replicate the distribution of both compressive and tensile stress inside the markers at stages 1 and 3 of the impact. The location offset test replicates the critical compressive stress produced at stage 2 of the impact with contact offset. On the other hand, the ASTM compression test, offset test, and location offset test are suitable for RRPMs on both types of pavement, while the ASTM longitudinal flexural test is more appropriate for RRPMs on flexible pavement than on rigid pavement because it generates tensile stress in the pattern that is more like what is produced inside the markers during the impact on flexible pavement. Furthermore, the loading rates for some laboratory tests can be differentiated for RRPMs on rigid and flexible pavement. The summary of these laboratory tests is shown in Table 19.

Table 19. Laboratory Test Summary.

Laboratory Tests		Tire-Marker Impact					
		Stage 1		Stage 2		Stage 3	
		Rigid	Flexible	Rigid	Flexible	Rigid	Flexible
Loading rates (mm/minute)	ASTM compression	N/A	N/A	4.0	3.0	N/A	N/A
	ASTM flexural	2.5	2.5	2.5	2.5	2.5	2.5
	Offset	4.0	4.0	N/A	N/A	4.0	4.0
	Location offset	N/A	N/A	5.0	4.0	N/A	N/A

CHAPTER 5. FIELD STUDY OF RRPMs

This chapter describes the field tests of RRPMs. The field study lasted 24 months, beginning in August 2005, and RRPM performance was evaluated every six months after the installment of RRPMs at the designated test decks. Generally, the field evaluation consists of retroreflectivity collection and visual observations. Visual observations of the markers are made regarding the marker case, lens surface, and lens interior, and marker conditions are rated in a scheme similar to the National Transportation Product Evaluation Program (NTPEP) *(21)*.

TEST DECK SETUP

The test decks were geographically selected at four sites all located in Texas: I-610 in Houston, I-35 in rural Laredo, FM 1179 in Bryan, and FM 230 in Lufkin. Figure 74 shows the geographical locations of the test decks. The test decks are surfaced with different types of pavement, i.e., concrete, asphalt, and seal coat. The test decks were set up on roadway facilities from interstate highways, to urban freeways, to rural highways.
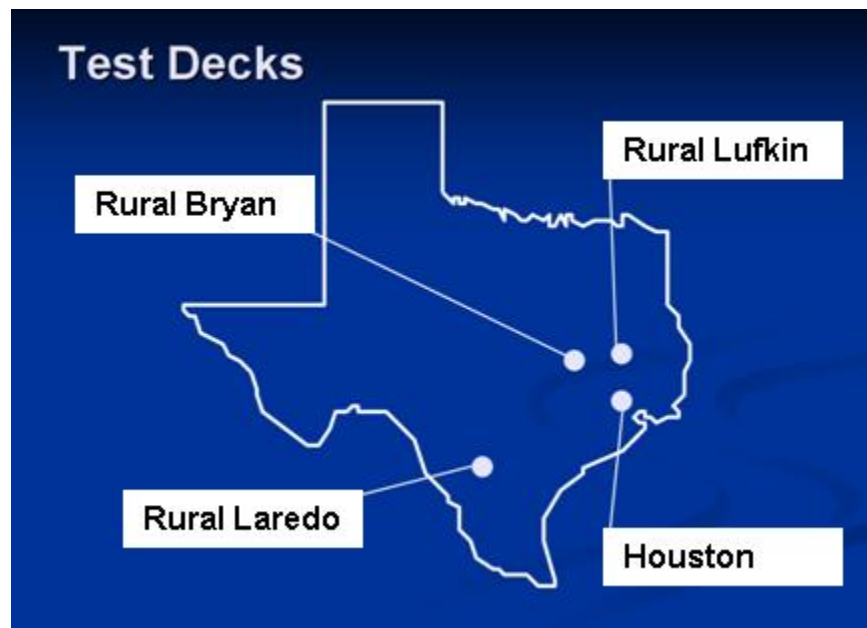
Figure 74. Locations of Test Decks.

Specific site characteristics for each deck are summarized as follows:

- The test deck on I-610 in Houston is an urban freeway segment serving a large traffic volume, with AADT between 200,000 to 250,000 vehicles per day. The pavement surface type is concrete.

- The test deck on I-35 in Rural Laredo is a segment of interstate highway with a high percentage of truck traffic (greater than 50 percent). The site happens to have a 1-mile concrete segment that provided an opportunity to compare RRPM performance with that of an asphalt surface under identical traffic and environmental conditions.

- The test deck on FM 1179 in Bryan is part of a rural highway on which a mid-volume traffic is usually served; it is a two-lane section with adequate shoulder width. Markers are placed in a two-way no passing zone. The pavement surface is seal coat.

- The test deck on FM 230 in Lufkin is a segment of rural highway that has the least traffic volume among the four decks. However, the location has a significant amount of logging truck traffic. The lane and shoulder are narrow, so conceivably the hits by logging trucks are significant, which is perceived as a potential cause for marker loss.

The specific site characteristics of the test decks are shown in Table 20.

Table 20. Site Characteristics of Test Decks.

Test Deck Site	Site Characteristics
I-610, Houston	6 lanes, concrete, high volume, innovative adhesive
I-35, rural Laredo	4 lanes, asphalt and concrete, high proportion trucks (> 50%)
FM 1179, rural Bryan	2 lanes, surface treatment, no shoulders, mid-volume, seal coat pavement
FM 230, rural Lufkin	2 lanes, surface treatment, narrow lanes (logging trucks), low volume, seal coat

Six models of RRPMs were installed at each test deck and they are listed in Table 21. Basically, the markers were installed in such a configuration that there were 12 marker groups at each test deck and 16 markers per group. Since six models of markers were selected, there were two groups of markers per model. The layout of markers at each test deck is illustrated in Figure 75. In addition, an extra two groups of markers, C80 and C88, were installed with a special adhesive at the test decks in Houston and Rural Laredo. The RRPMs installed at the test decks on

the interstate highways and urban freeways are in white with a white lens, while on rural highways they are in yellow with a yellow lens.

Table 21. RRPM Models Installed at the Test Decks.

Manufacturer	Manufacturer's Model No.
APEX Universal, Inc.	921 AR
APEX Universal, Inc.	9003
Avery Dennison (AD)	C80
Avery Dennison	C88
Ray-O-Lite (RO)	ARC II 9700
3M	290

Figure 75. Test Deck RRPM Layout.

The selection of the six RRPM models was made after discussions with TxDOT staff. They include models such as Avery Dennison C88 and 3M 290 that are extensively used throughout the state. The Ray-O-Lite ARC II model is included since it has historically performed well under high traffic demand conditions. It is also a more expensive type of marker, so its inclusion can shed some light on whether more expensive markers will have better performance. Avery Dennison C80 was a new model at the time of the project inception and was not on the state's prequalified product list (QPL). The Apex 921 AR is a product that had prior performance issues and had been removed from the QPL. The APEX 9003 is a new product that the manufacturer wished to be added to the QPL.

111

The RRPMs were initially installed at all four test decks in August 2005. The field evaluation started six months after the installation and has been conducted every six months until reaching the two-year mark. Initially, the markers were brand new and their retroreflectivity had been measured before they were installed in the field. The researchers observed the marker conditions and measured their retroreflectivity during each field evaluation. They used a 1200RPM retrometer from Gamma Scientific to collect the lens retroreflectivity of each marker and rated the conditions of those markers based on visual observation. In addition, the team also took pictures of the markers that had typical damages during each visit. Different problems relative to retroreflectivity, marker retention, and structural durability were revealed at different test decks.

TEST DECK RESULTS

Next, the results of the field study of RRPMs were demonstrated. The results consist of a summary of retroreflectivity measures, marker ratings, and types of marker damage at each test deck. The retroreflectivity measures and marker ratings for each marker brand were averaged, and the trend of deterioration was plotted over the two-year period. RRPM performance at different test decks was also compared to investigate how it relates to roadway characteristics and pavement surface. The detailed data for retroreflectivity and RRPM ratings are provided in Appendix C in Table 27 through Table 35.

Laredo

The rural Laredo test deck actually has two sections. One is an asphalt surface, and the other is a concrete surface. Consequently, the results for these two sections are presented separately.

Asphalt Surface

The average retroreflectivity measures and marker ratings for markers on asphalt pavement at the rural Laredo deck are summarized in Figure 76 and Figure 77. The rating values in Figure 77 are averages from the marker case, lens interior, and lens surface. It is evident that RRPM retroreflectivity underwent the most significant plunge in the first six months after the

installation, and the rate of drop gradually declined. Not much change occurred between the 18-month and two-year marks. The ratings of marker condition show more randomness, but the overall condition of all the markers deteriorated during the two-year evaluation.
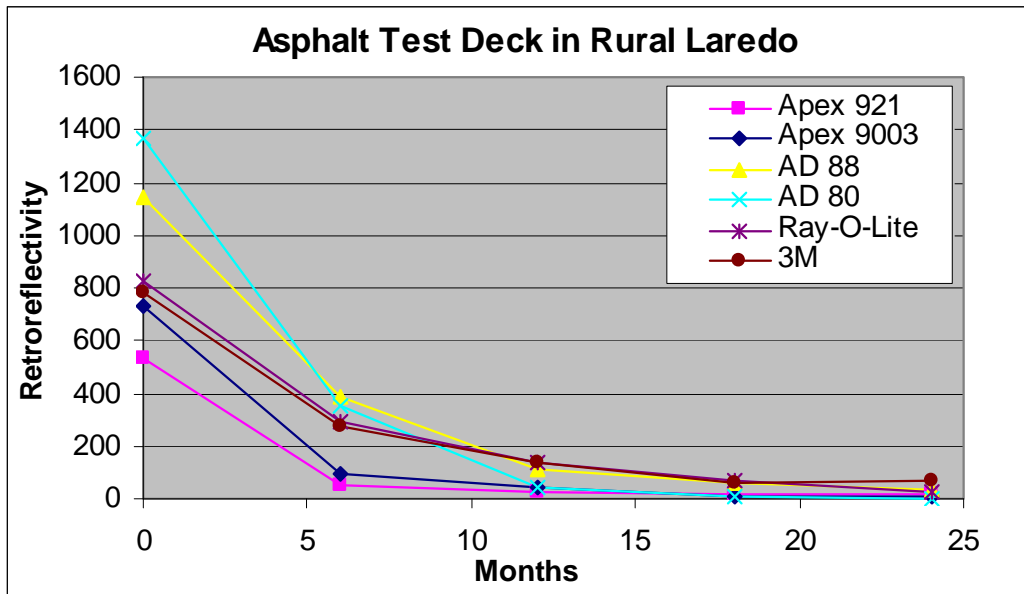
Figure 76. RRPM Retroreflectivity at Asphalt Test Deck in Rural Laredo.
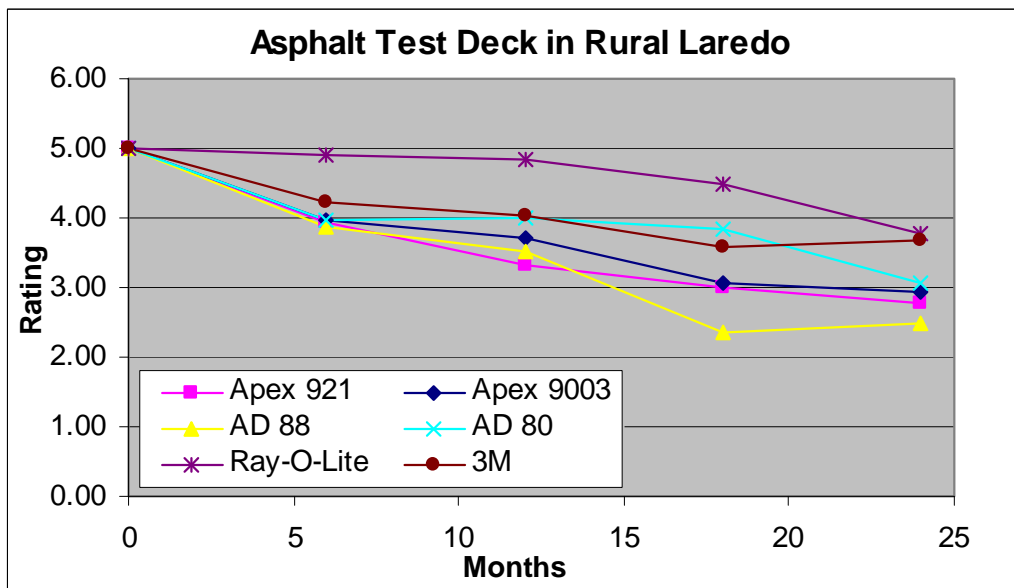
Figure 77. RRPM Rating at Asphalt Test Deck in Rural Laredo.

The primary types of marker damage observed on asphalt pavement at the deck are fracture from the mid-bottom of the markers, cracks on the top edges and non-lens side of the markers, and damage to the interior lens. Figure 78 shows the markers that have these typical damages.

Figure 78. Typical RRPM Damage on Asphalt Pavement in Rural Laredo.

Figure 78. Typical RRPM Damage on Asphalt Pavement in Rural Laredo (Continued).

Concrete Surface

The average retroreflectivity measures and marker ratings for RRPMs installed on the roadway segment with a concrete surface at the rural Laredo deck are summarized in Figure 79 and Figure 80. The rating values in Figure 80 are averages from the marker case, lens interior, and lens surface. Similar deterioration trends of marker retroreflectivity and overall condition are demonstrated compared to those for markers on concrete pavement.
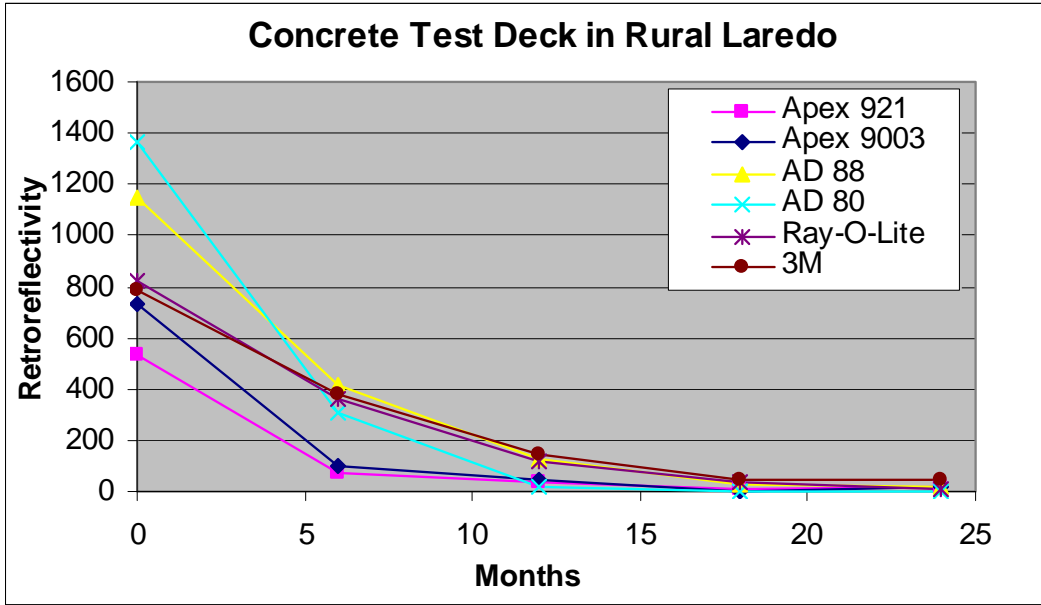
Figure 79. RRPM Retroreflectivity at Concrete Test Deck in Rural Laredo.
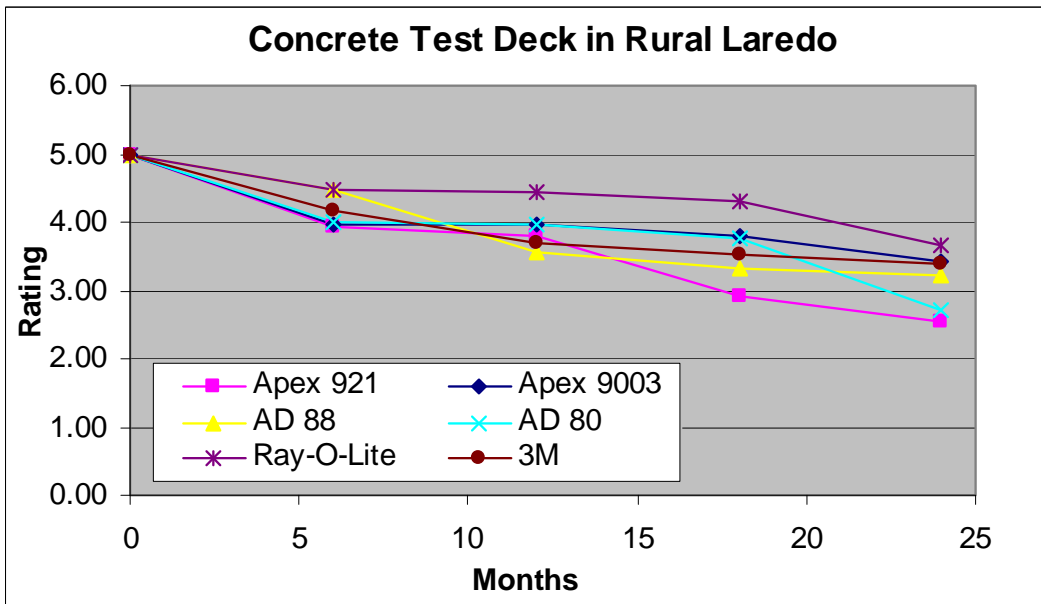
Figure 80. RRPM Rating at Concrete Test Deck in Rural Laredo.

In addition to the types of damages that occurred to the RRPMs observed on asphalt pavement, i.e., cracks on top edges and interior lens damage, a crack at the non-lens side proved to be a significant type of damage on a concrete surface; the finite element analysis demonstrated that tire contact with an offset to the center of the marker could produce more stress inside the

116

marker, especially at the top edge and non-lens side of the marker. However, on concrete pavement a few of the RRPMs had fractures from the mid-bottom of the markers which is a prevailing type of structural damage to several brands of markers on asphalt pavement at the deck. Figure 81 shows the representative structural failures for markers on concrete pavement in rural Laredo two years after installation.

Figure 81. Typical RRPM Damage on Concrete Pavement in Rural Laredo.
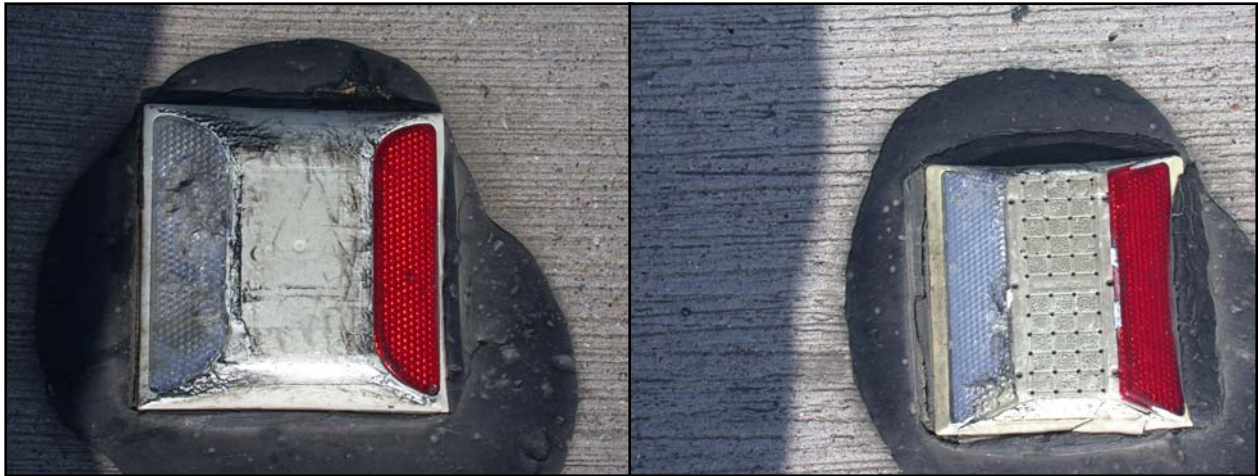
Figure 81. Typical RRPM Damage on Concrete Pavement in Rural Laredo (Continued).

Another issue is that a few of the markers were removed by traffic on asphalt pavement while many more were lost on the concrete pavement deck, but the number lost on the concrete surface deck in Laredo was much less than that at the Houston deck, which will be discussed next. The researchers believe that markers are more vulnerable to traffic with respect to their retention on concrete pavement than on asphalt pavement since the previous finite element analysis indicated that markers on concrete pavement receive a larger magnitude of shear interface force between marker base and pavement surface compared to those on asphalt pavement.

Houston

The Houston test deck is located on I-610, which has multiple lanes and serves a huge volume of traffic every day. This deck underwent the most significant problem of marker loss compared to other decks. The field evaluation was halted at the one-year mark; few markers remained on the road when the 18-month evaluation was planned. In addition, two brands of markers were replaced by the city within six months after installation, so only four brands of markers were evaluated at this deck. The average retroreflectivity measures and marker ratings for RRPMs at the Houston deck are available for 12 months and are summarized in Figure 82 and Figure 83. The rating values in Figure 83 are averages from the marker case, lens interior, and lens surface.
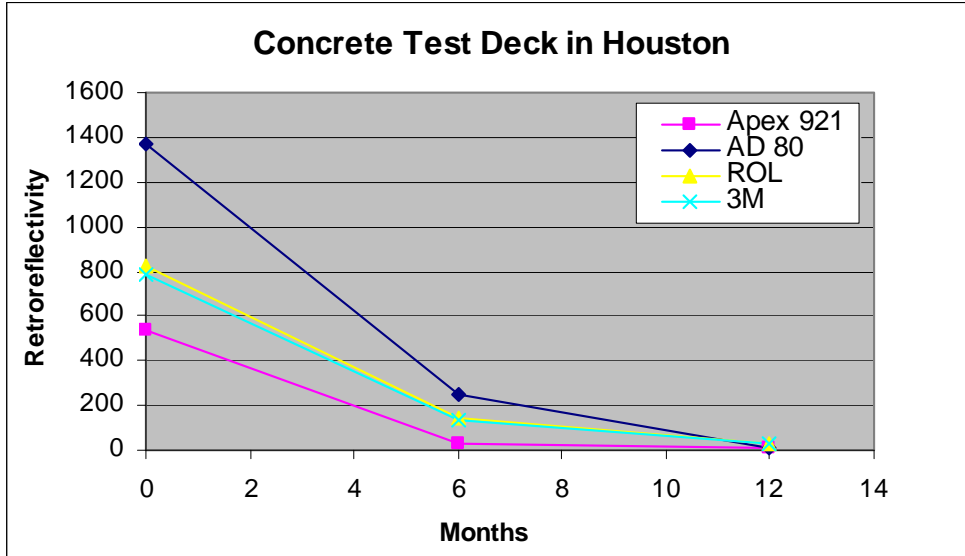
Figure 82. RRPM Retroreflectivity at Concrete Test Deck in Houston.
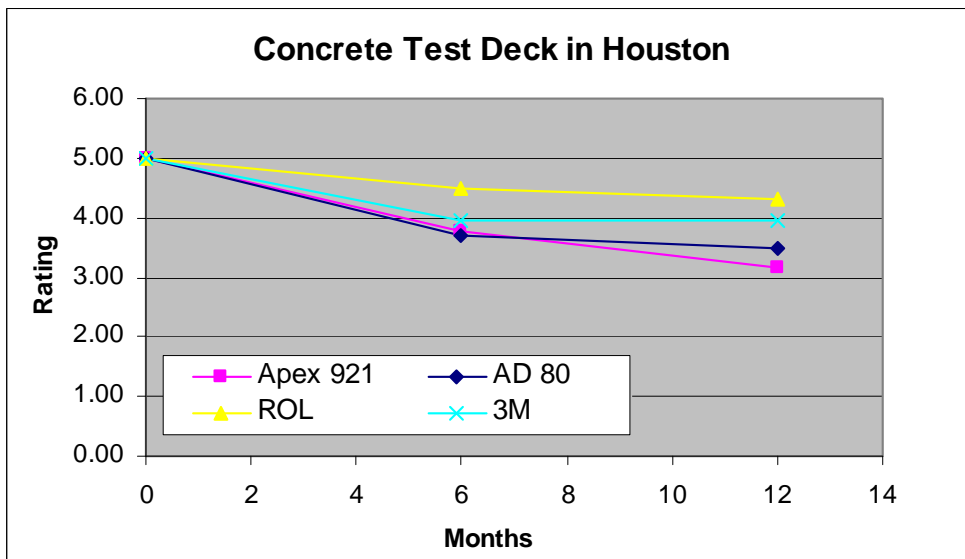
Figure 83. RRPM Rating at Concrete Test Deck in Houston.

The prevailing type of damage to the markers at this deck appears to be cracks at the top edges and corners of the markers. In addition, some markers had holes in the close-to-lens side of the top surface; some markers' top surfaces were sheared off, similar to some markers on the concrete pavement at the Laredo deck and others were split in half. Figure 84 shows these types of damages at the Houston deck.

Figure 84. Typical RRPM Damage on Concrete Pavement in Houston.

Lufkin

Rural Lufkin has the least traffic volume among the four test decks. The average retroreflectivity and marker ratings for a 24-month period are summarized in Figure 85 and Figure 86.
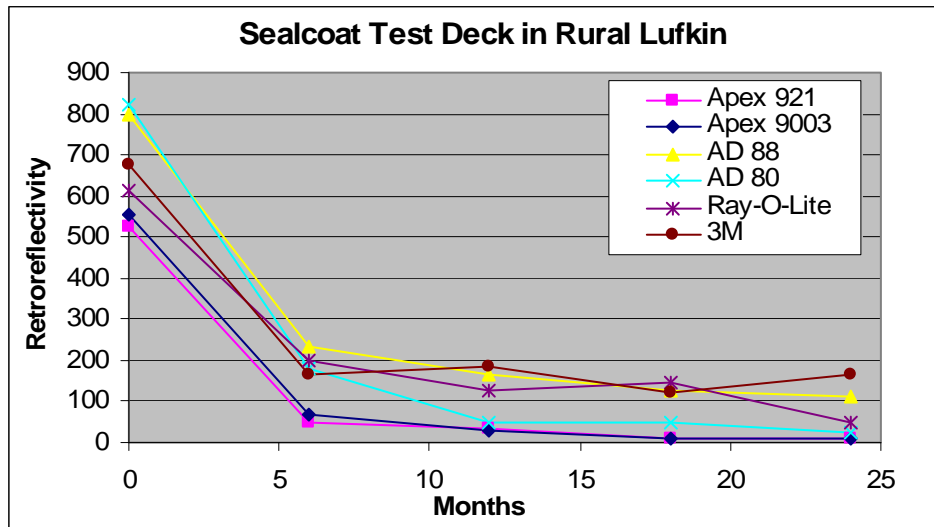
Figure 85. RRPM Retroreflectivity at Seal Coat Test Deck in Lufkin.
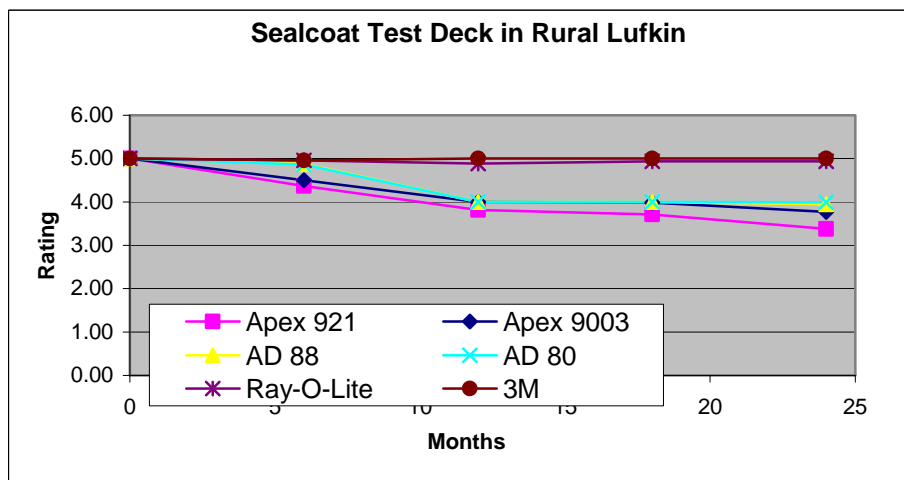
Figure 86. RRPM Rating at Seal Coat Test Deck in Lufkin.

The major marker damage observed at this deck includes cracks at the top edges of the markers, fracture at the mid-bottom of the markers, markers sinking into the pavement, damage

to the interior lens, and shear-off to the marker body. Figure 87 shows these types of damages to markers at the Lufkin deck.

Figure 87. Typical RRPM Damage on Seal Coat Pavement in Lufkin.

Figure 87. Typical RRPM Damage on Seal Coat Pavement in Lufkin (Continued).

Bryan

The deterioration trends of the marker retroreflectivity and ratings at the Bryan deck are shown in Figure 88 and Figure 89.
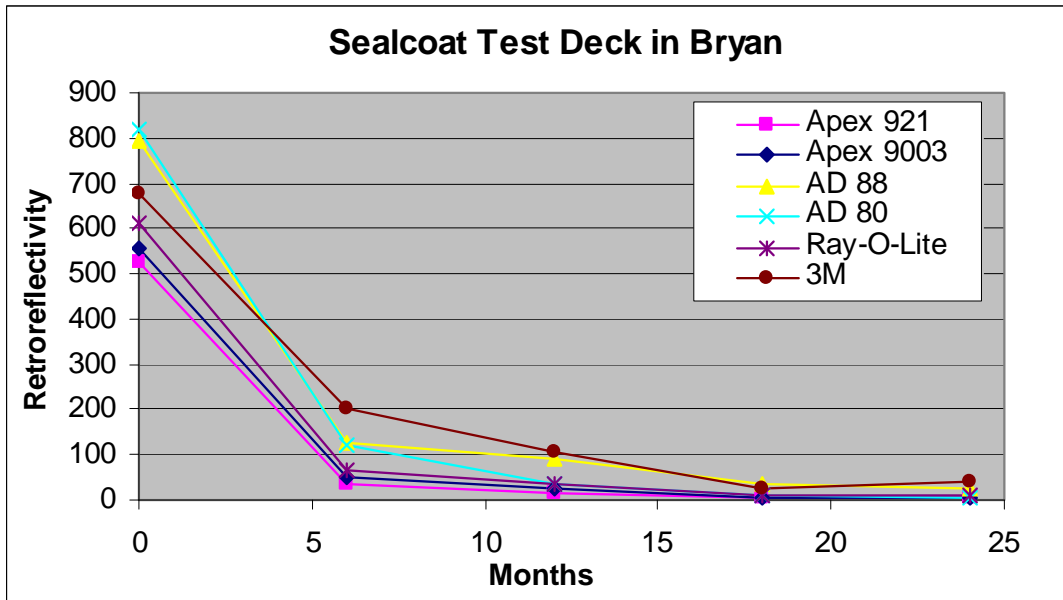
Figure 88. RRPM Retroreflectivity at Seal Coat Test Deck in Bryan.
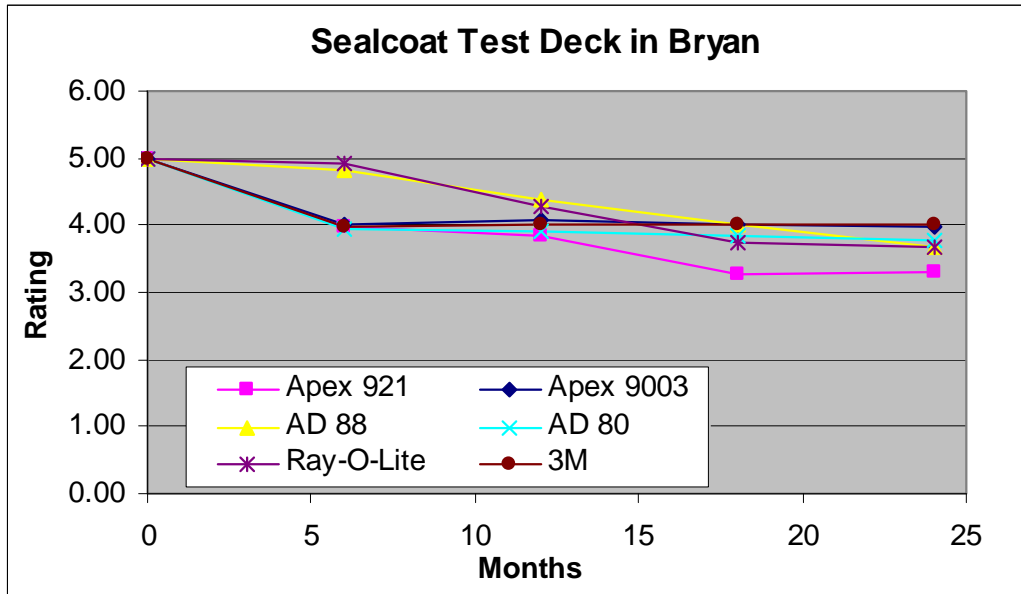
Figure 89. RRPM Rating at Seal Coat Test Deck in Bryan.

RRPMs at this deck primarily have such types of damage as cracks at the top edges and upper lens, shear-off of the marker's top surface, slight fracture from the mid-bottom of the markers, markers sinking into the pavement, loss of marker lens, and damage to the interior lens. Figure 90 shows typical damage on the Bryan deck.

Test Deck Marker Performance Comparison

Test decks with different ADT, surface types, and roadway types were selected for the purpose of comparing marker performance under different external conditions. This section gives insight into the effects of external factors on RRPM performance, both in retroreflectivity and physical conditions over time.

Figure 91 and Figure 92 show retroreflectivity and rating change over time for 3M and Ray-O-Lite on the Laredo deck, which has both a concrete and asphalt surface. It appears that for the first year after installation, there was no consistency as to whether either marker performed better on concrete or asphalt. However, in the second year, the retroreflectivity values as well as rating values were lower for the concrete surface for both marker models.

Figure 90. Typical RRPM Damage on Seal Coat Pavement in Bryan.
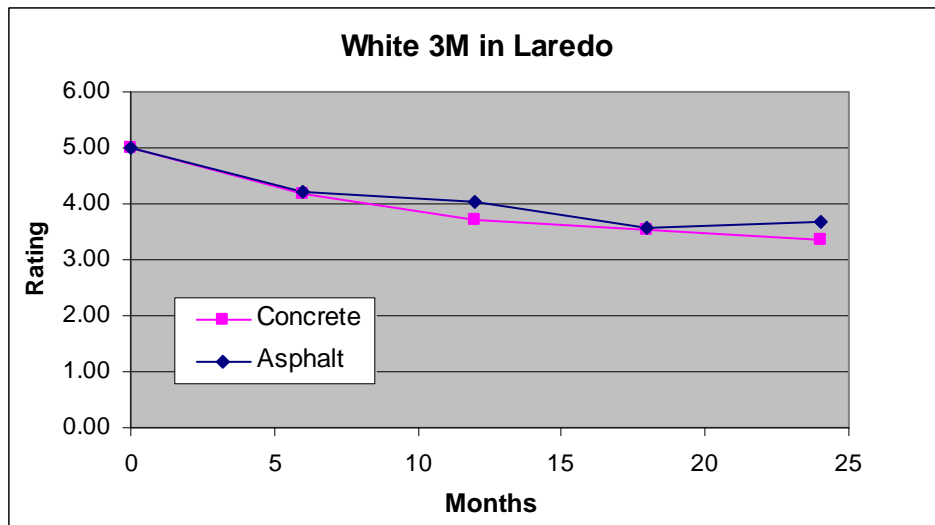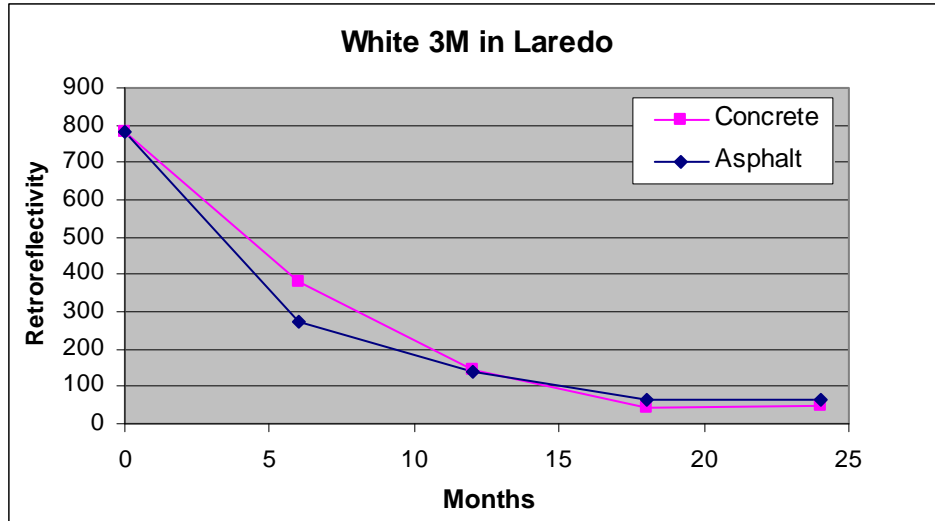
Figure 91. Performance of 3M Marker on Laredo Deck.
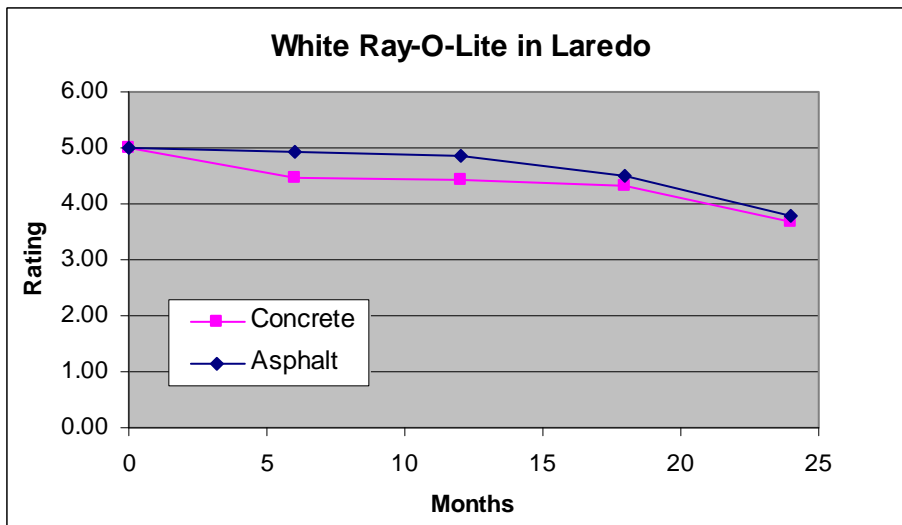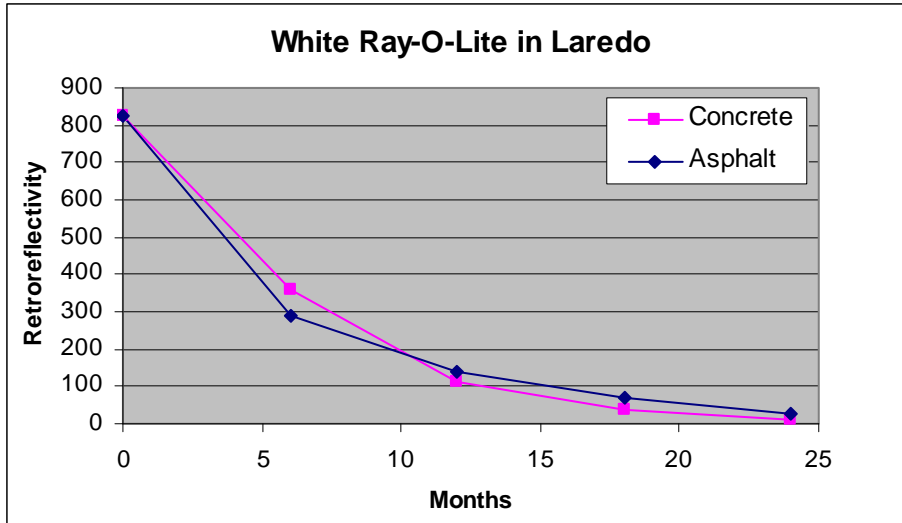
Figure 92. Performance of Ray-O-Lite Marker on Laredo Deck.

Figure 93 and Figure 94 compare retroreflectivity and physical rating on a concrete surface for 3M and Ray-O-Lite between the Houston and Laredo decks. The Houston deck has a much higher ADT, while the Laredo deck has a much higher truck percentage. This comparison is only for the first 12 months because the Houston deck only had one year of data. It can be clearly seen that the retroreflectivity values are much lower on the Houston deck for both marker models, indicating more ADT leads to faster degrading of retroreflectivity. There was no apparent difference in rating between the two locations for either marker model.
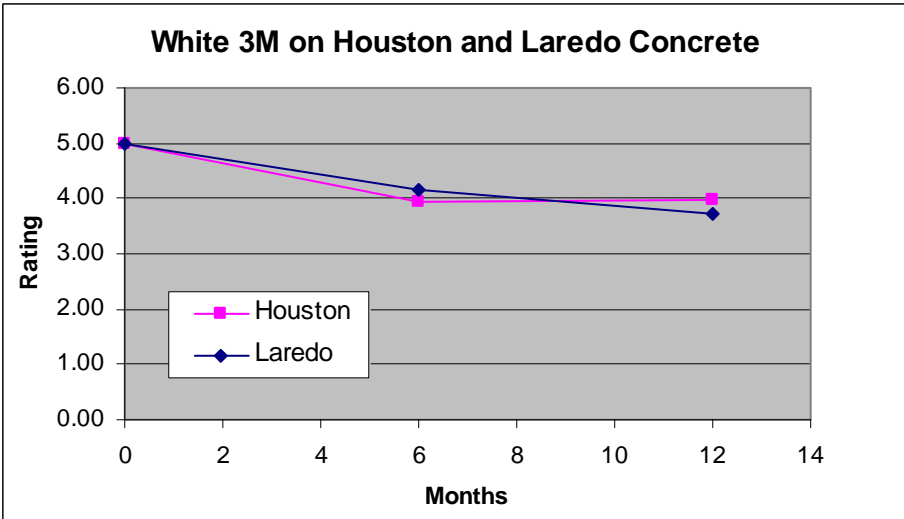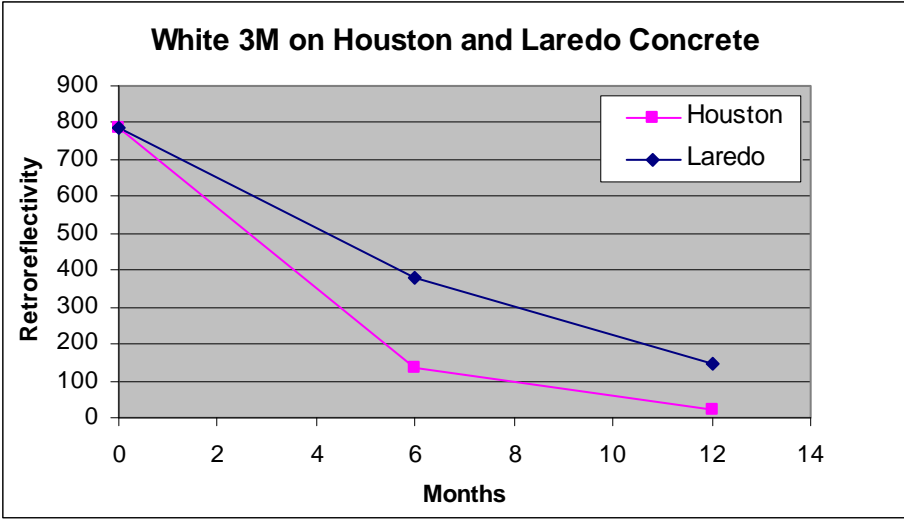
Figure 93. Performance of 3M Marker on Houston Deck.
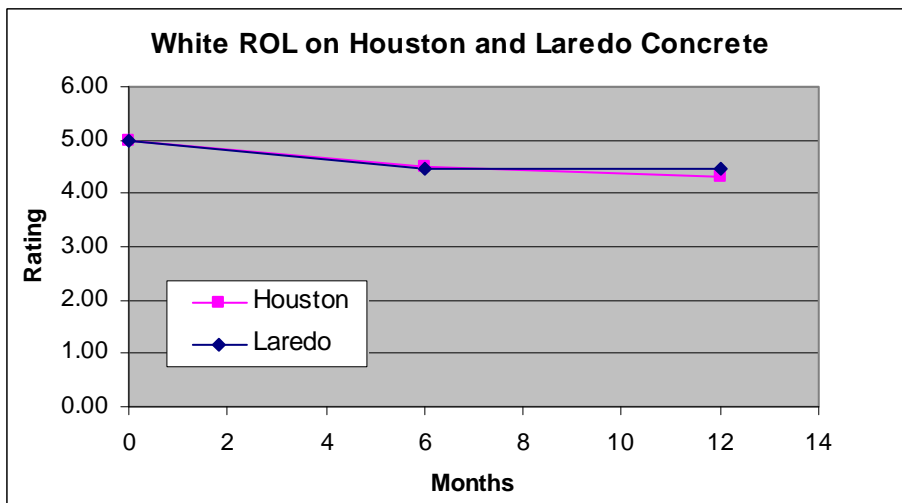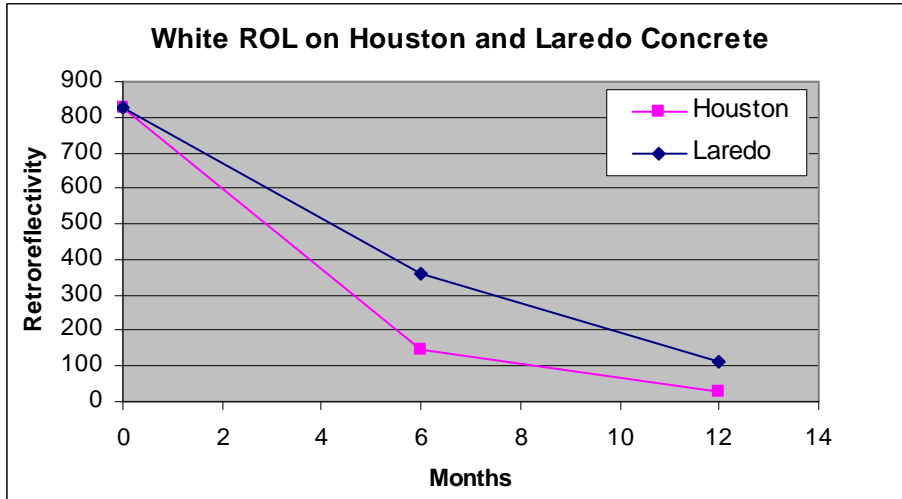
Figure 94. Performance of Ray-O-Lite Marker on Houston Deck.

Figure 95 and Figure 96 compare retroreflectivity and rating on two seal coat locations, Bryan and Lufkin. The marker models for this comparison are AD88 and AD80. The Bryan deck has a much higher ADT and lower retroreflectivity values. This again shows that higher ADT leads to fast degrading of retroreflectivity. The rating, however, did not yield consistent results for the two locations, again indicating ADT may not directly affect marker damage situations.
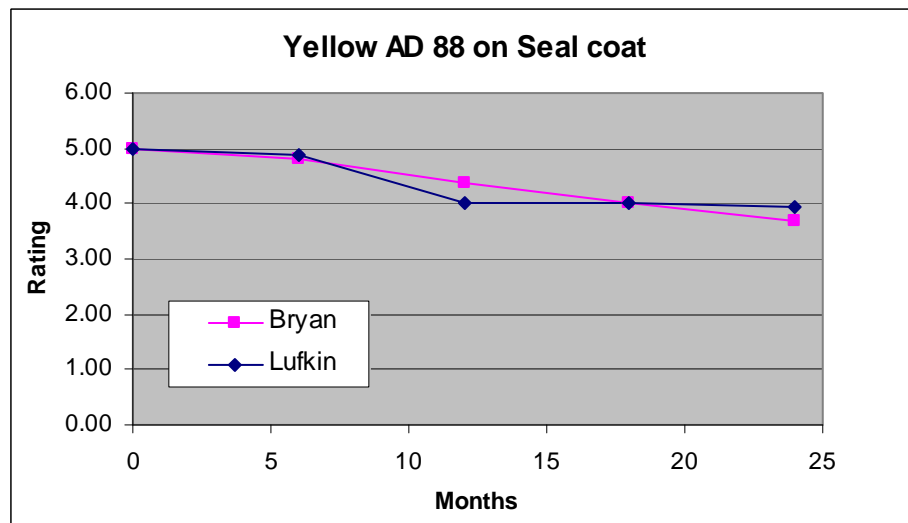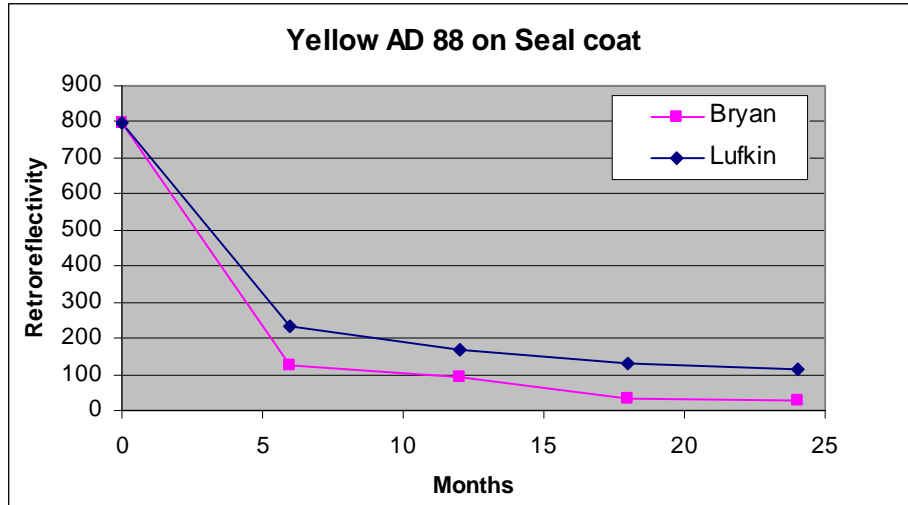
Figure 95. Performance of AD88 Marker on Seal Coat Surface.
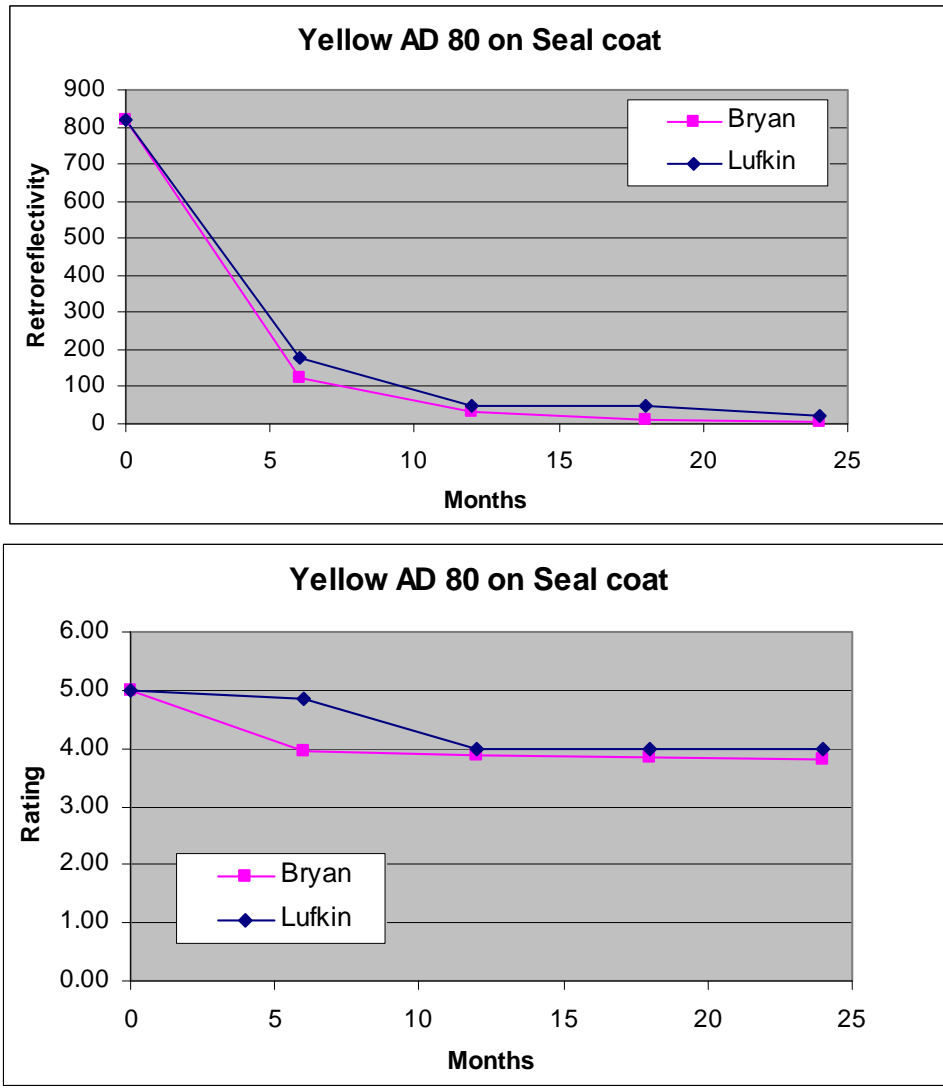
Figure 96. Performance of AD80 Marker on Seal Coat Surface.

Figure 97 and Figure 98 compare performance of AD88 and AD80 on two flexible pavement surfaces, asphalt concrete on the Laredo deck and seal coat on the Lufkin deck. Because the Laredo deck is a freeway section while the Lufkin deck is a two-lane FM road, the markers on the two decks are of different color. The white markers always have higher initial values than yellow ones of the same brand (the only difference is the color). Nevertheless, the retroreflectivity of the white models on the Laredo deck dropped below the values of the yellow ones on the Lufkin deck after 12 months. This is again evidence that the degrading of retroreflectivity is mainly determined by the ADT. The marker condition rating is always lower for Laredo due to high overall volume and high truck volume. The rating is not significantly

131

different on the two surfaces for AD80 because AD80 has been shown to be structurally sound and did not get easily damaged even under very high ADT or high truck traffic.
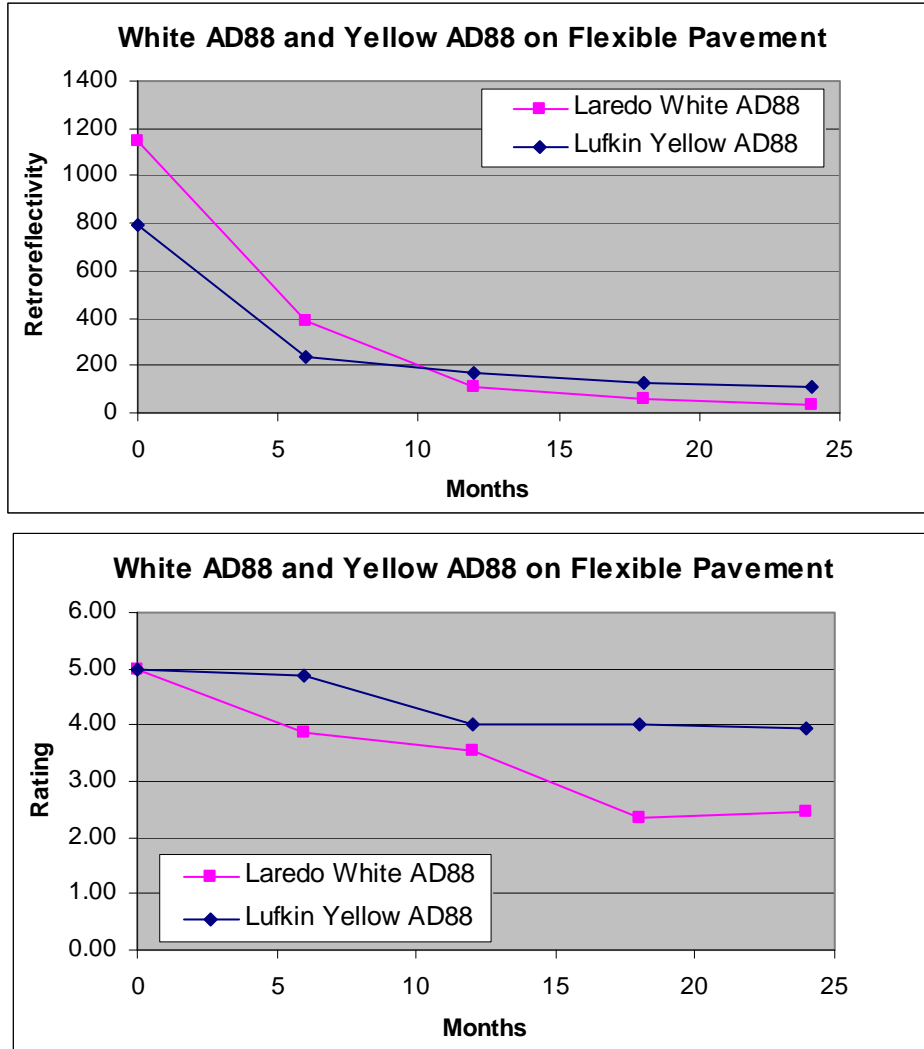
Figure 97. Performance of AD88 on Flexible Pavement.

White AD80 and Yellow AD80 on Flexible Pavement

White AD80 and Yellow AD80 on Flexible Pavement

(Retroreflectivity vs Months)
- Laredo White AD80
- Lufkin Yellow AD80

White AD80 and Yellow AD80 on Flexible Pavement

(Rating vs Months)
- Laredo White AD80
- Lufkin Yellow AD80
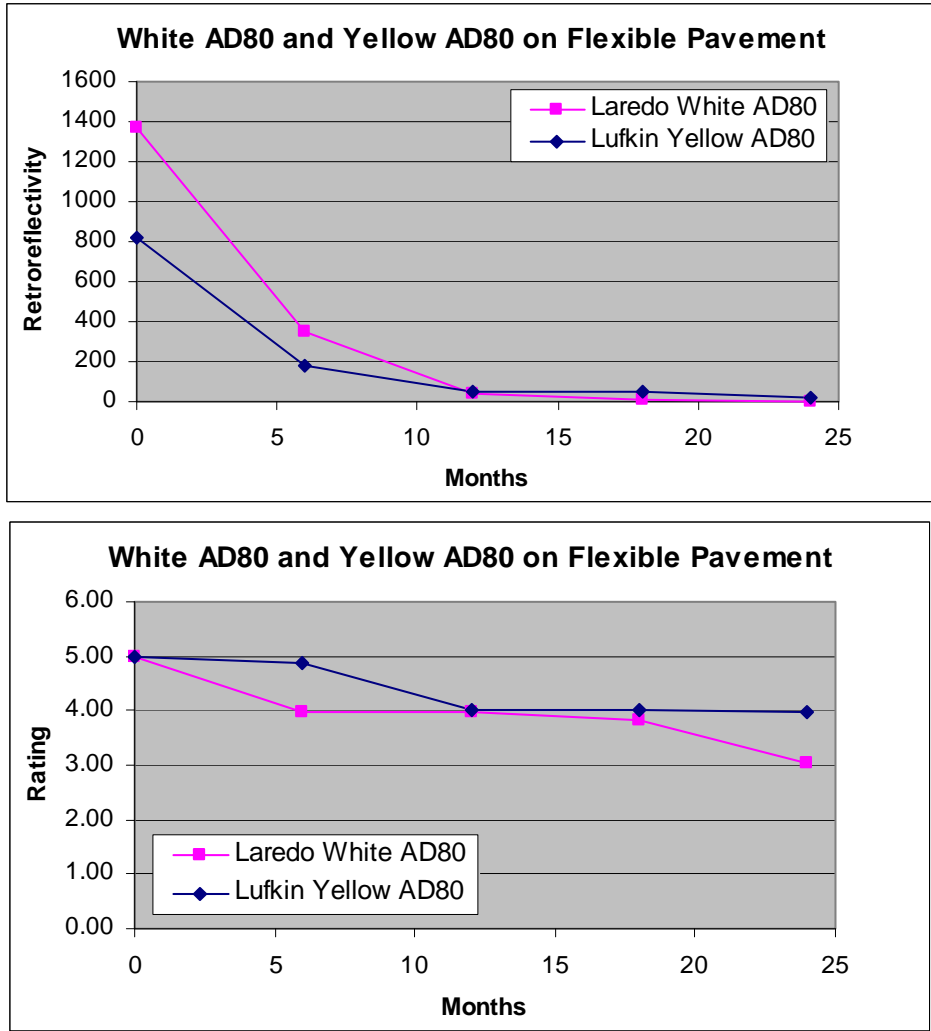
Figure 98. Performance of AD80 on Flexible Pavement.

Summary of Field Test Results

This section summarizes field test findings based on the data and results presented earlier. This summary intends to highlight findings regarding marker performance under various external factors. Marker performance between brands will also be briefly discussed.

The degrading of retroreflectivity is primarily determined by ADT. This was consistently shown by the results on all decks. Retroreflectivity also varies significantly between marker models. It was found that both Apex models and AD80 have some serious retroreflectivity performance issues. The average retroreflectivity values of these RRPM models all dropped below 50 after 12 months, even on low traffic locations such as the Bryan and Lufkin decks. Of

particular concern was the drastic drop in retroreflectivity between 6 months and 12 months for AD80, which has the highest average initial retroreflectivity value among all models. This indicates a potential design flaw with the retroreflective mechanism for this particular marker brand. For the Houston deck, because of the extremely high ADT, the retroreflectivity values of all models dropped to very low values after 12 months. This indicates that for high ADT roadways such as I-610, the controlling factor for service is probably the retroreflectivity. No RRPM brands were found to provide adequate retroreflectivity after one year. For lower volume roads, such as the Lufkin deck location, retroreflectivity is adequate after 18 to 24 months for AD80, 3M, and Ray-O-Lite. For the Laredo and Lufkin decks, other than the Apex models and AD80, the retroreflectivity at the end of 12 months was adequate but degraded further in the second year to levels that may not be considered adequate. This, however, is a judgment call since there is no standard for the minimum retroreflectivity value for RRPMs. Comparing the retroreflectivity values on two surface types at the Laredo deck; the retroreflectivity values are slightly lower on concrete than on asphalt. This could be because lens and case damage is more severe on concrete, as will be discussed later. The physical damage to the case, lens, and lens interior reduces retroreflectivity; a correlation between marker physical condition and retroreflectivity was observed during data collection and analysis.

For marker damage and rating, there are noticeable differences on different types of surfaces. First, the damage on concrete seemed more severe as indicated by the lower average rating for the concrete sub-deck than the asphalt sub-deck of the Laredo deck. This can be explained by the rigid nature of the concrete surface, which does not deform, so the markers and the adhesive absorb more energy from tire impacts, resulting in more severe damage. Also, different damage types were found, particularly with the two Apex models. It was observed that both Apex models had cracks from the mid-bottom up on flexible pavement (asphalt or seal coat). This type of damage was observed on virtually every Apex marker. On the Laredo test deck, the Apex markers were split into two halves on the asphalt surface, which was not observed on the concrete surface. AD88 also seemed to have more case cracks on asphalt than on concrete. The failure of the Apex models on asphalt indicates an inadequate tensile strength of the markers because the bottom of a marker has higher tensile stress, as shown in the FEM analysis; this seems to be a design problem. On a concrete surface, other types of damages to the case and lens are more severe, leading to an overall lower rating on concrete than on asphalt.

For a particular marker, there appears to be a general correlation between marker rating and retroreflectivity at a given time. This is not surprising since damage to the case, lens surface, or interior reduces retroreflectivity. There are, however, some particularities with some marker models. For example, AD80 has a consistently high case condition rating, but its retroreflectivity is always very low after one year. It was also found that 3M markers can maintain high retroreflectivity values even if they are severely damaged as long as there is a piece of retroreflective material left. This is because the technology used by 3M is different from that of other manufacturers. For other marker brands, once the lens interior is affected water entering through the cracked lens cover reduced the retroreflectivity.

Overall, Ray-O-Lite and 3M seem to perform better than the rest of the brands, as they both retained reasonable values of retroreflectivity, and damage conditions were less severe even for high traffic locations. Apex models performed poorly, as they had very low retroreflectivity after one year. All Apex markers that were installed cracked, and eventually broke into two halves on asphalt. AD80 was structurally sound with no severe damage to the case, even for high traffic locations. However, its retroreflectivity decreased drastically in the first year and stayed at a very low level after one year. AD88 seemed to have more cracks all over the marker, especially on high traffic roads.

Test deck evaluations did not have mass failure, in terms of marker loss, on any of the decks. This is an indication even though regular contractors installed all the markers on the decks, they appeared to have paid more attention to the installation process knowing the markers would be tested and evaluated, which otherwise would have affected the durability significantly. Better installation quality on the test decks, compared to that of regular contract installations was observed. During a field visit to a TxDOT district, researchers were able to observe the installation quality as soon as the contractor left the job site. This site was not one of the test decks evaluated in this research. Problems such as inadequate bitumen pad size, improper adhesive treatment and noticeable voids between the marker bottom and adhesive were found. These problems were not found at the test decks evaluated in this research. These findings signify the importance of inspection and quality control by both the contractor and TxDOT during marker installation. The only marker model that was found lost occasionally was AD80. This may be due to its smoother bottom surface (compared to potted markers). However, the loss percentage was rather small and only took place on the Laredo and Houston decks.

CHAPTER 6. LAB TESTS

This section of the report describes laboratory testing of the RRPMs. The primary objective of the testing was to develop a test method or methods that would allow TxDOT to quickly and easily evaluate RRPMs from different manufacturers. While ASTM D 4280 provides testing procedures that evaluate performance of RRPMs, it was determined that the standard did not correlate well with in-service performance. The testing was performed at the Structural and Materials Testing Laboratory in the Zachry Department of Civil Engineering at Texas A&M University in College Station, Texas.

BACKGROUND

ASTM standard D 4280 provides testing criteria for non-snowplowable RRPMs (*6*). Brief testing procedures for compression and flexural tests are provided in the testing practices in Chapter 2.

LONGITUDINAL FLEXURAL STRENGTH

Section 9.2.1 of ASTM D 4280 provides a method for determining the flexural strength of an RRPM using a simple three-point bend test. The marker is placed with the marker base down on two 1/2-inch wide supports extending beyond either side of the marker. A load is then applied at mid-span such that the direction of flexural stress is parallel to the direction of traffic. Elastomeric pads are used at all support and load points. The test is performed using displacement control with a rate of 0.2 inch/minute. Figure 99 provides a view of a typical test setup.

Figure 99. Test Setup for ASTM D 4280
Longitudinal Flexural Strength.

ASTM D 4280 requires a minimum flexural strength of 2000 lb for an RRPM. Tests of all six types of RRPMs evaluated in this study exceeded this strength.

COMPRESSIVE STRENGTH

Section 9.2.2 of ASTM D 4280 also provides a test procedure to measure the compressive strength of a marker. With the marker supported on a flat steel surface, a compressive force is applied perpendicular to the plane of the marker. Elastomeric pads are used at the base and at the load point. Using load control, the compressive force is applied at a rate of 0.2 inch/minute. Figure 100 provides a view of a typical test setup.

Figure 100. View of ASTM D 4280 Compression Test.

ASTM D 4280 requires the marker to support a load of 6000 lb with breakage of significant deformation. Tests of all six types of RRPMs evaluated in this study exceeded this strength. The marker identification that is used for the laboratory procedures is presented in Table 22.

Table 22. Marker Identification Used in Lab Tests.

Marker No.	Type
1	AD80
2	AD88
3	ARCII
4	3M
5	921 AR
6	9003

ADDITIONAL TEST PROCEDURES

In order to better correlate field performance with laboratory test results, several additional tests were developed and evaluated using six different RRPM types. These included:

- longitudinal fatigue test,

- tension test,

- poke test, and

- pendulum impact test.

The following sections describe each test and provide a summary of the test results.

Longitudinal Fatigue Test

The longitudinal flexural test described in ASTM D 4280 was modified for repetitive loading. This allowed the evaluation of the RRPMs for their fatigue performance and replicated the type of loading RRPMs experience from typical traffic loading. Instead of a monotonic increasing load to failure, a cyclic load of 2000 lb was used with a minimum load of 100 lb. Elastomeric pads were used at all support and load points. Figure 101 shows a Type 4 RRPM in the fatigue test setup. The maximum flexural stress in the marker from this type of loading occurred in its base at mid-span. Consequently, failure usually occurred due to the development of a crack at this location. The number of cycles to failure varied depending on the type of RRPM. For example, Type 3 RRPMs ranged from 20 to 55 cycles, while Type 5 ranged from 5 to 111 cycles. Shear failures also occurred in some markers at their support points. This was particularly true for the markers that tapered in plan view at their supported edges.

**Figure 101. Close-up View of RRPM in Longitudinal
Fatigue Test Setup.**

Relatively wide scatter of the test results occurred from this test method, without revealing any superior performance of one type of marker over another. Additionally, it was found that the test was relatively difficult to set up and time-consuming in order to achieve satisfactory results. Therefore, this test method was not pursued further as a means of providing a rapid and simple screening process for RRPMs.

Tension Test

The field performance evaluation of the RRPMs indicated that a possible failure mode was the separation of its outer shell from either its base or potting material. Consequently, under normal usage, the bonding between the outer shell of the marker and its base or potting material deteriorated with time. A simple tension test was developed that would evaluate the integrity of the bond between the outer shell of the marker and either the potting material or the inner structure of the marker. A test of this type is not covered in the current ASTM D 4280 standard. There was no direct means of attaching to or gripping any of the markers so that the specimens could be pulled in tension. Consequently, steel tee-tabs were fabricated that were then adhesively attached to both the top and bottom of the RRPM (see Figure 102 and Figure 103). The mating surface of the tee-stubs was roughened to provide a stronger bond of the adhesion.

Through repeated attempts, which included different roughened surfaces and adhesive types, failure occurred in the adhesive prior to failure of the bond between the outer shell and inside structure of the marker. Figure 104 shows the top surface of a Type 4 RRPM after an unsuccessful test where failure occurred in the adhesive. While some damage occurred in the marker itself, as evidenced by the cracking at the lower portion of the marker, the adhesive bond failed prior to separation of the outer shell. Given the difficulty of getting a strong enough adhesive bond between the outer shell and fixture needed to test a marker in tension, it was concluded that this test method was impractical as a screening process for TxDOT. Additional efforts and testing were not pursued.
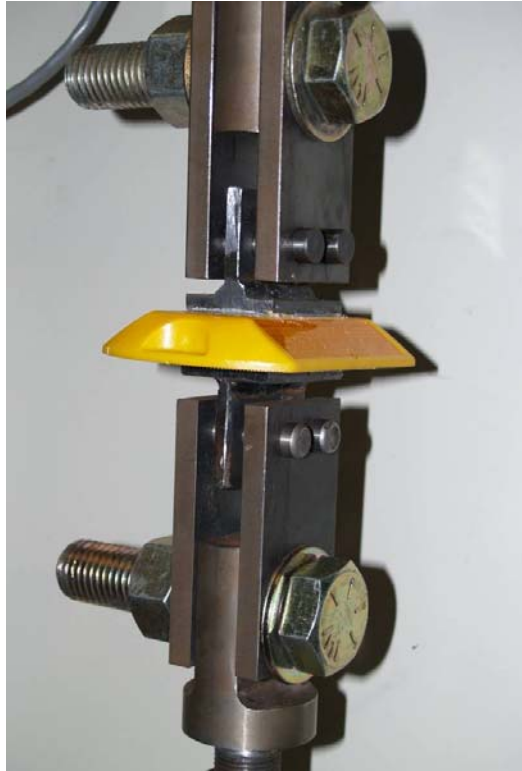
Figure 102. View of RRPM Type 3 and Tee-Stubs Inserted into Tension Test Fixtures.
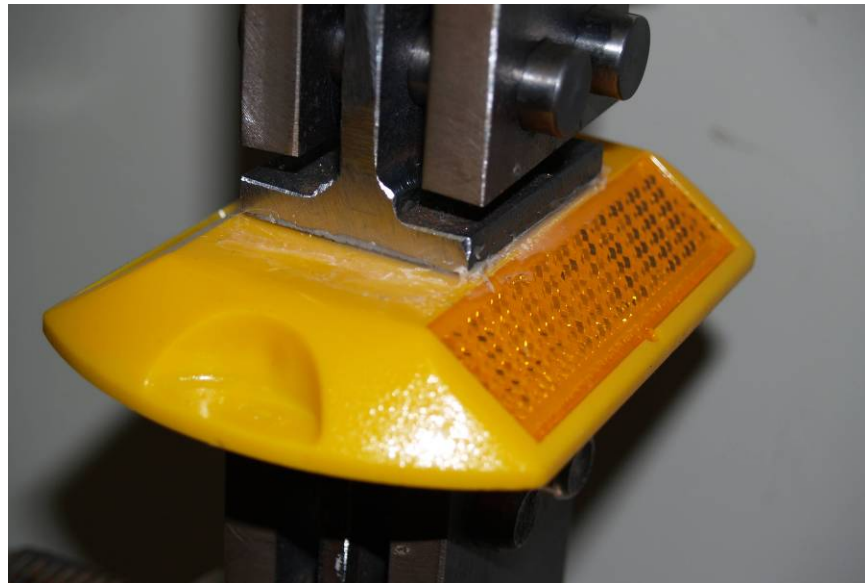
Figure 103. Close-up View of Type 3 RRPM Showing Steel Tee-Stub Adhered to Its Top.
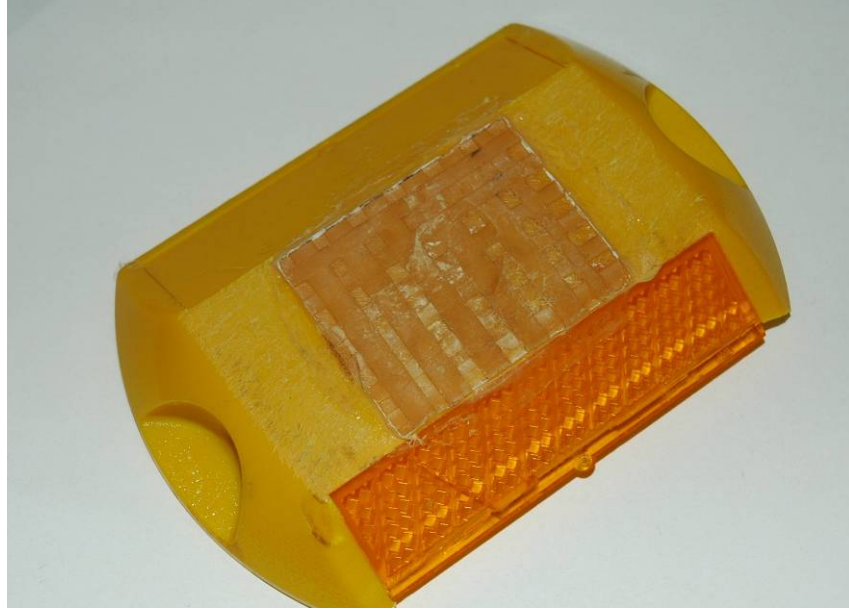
Figure 104. Top View of Type 3 RRPM after Unsuccessful Test.

Poke Test

The poke test was developed to evaluate the strength of the marker shell to concentrated points of force. This force would simulate the damage imposed by a hard object, such as gravel or a piece of rock. Both a 1-inch diameter steel ball (Figure 105) and a 1/2-inch rounded steel rod (Figure 106) were used to apply the compression force at various locations on top of the marker (Figure 107). The tests were run using displacement control, and the peak compressive force was recorded. Through preliminary testing it was found that the 1/2-inch steel rod shown in Figure 106 was easier to test with and gave more consistent results. Consequently, additional testing was performed with that setup.
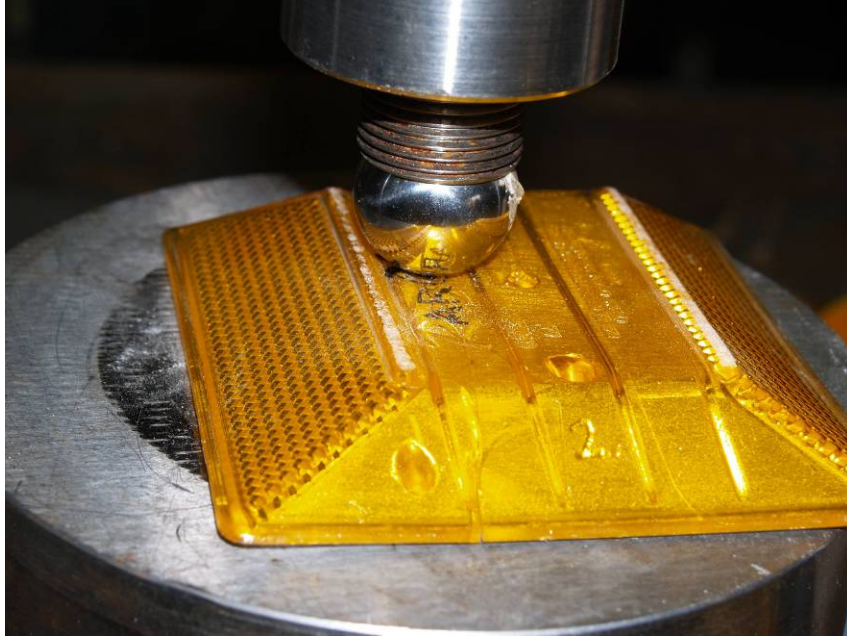
Figure 105. Poke Test with 1-Inch Diameter Steel Ball.

Figure 106. Poke Test with Rounded 1/2-Inch Diameter Rod.
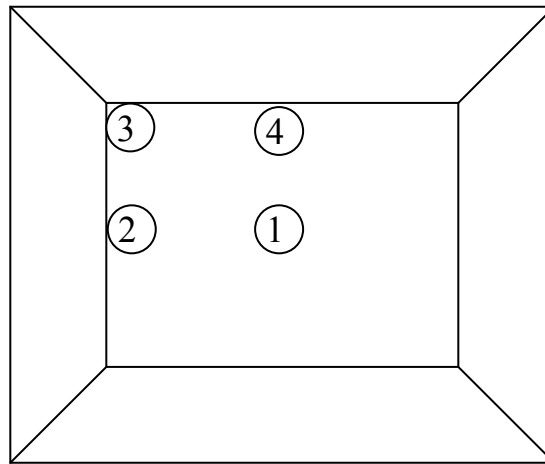
**Figure 107. RRPM Impact Locations
for Poke Tests.**

The results from the poke test for one series of tests using all six types of RRPMs are shown in Table 23. As indicated by these data, the results varied by marker and by location point on the marker. Type 4 consistently gave the lowest compressive forces, ranging from 1160 to 1920 lb. The other five markers failed with a minimum compressive force no lower than 2200 lb. Higher strengths were found when the force was applied at the center of the marker (Location 1) rather than at a corner or side.

Table 23. Poke Test Results (in Pounds) for 1/2-Inch Diameter Steel Rod.

Marker No.	Location			
	1	**2**	**3**	**4**
1	2650	2900	2550	2200
2	6610	3960	4060	4720
3	3790	3470	2960	4090
4	1920	1160	1250	1570
5	5430	2170	2710	2930
6	2830	2990	3970	4690

The poke test was relatively simple to run with the correct testing frame. The test results were consistent between different test series with the same types of markers. However, it was found that the test results did not correlate well with the observed field performance for the RRPMs. For example, the Type 4 RRPM consistently failed with the lowest compressive forces but generally performed well in the field. The low compressive forces for this marker can be attributed to its cell structure composition. This resulted in weak locations on its top surface. However, this effect was localized and did not appear to affect its field performance.

Pendulum Impact Test

Review of the in-field performance indicated that failure of RRPMs initiated with the fracture of their outer shell. These failures could be caused by something as simple as a stone wedged in the tire tread of a vehicle. Consequently, failure occurred due to the impact (dynamic loading) of a hard small object with the surface of the RRPM. Therefore, a testing procedure was needed that evaluated the ability of the RRPMs to absorb energy of impact type loading.

It was decided to design and fabricate a pendulum-like device that could deliver an impact load to a marker. The device that was developed is called a RRPM pendulum impact test device and is shown in Figure 108. The impact force is delivered to the RRPM by the end of a 1-inch rounded steel rod at the end of a swinging arm. The marker is supported in the vertical position by a small metal sleeve and a simple metal clip that holds it against an elastomeric pad (0.125-inch, 70 Shore A). All of these components are mounted on what was originally a bidirectional machining vise. This allowed both horizontal and vertical positioning of the marker relative to the steel rod and its impact point. This adjustable support for the RRPM can be seen in Figure 109.

Figure 108. Overall View of Pendulum Impact Device.
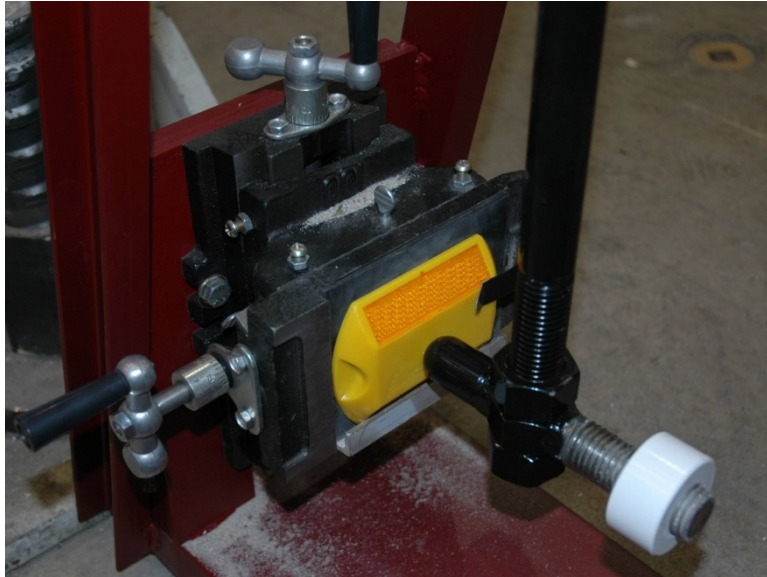
Figure 109. View of Marker Adjustable Support.

Different weights can be added to the end of the pendulum arm to increase the force exerted on the marker at impact. The set of five weights is shown in Figure 110, and their corresponding weights are given in Table 24. This set allows for six different impact forces, including using the pendulum arm (8.54 lb) without any added weight. By testing each RRPM brand to the set of six different levels of impact forces, better measurement of impact performance can be determined when comparing RRPM brands and types.

Figure 110. Set of Five Weights for Pendulum Impact Device.

Table 24. Pendulum Impact Device Weights.

Weight Number	Weight (lb)
1	0.35
2	0.69
3	1.36
4	1.73
5	2.06

The use of the adjustable marker support allows for a variation of impact locations on the marker. To fully evaluate each marker, it was determined that four impact locations were needed, as summarized in Figure 107. These locations are the same locations that were used for the poke test. Each of the four positions shown was easily achieved for each of the six RRPMs tested. The damage caused by the impact, if any, varied depending on the location of the impact and the type of RRPM. For example, an impact at Location 1 (center) or Location 2 (side) resulted in damage to the shell of the RRPM and/or cracking at the base or in the potting material. An impact at Location 3 (corner) or Location 4 (top) often resulted in damage to the reflector. A description of damage observed for these series of tests is summarized in Table 25 along with a corresponding identification code used to summarize the test results.

Table 25. Summary of Damage Descriptions and Identification Codes.

Code	Description of Damage
A	No distress (except local at impact point)
B	Minor reflector separation
C	Minor cracking in reflector/base
D	Reflector cracking
E	Base cracking
---	Not tested

The six RRPMs evaluated in this study were tested in the pendulum impact device using all six weight configurations at each of the four impact positions. Each marker was examined after testing to determine if damage occurred and, if so, to what extent and type. The condition of the marker was then rated according to Table 25 and summarized in Table 26.

149

Table 26. Summary of Pendulum Impact Tests.

Location 1						
Marker No.	**Weight No.**					
	0	**1**	**2**	**3**	**4**	**5**
1	A	A	A	A	A	A
2	---	---	---	---	E	E
3	---	---	---	---	E	E
4	---	---	---	---	A	A
5	E	E	E	E	E	E
6	E	E	E	E	E	E
Location 2						
Marker No.	**Weight No.**					
	0	**1**	**2**	**3**	**4**	**5**
1	A	A	A	A	A	A
2	E	E	---	---	---	---
3	E	E	---	---	---	---
4	---	---	---	---	A	A
5	E	E	E	E	E	E
6	E	E	E	E	E	E
Location 3						
Marker No.	**Weight No.**					
	0	**1**	**2**	**3**	**4**	**5**
1	A	A	B	B	C	C
2	E	E	---	---	---	---
3	E	E	---	---	---	---
4	---	---	---	---	A	A
5	E	E	E	E	E	E
6	E	E	E	E	E	D
Location 4						
Marker No.	**Weight No.**					
	0	**1**	**2**	**3**	**4**	**5**
1	B	B	C	C	C	C
2	E	E	---	---	---	---
3	A	A	E	E	---	---
4	---	---	---	---	A	A
5	B	E	E	E	E	E
6	B	E	E	E	E	E

Use of the pendulum impact device is relatively easy. It is semi-portable in that its weight is approximately 120 lb, exclusive of any external weight that is used to stabilize and prevent movement of the device at impact. The external stabilizing weight can be eliminated by fastening the base of the device to a concrete floor or other suitable rigid surface.

Temperature Effects

The test results presented above were all performed at an ambient temperature between 70°F and 75°F. A limited number of tests were conducted at temperatures below this temperature to determine if there were any adverse effects on the test results and, hence, correlation to field performance. The two lower temperatures investigated were 40°F and 0°F. These test temperatures were selected due to their relative ease in achieving: normal refrigerator temperature for 40°F and normal freezer temperature for 0°F. (These temperatures are used by AASHTO in evaluating the fracture toughness of bridge steels.) The test results for the poke test showed no significant effect of temperature. While the process of reducing the temperature of the marker prior to testing was relatively simple, keeping the proper temperature during testing was found to be more difficult. Given the relatively low density of the RRPMs, they had a tendency to warm either due to the time it took to set up the test or because of the mass of the test fixture. For example, the support fixture shown in Figure 100 provided a large heat source for a marker that was placed on it. As a consequence of these difficulties and the lack of significant influence on the test results, it was decided to perform all tests at room temperature.

SUMMARY AND RECOMMENDATION

In addition to the ASTM compressive test and longitudinal flexural strength tests, several additional tests, including the longitudinal fatigue test, tension test, poke test, and pendulum impact test, were developed and evaluated. Test results were compared with field results on six test RRPM models. The following conclusions were reached:

- All RRPM models passed the ASTM compressive test and longitudinal flexural strength tests. Since many of the marker models have known performance problems that were also displayed in the field test, the two ASTM tests were proven to be inadequate to describe the RRPM's performance.
- The longitudinal fatigue test was found to be inconsistent with the results of multiple tests, and it is a difficult test to conduct.
- The tension test is difficult to set up and impractical due to the difficulty of getting a strong enough adhesive bond.

- The poke test is easy to run and produced consistent results between different runs with the same marker model. However, its results do not consistently correlate with field performance.

- The pendulum impact test is easy to run and it is semi-portable. It produced very consistent results between different runs on the same marker models. Also, the pendulum test results on all six test marker models were consistent with that of the field performance of RRPMs obtained from the field test deck.

The researchers recommend the pendulum impact test be adopted by TxDOT for product qualification and also for sampling of products for quality control purposes.

CHAPTER 7. CONCLUSIONS AND RECOMMENDATIONS

Over a three-year period, researchers conducted the following tasks to identify the causes of RRPM failure and to evaluate marker performance on the field decks and in the lab, so as to develop new lab tests:

- Researchers conducted a survey of TxDOT districts and RRPM manufacturers to gather information on existing testing procedures and marker field performance.

- Researchers performed field visits to observe RRPM failure modes and the installation process.

- Four field test decks were installed and monitored. Retroreflectivity and physical condition data were collected on six selected RRPM models at four deck locations that were selected based on traffic condition, pavement surface type, geographic, and other environmental factors.

- Researchers conducted different lab tests. The tests included currently recommended ASTM tests, modified ASTM tests, and other newly developed tests.

- Researchers also conducted an FEM of RRPMs under tire-marker impact and in a lab environment to gain insights into the correlation between lab test results and actual field performance by comparing the stresses inside the RRPMs.

- The researchers conducted analyses to correlate lab and field test performances.

- Finally, researchers recommended a developed lab test procedure that correlated well with field performance.

This research yielded several important findings with respect to RRPM performance and testing methods, some of which are:

- Performance of RRPM products has a wide range. The quality and performance of an RRPM product is related to marker model, materials, and technologies used.

- Performance (physical condition and retroreflectivity) of RRPM products also depends on traffic volume, truck traffic, and pavement surface type. Retroreflectivity degrading is directly related to ADT. High truck traffic significantly deteriorates marker physical condition. It deteriorates more rapidly on a concrete surface, but some models perform poorer on a flexible surface due to cracking of the marker case.

- No marker models were found to withstand high traffic volumes beyond one year on

high traffic roadways such as I-610 in Houston.

- On low traffic roads such as FM 230 in the Lufkin District, several marker brands displayed reasonable physical condition and retroreflectivity level at the end of the two-year evaluation period.

- There is a correlation between marker physical condition and retroreflectivity values. From field observation, marker damage, especially damage to the lens surface and lens interior, is directly related to the deterioration of retroreflectivity.

- Marker retention is directly related to installation quality. Poor installation was observed during field visits, while installation quality was high at all four field decks. No significant marker loss problems were reported in several TxDOT districts on the field decks.

- Constrained by the markers currently available on the market, researchers did not find any "super" marker that could last for more than three years on high traffic roads.

- Existing lab testing methods do not produce results consistent with field performance. All RRPM products passed ASTM tests, but their performance varied considerably.

- Many of the existing lab tests and the new lab tests developed and evaluated in this project failed to produce consistent results and could not correlate with field performance.

Based on the findings from this project, the researchers make the following recommendations to TxDOT:

- There is a critical need to emphasize the quality of RRPM installation because it is directly related to their retention and performance in the field. Installation quality can be improved by enhancing TxDOT inspection or adopting warranty specifications that require the contractor to replace missing markers within a certain time from the installation.

- TxDOT's current RRPM replacement schedule is reasonable for the products currently available on the market. Based on the performance of the marker brands evaluated in this project, on high traffic interstates, markers should be replaced yearly. On low traffic roadways, markers can be replaced every two or three years.

- The researchers also recommend conducting the pendulum impact test for the purpose of marker qualification and quality control.

154

REFERENCES

1.   Federal Highway Administration, U.S. Department of Transportation. *Manual on Uniform Traffic Control Devices for Streets and Highways.* Washington, D.C., 2003.

2.   R. McNees and J. S. Noel. *State-of-the-Art and Objectives of Reflective Raised Pavement Markers.* Report No. 322-1. Texas Transportation Institute, College Station, Texas, 1986.

3.   J. T. Tielking and J. S. Noel. *On the Retention of Reflective Raised Pavement Markers.* Report No. 477-1F. Texas Transportation Institute, College Station, Texas, 1988.

4.   V. J. Pezoldt. *Raised Pavement Marker Retroreflectivity.* Report No. 1151-1F. Texas Transportation Institute, College Station, Texas, 1990.

5.   G. L. Ullman. *Retroreflective Raised Pavement Markers: A Two-Year Field Evaluation in Texas.* Report No. 1946-3. Texas Transportation Institute, College Station, Texas, 1994.

6.   ASTM International. *Standard Specification for Extended Life Type, Nonplowable, Raised Retroreflective Pavement Markers.* Publication ASTM D4280-03. West Conshohocken, Pennsylvania, 2003.

7.   J. Migletz, J. K. Fish, and J. L. Graham. *Roadway Delineation Practices Handbook.* Report No. FHWA-SA-93-001. Federal Highway Administration, U.S. Department of Transportation, Washington, D.C., 1993.

8.   J. L. Pline. *Traffic Control Devices Handbook.* Institute of Transportation Engineers, Washington, D.C., 2001.

9.   A. R. Grant and J. R. Bloomfield. *Guidelines for the Use of Raised Pavement Markers.* Report No. FHWA-RD-97-152. Federal Highway Administration, U.S. Department of Transportation, Washington, D.C., 1998.

10.   H. B. Rushing, J. O. Burt, and E. J. LeBlanc. *Evaluation of Raised Pavement Markers.* Report No. 68-1T. Louisiana Department of Highways, Baton Rouge, Louisiana, 1968.

11.   J. G. Pigman, K. R. Agent, and R. L. Rizenbergs. *Evaluation of Raised Pavement Markers.* Kentucky Department of Transportation, Lexington, Kentucky, 1975.

12.   S. Q. Kidd. *An Evaluation of Reflective Markers: Final Report.* Report No. MSHD-RD-90-67-4. Mississippi State Highway Department, Jackson, Mississippi, 1990.

13.   R. McNees and J. S. Noel. *Reflectivity Retention of Reflective Raised Pavement Markers.* Report No. 322-2. Texas Transportation Institute, College Station, Texas, 1986.

14.   R. McNees and J. S. Noel. *Retention of Reflective Raised Pavement Markers.* Report No. 322-3. Texas Transportation Institute, College Station, Texas, 1986.

15.   R. McNees and J. S. Noel. *Executive Summary, Significant Results and Assorted Tests and Procedures for Reflective Raised Pavement Markers.* Report No. 322-4F. Texas Transportation Institute, College Station, Texas, 1986.

16.   G. L. Ullman. *Retroreflective Raised Pavement Marker Field Testing: Initial Interim Report*. Report No. 1946-1. Texas Transportation Institute, College Station, Texas, 1992.

17.   G. L. Ullman. *Retroreflective Raised Pavement Marker Field Testing: Results of the First Year Evaluation*. Report No. 1946-2. Texas Transportation Institute, College Station, Texas, 1994.

18.   HAPI Asphalt Pavement Guide. Pavement Types. http://www.hawaiiasphalt.com/HAPI/modules/04_pavement_types/04_pavement_types.htm, accessed November 11, 2006.

19.   HAPI Asphalt Pavement Guide. Pavement Structure. http://www.hawaiiasphalt.com/HAPI/modules/08_structural_design/08_pavement_structure.htm, accessed November 11, 2006.

20.   California Department of Transportation Engineering Services. *Method of Testing for Specification Compliance of Non-reflective and Retroreflective Pavement Markers.* California Department of Transportation, Sacramento, California, 2003.

21.   National Transportation Product Evaluation Program (NTPEP). *Project Work Plan for the Field and Laboratory Evaluations of Raised Pavement Markers and Adhesives.* American Association of State Highway and Transportation Officials, Washington, D.C., 2004.

22.   K. M. Marshek, W. R. Hudson, R. B. Connell, H. H. Chen, and C. L. Saraf. *Experimental Investigation of Truck Tire Inflation Pressure on Pavement-Tire Contact Area and Pressure Distribution.* Report No. 386-1. Center for Transportation Research, University of Texas at Austin, Austin, Texas, 1985.

23.   F. L. Roberts, J. T. Tielking, D. Middleton, R. L. Lytton, and K. Tseng. *Effects of Tire Pressures on Flexible Pavements*. Report No. 372-1F. Texas Transportation Institute, College Station, Texas, 1986.

24.   D. Cebon. *Handbook of Vehicle-Road Interaction*. Swets and Zeitlinger Publications, Lisse, Netherlands, 1999.

25.   Y. Xu, L. Jia, and J. Zhang. Modeling Tire/Road Contact Using Piecewise Ritz Procedure. In *Journal of Terramechanics*, Vol. 42, Issue 2, 2005, Elsevier, Amsterdam, Netherlands, pp. 99-113.

26.   H. Rothert, H. Idelberger, W. Jacobi, and G. Laging. On the Finite Element Solution of the Three-Dimensional Tire Contact Problem. In *Nuclear Engineering and Design*, Vol. 78, Amsterdam, Netherlands, 1984, pp. 363-375.

27.   P. F. J. Abeels. Tire Deflection and Contact Studies. In *Journal of Terramechanics*, Vol. 13, Elsevier, Amsterdam, Netherlands, 1976, pp. 183-196.

28.   C. W. Mousseau and G. M. Hulbert. An Efficient Tire Model for the Analysis of Spindle Forces Produced by a Tire Impacting Large Obstacles. In *Computer Methods in Applied Mechanics and Engineering*, Vol. 135, Number 1, Elsevier, Amsterdam, Netherlands, 1996, pp. 15-34.

29.   A. V. Pesterev, L. A. Bergman, C. A. Tan, and B. Yang. Assessing Tire Forces due to Roadway Unevenness by the Pothole Dynamic Amplification Factor Method. In *Journal of Sound and Vibration*, Vol. 279, Issues 3-5, Elsevier, Amsterdam, Netherlands, 2005, pp. 817-841.

30.   R. P. H. Bonse and S. H. Kuhn. Dynamic Forces Exerted by Moving Vehicles on a Road Surface. In *Flexible Pavement Design Research*, Vol. 233, Highway Research Board, Washington, D.C., 1959, pp. 9-32.

31.   R. W. Hansen, C. Bertrand, K. M. Marshek, and W. R. Hudson. *Truck Tire Pavement Contact Pressure Distribution Characteristics for Super Single 18-22.5 and Smooth 11R24.5 Tires.* Report No. 1190-1. Center for Transportation Research, University of Texas at Austin, Austin, Texas, 1989.

32.   D. A. Philips. *Finite Element Analysis of a Shaft-Rotor System.* Master's thesis, Virginia Polytechnic and State University, Blacksburg, Virginia, 2001.

33.   Lecture Notes. Finite Element Methods. http://www.st.bv.tum.de/content/teaching/ifem/ifem.html#notes, accessed January 8, 2006.

34.   S. S. Rao. *Finite Element Method in Engineering, First Edition.* Pergamon Press, Oxford, United Kingdom, 1982.

35.   R. K. Livesley. *Finite Elements: An Introduction for Engineers, First Edition.* Cambridge University Press, Cambridge, United Kingdom, 1983.

36.   Finite Element Analysis. Wikipedia, the Free Encyclopedia. http://en.wikipedia.org/wiki/Finite_element_analysis, accessed May 30, 2005.

37.   Altair Hypermesh. http://www.altair.com/software/hw_hm.htm, accessed June 20, 2005.

38.   LS-DYNA. http://www.lstc.com/, accessed June 20, 2005.

39.   Altair Hyperview. http://www.altair.com/software/hw_hv.htm, accessed June 20, 2005.

40. D. Luskin and M. Walton. *Effects of Truck Size and Weights on Highway Infrastructure and Operations.* Project Summary Report 2122-S. Center for Transportation Research, University of Texas at Austin, Austin, Texas, 2001.

41. Von Mises Stress. Wikipedia, the Free Encyclopedia. http://en.wikipedia.org/wiki/Von_Mises_stress, accessed February 10, 2006.

APPENDIX A. FEM CALIBRATION RESULTS

Appendix A provides Figure 111 to Figure 118. The figures show the comparisons between experimental and simulation results. There are two kinds of results:

1. displacement of the top surface of the marker in millimeters and
2. strains in strain gauges 1-6.

Figure 111 shows the comparison of displacements (in millimeters) of the top surface of the marker from the experiment and the simulation for RRPM Type A. Figure 112 to Figure 114 show the comparisons of strains in strain gauges 1-6 for RRPM Type A. Figure 115 shows the comparison of displacements (in millimeters) of the top surface of the marker from the experiment and the simulation for RRPM Type B. Figure 116 to Figure 118 show the comparisons of strains in strain gauges 1-6 for RRPM Type B.
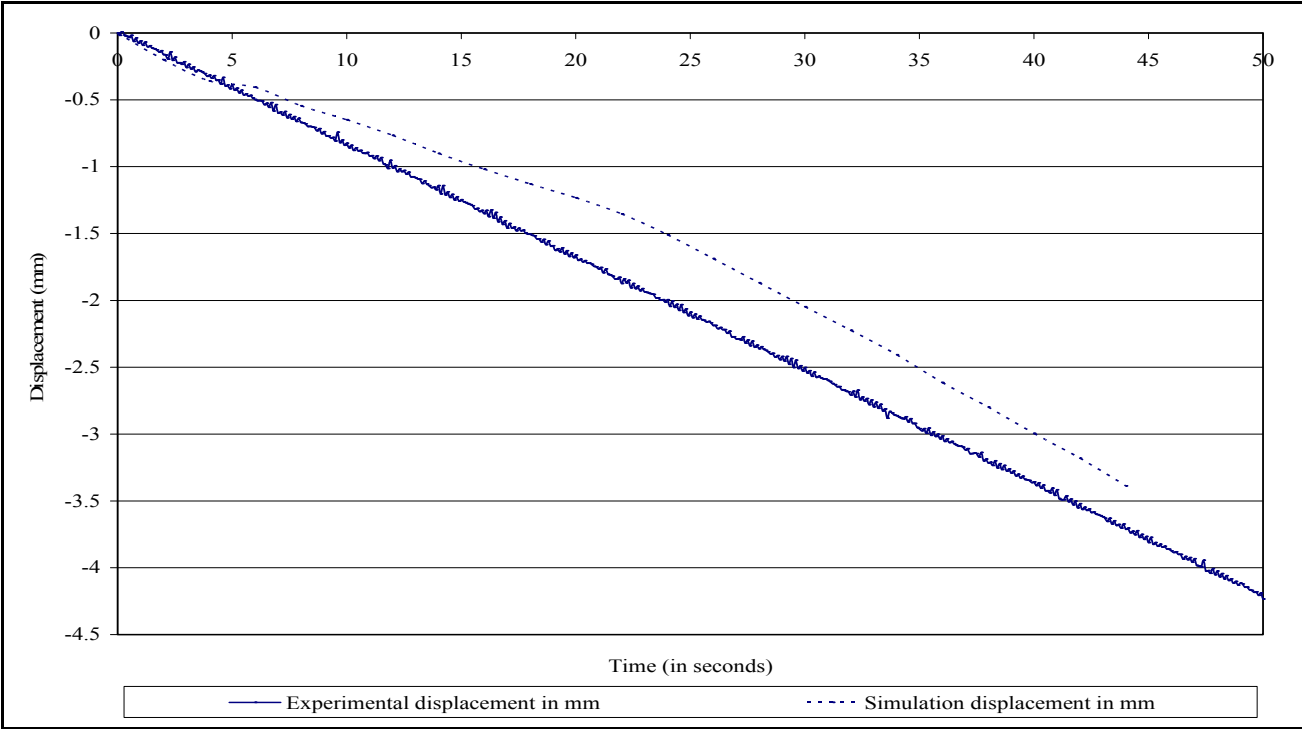
**Figure 111. Experiment versus Simulation for RRPM Type A—
Displacement of Top Surface of Marker in Millimeters.**
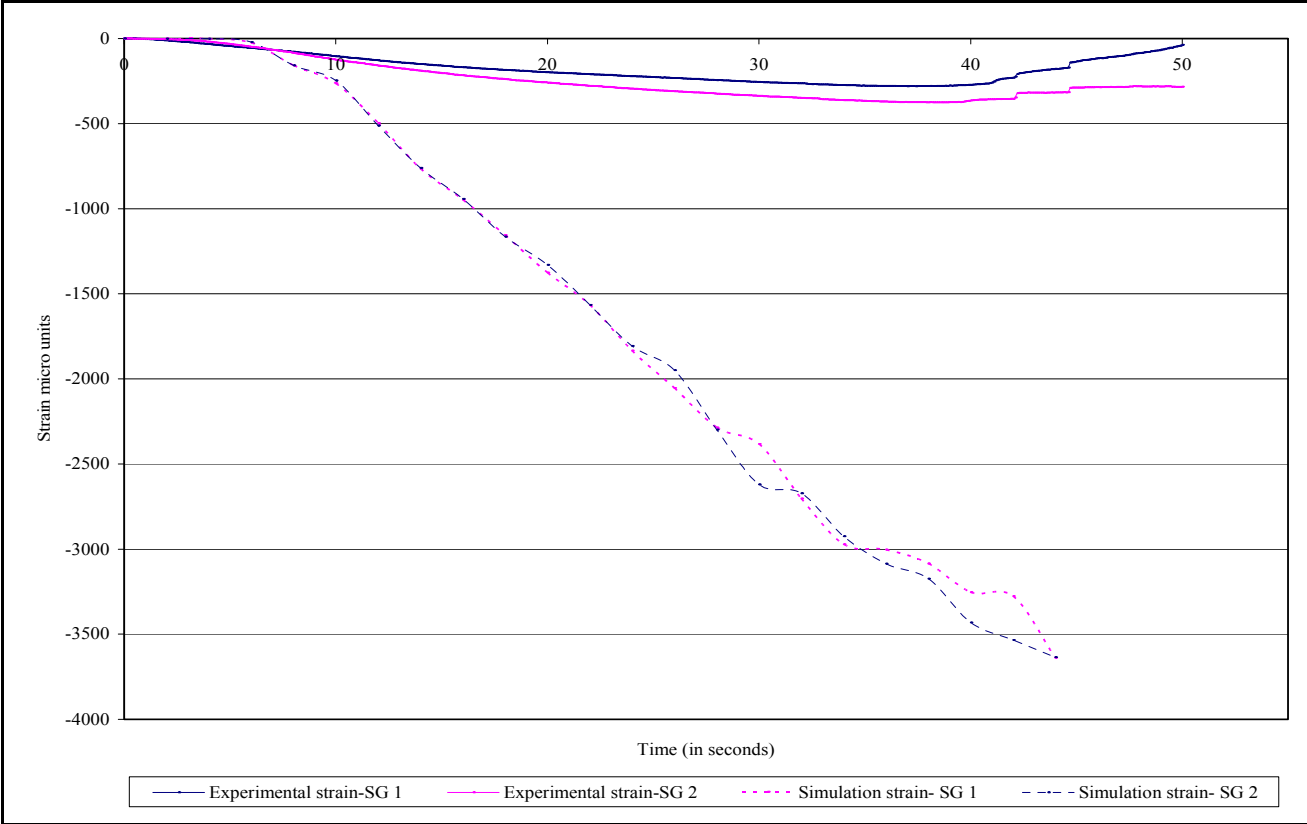
**Figure 112. Experiment versus Simulation for RRPM Type A—
Strains from Strain Gauges 1 and 2.**
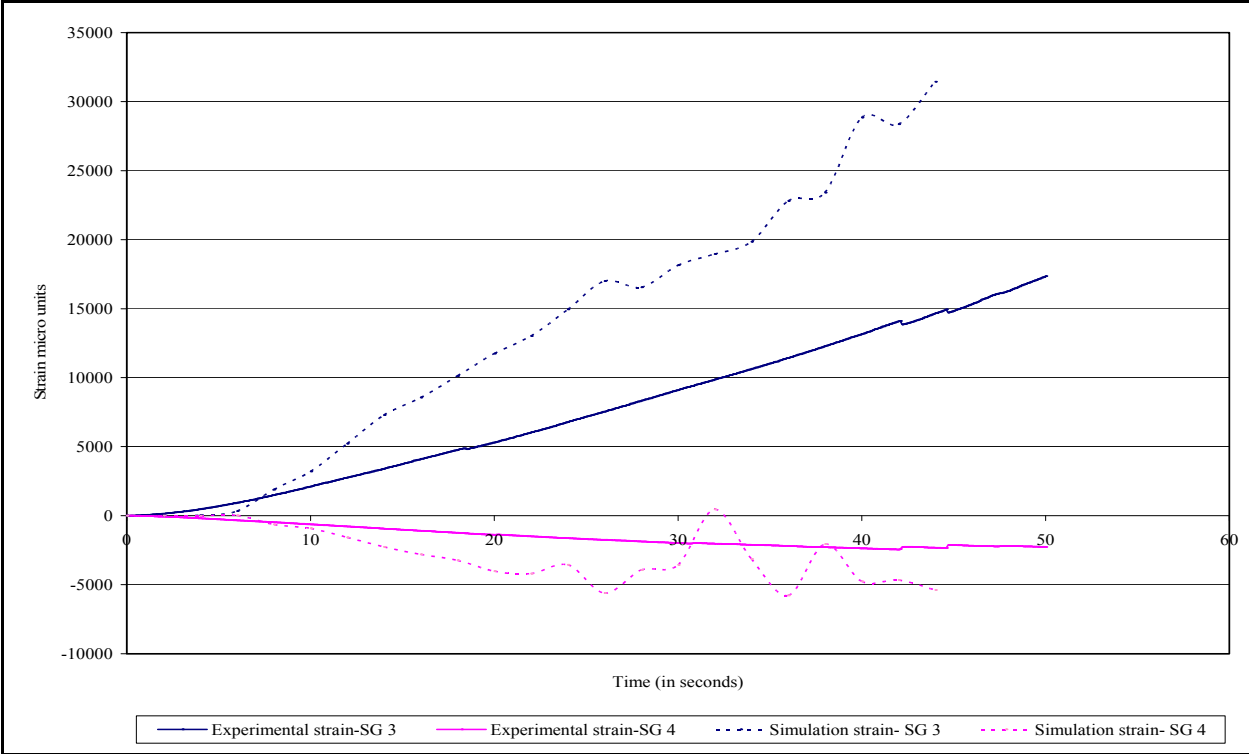
**Figure 113. Experiment versus Simulation for RRPM Type A—
Strains from Strain Gauges 3 and 4.**
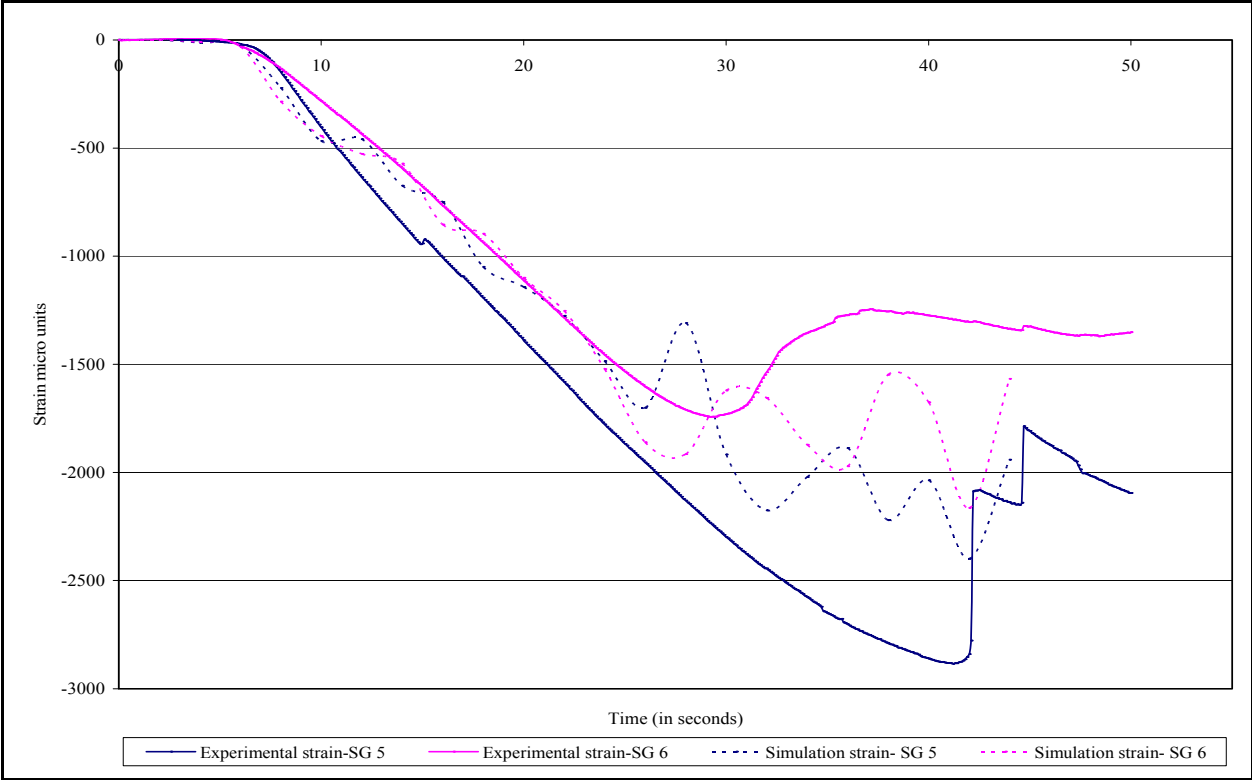
**Figure 114. Experiment versus Simulation for RRPM Type A—
Strains from Strain Gauges 5 and 6.**
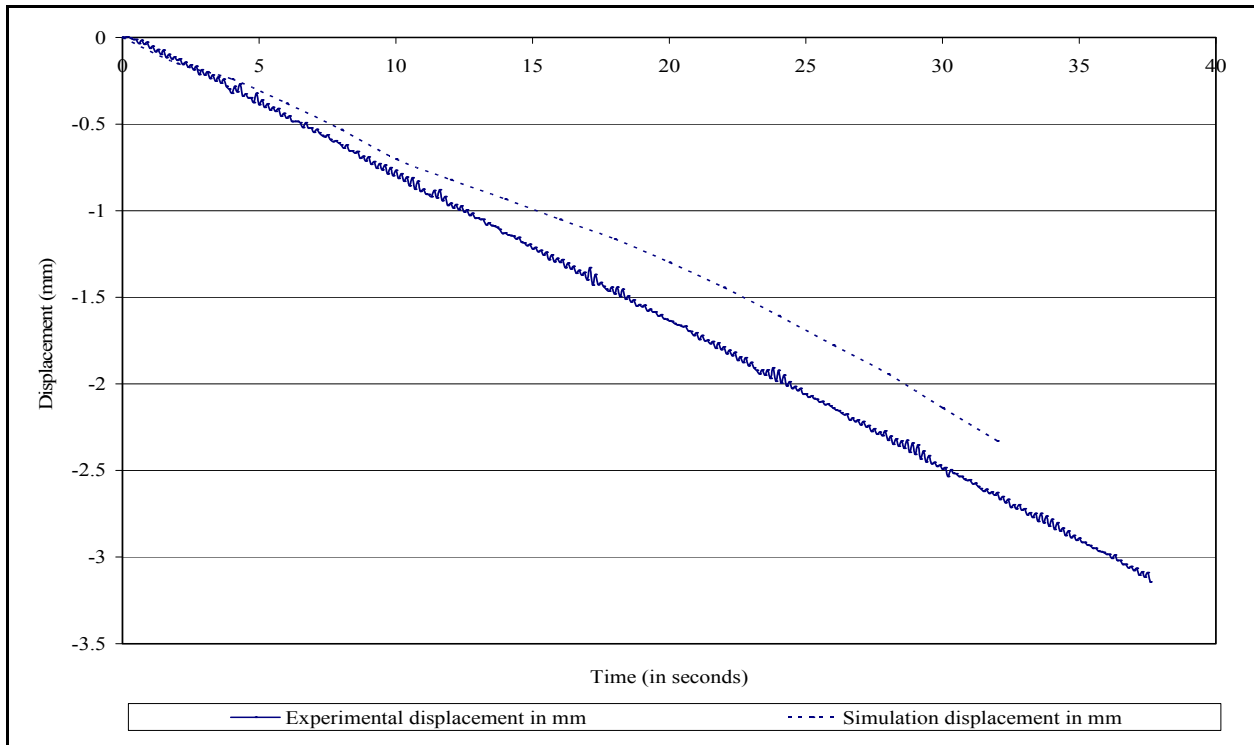
**Figure 115. Experiment versus Simulation for RRPM Type B—
Displacement of Top Surface of Marker in Millimeters.**
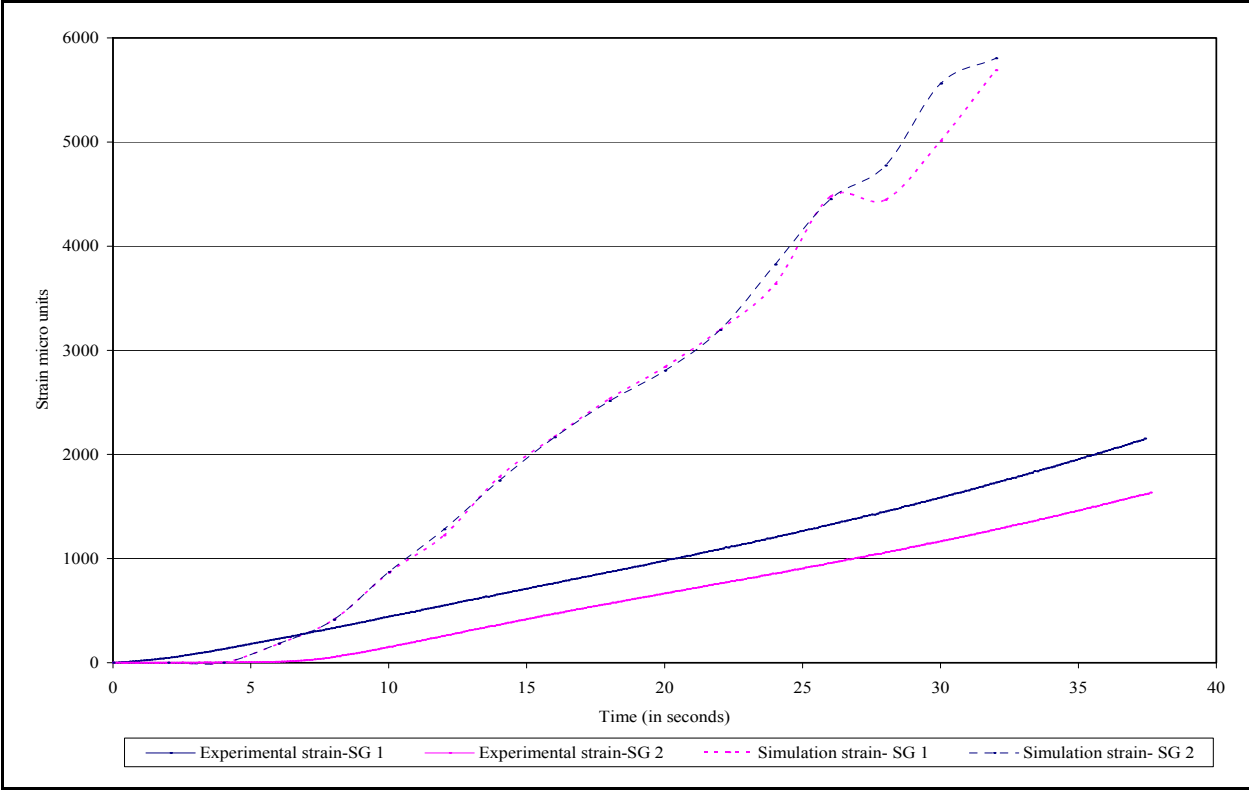
Figure 116. Experiment versus Simulation for RRPM Type B—Strains from Strain Gauges 1 and 2.
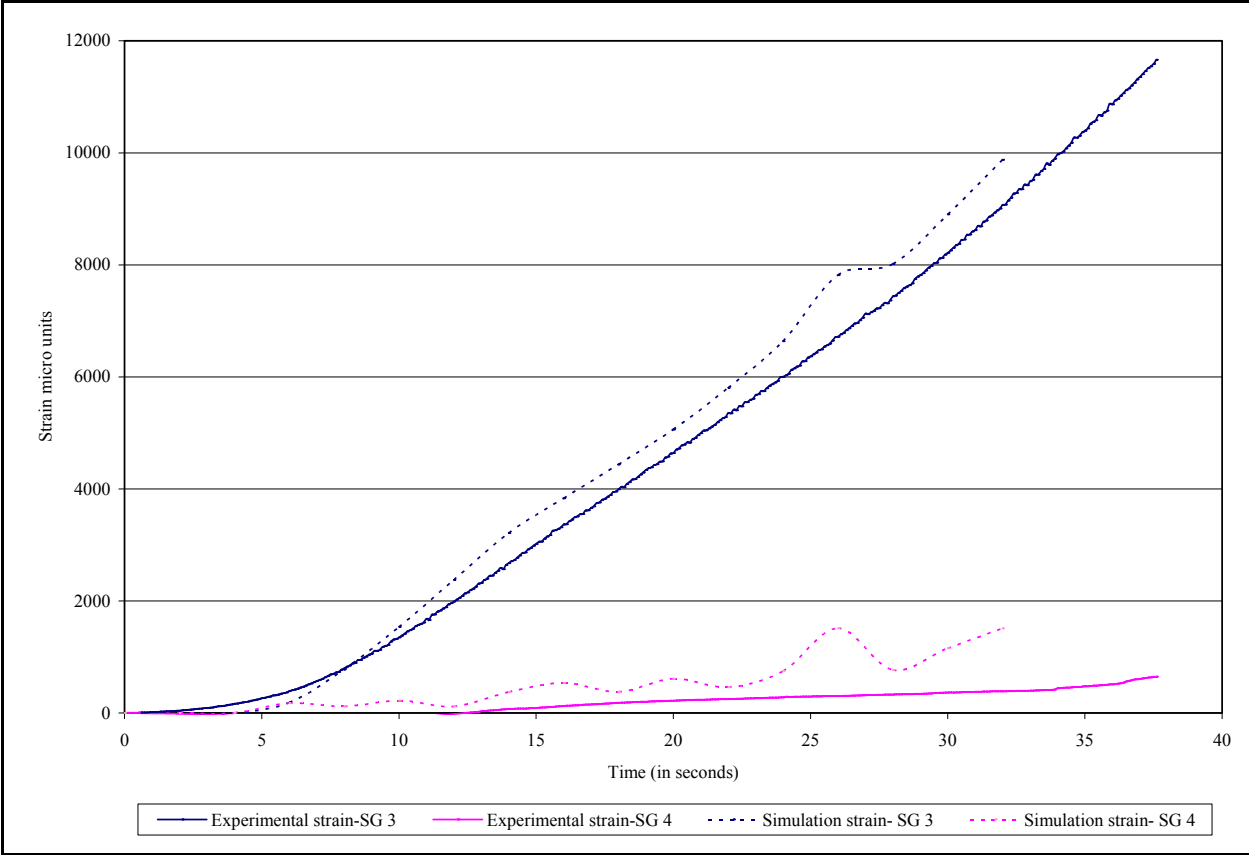
**Figure 117. Experiment versus Simulation for RRPM Type B—
Strains from Strain Gauges 3 and 4.**
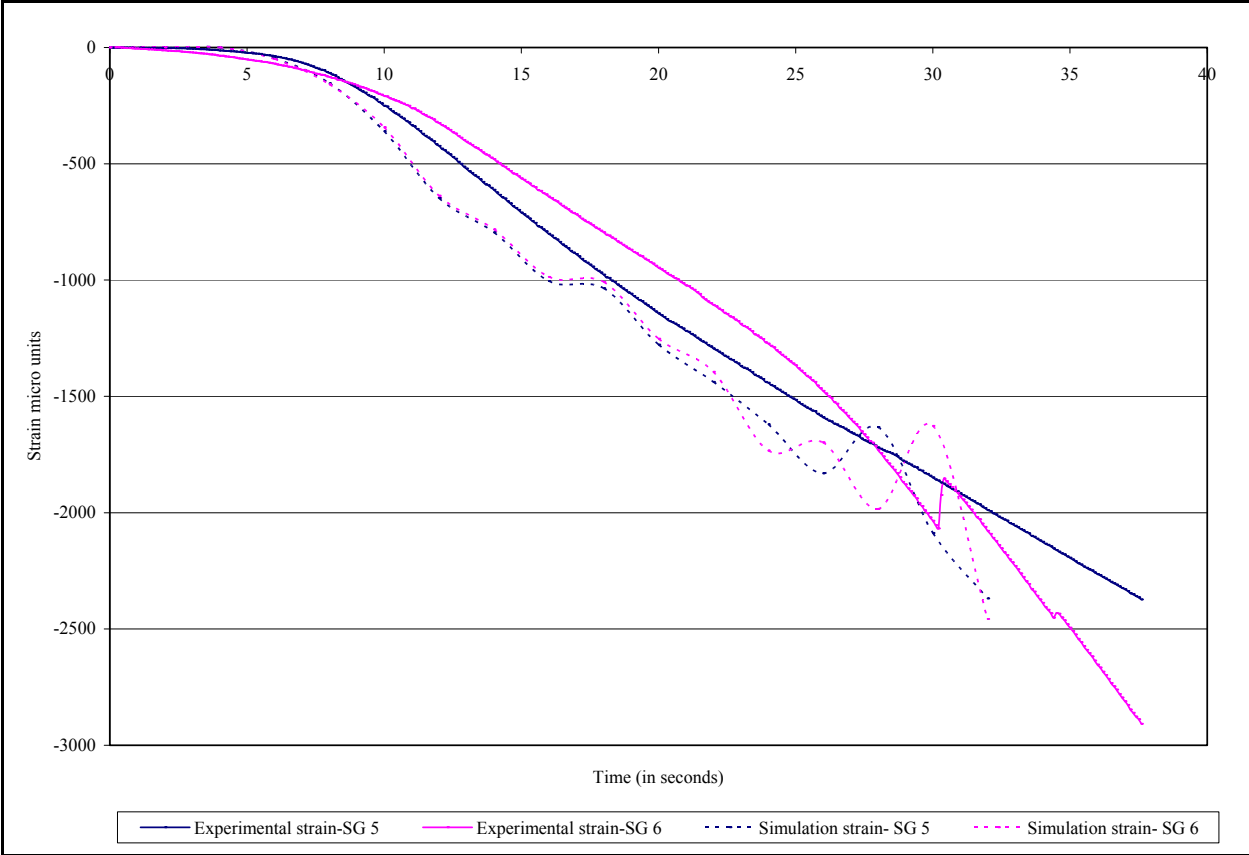
**Figure 118. Experiment versus Simulation for RRPM Type B—
Strains from Strain Gauges 5 and 6.**

APPENDIX B. COMPARISON OF LABORATORY TEST SIMULATIONS

Appendix B provides Figure 119 to Figure 124. Figure 119, Figure 121, and Figure 123 show the percentage differences between Von Mises stresses from the six laboratory test simulations and each stage of the tire-marker impact simulation in finite elements 1-6 for RRPM Type A. Figure 120, Figure 122, and Figure 124 show the percentage differences between Von Mises stresses from the six laboratory test simulations and each stage of the tire-marker impact simulation in finite elements 1-6 for RRPM Type B.
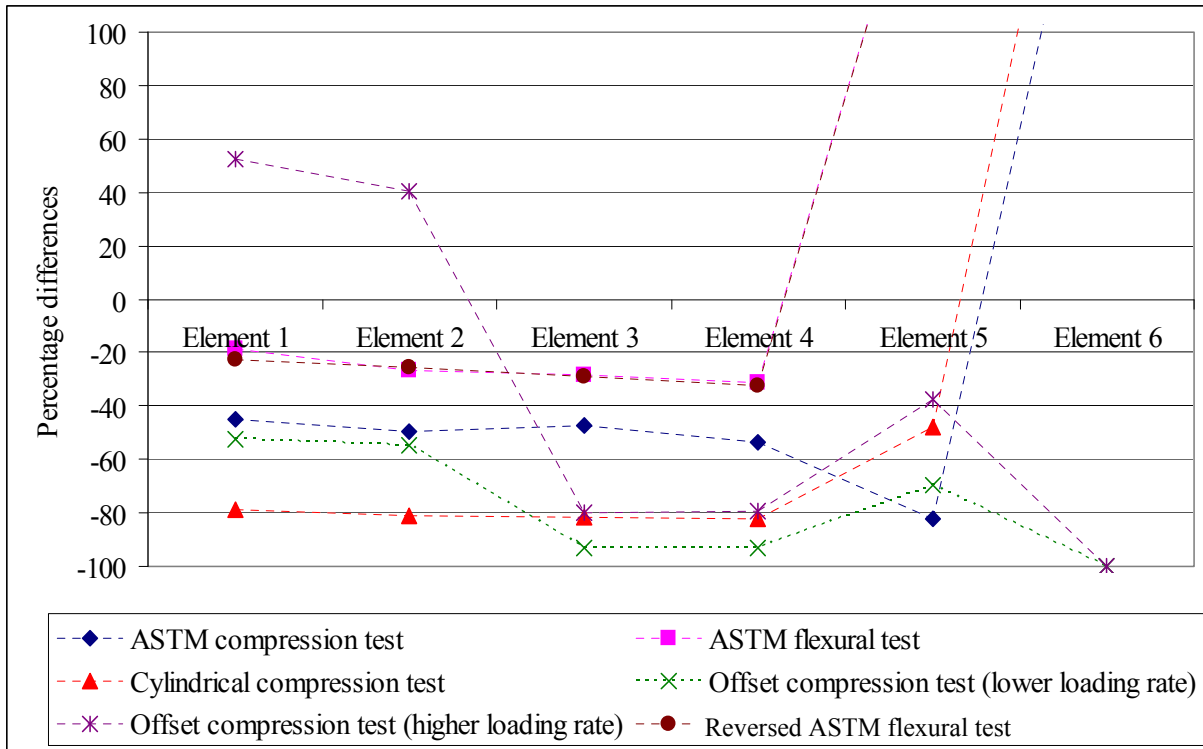
Figure 119. Percentage Differences between Von Mises Stresses from Six Laboratory Test Simulations and Stage 2 of Tire-Marker Impact Simulation in Finite Elements 1-6 (RRPM Type A).
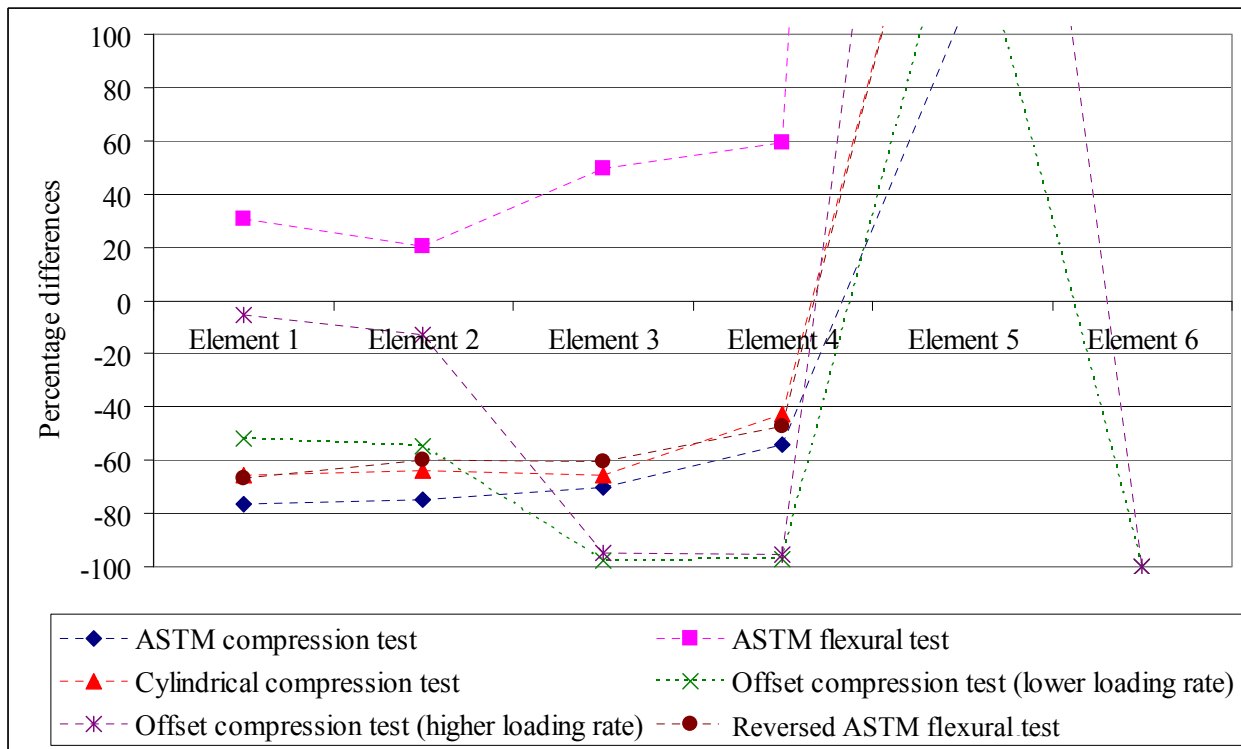
Figure 120. Percentage Differences between Von Mises Stresses from Six Laboratory Test Simulations and Stage 2 of Tire-Marker Impact Simulation in Finite Elements 1-6 (RRPM Type B).
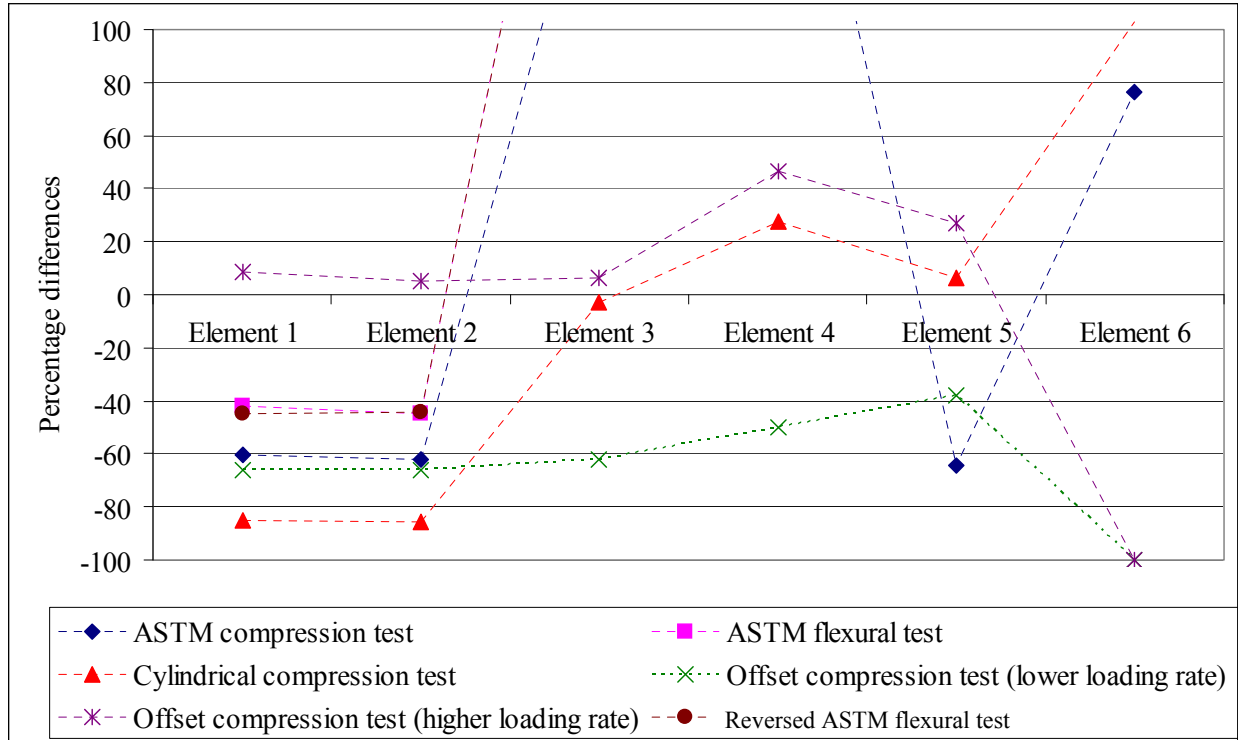
Figure 121. Percentage Differences between Von Mises Stresses from Six Laboratory Test Simulations and Stage 1 of Tire-Marker Impact Simulation in Finite Elements 1-6 (RRPM Type A).
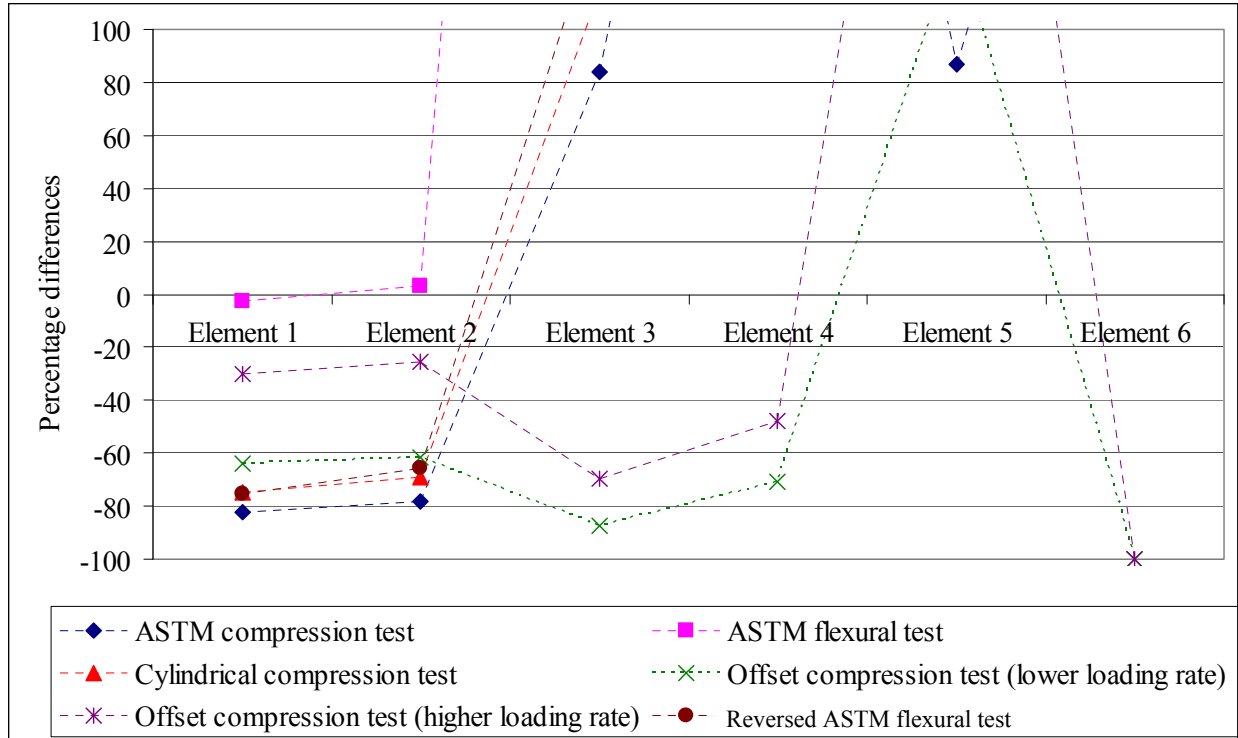
Figure 122. Percentage Differences between Von Mises Stresses from Six Laboratory Test Simulations and Stage 1 of Tire-Marker Impact Simulation in Finite Elements 1-6 (RRPM Type B).
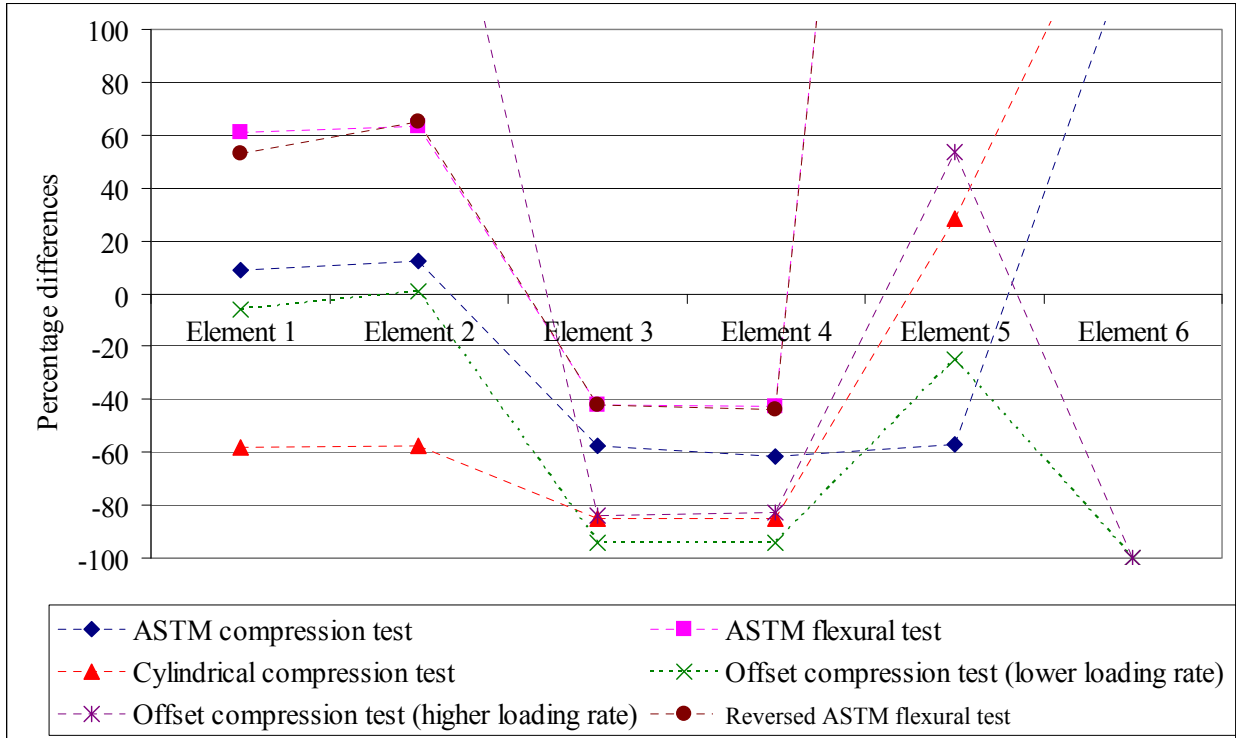
Figure 123. Percentage Differences between Von Mises Stresses from Six Laboratory Test Simulations and Stage 3 of Tire-Marker Impact Simulation in Finite Elements 1-6 (RRPM Type A).
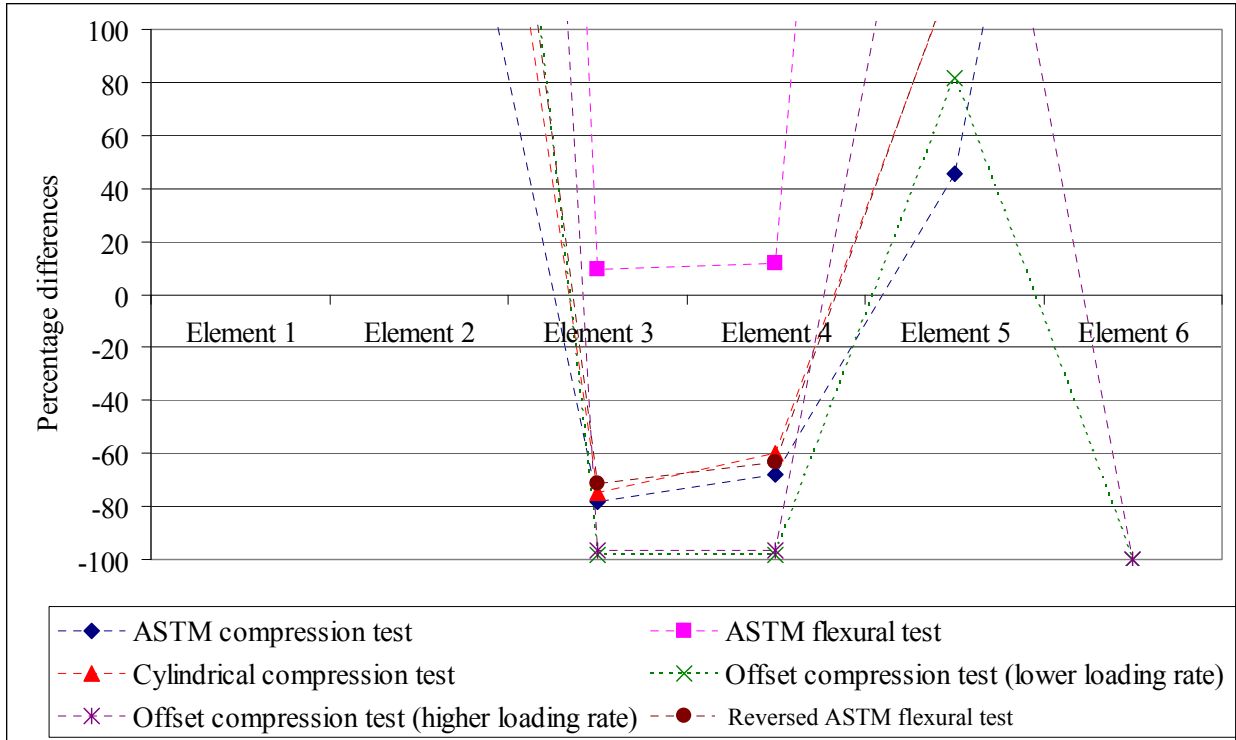
Figure 124. Percentage Differences between Von Mises Stresses from Six Laboratory Test Simulations and Stage 3 of Tire-Marker Impact Simulation in Finite Elements 1-6 (RRPM Type B).

APPENDIX C. FIELD DATA FOR RETROREFLECTIVITY AND MARKER RATING

Table 27. Retroreflectivity Values for New Markers.

		Apex 921	Apex 9003	AD88	AD80	Ray-O-Lite	3M
White	Average	535.9	731.9	1148.0	1368.5	826.9	784.8
	STD*	256.5	233.7	324.8	203.2	185.2	160.2
	Max.	980	1499	1645	1723	1241	1073
	Min.	139	363	546	980	555	391
Yellow Combined	Average	525	556	796	821	613	677
	STD	186.1	247.0	123.1	114.2	144.9	153.1
	Max.	966	1271	1077	1117	894	974
	Min.	221	185	622	579	329	257

* STD: standard deviation

Table 28. Six-Month Retroreflectivity Values from Field Decks.

		Apex 921	Apex 9003	AD88	AD80	Ray-O-Lite	3M	AD80 with GulfStates
Houston	Average	32.9	43.3	157.6	245.5	146.6	133.9	220.2
White/concrete	STD	9.17878	16.13988	52.84312	86.16613	53.12655	49.9905	117.19
	Max.	48	87	251	355	239	221	355
	Min.	17	20	81	48	42	66	48
Laredo	Average	52.7	95.8	388.8	351.2	288.2	274.0	
White/asphalt	STD	22.89	30.59	160.85	88.19	54.84	106.91	
	Max.	108	178	603	534	397	491	
	Min.	21	34	13	134	219	46	
Laredo	Average	76.1	97.9	413.8	305.7	361.4	381.5	393.8
White/concrete	STD	26.15	22.99	128.64	80.42	93.10	147.74	117.92
	Max.	114	151	668	518	559	583	668
	Min.	21	65	139	158	242	86	241
Bryan	Average	35.8	51.7	127.2	122.1	66.8	201.9	
Yellow/seal coat	STD	14.03	35.93	53.39	27.69	40.48	68.18	
	Max.	70	161	289	177	175	424	
	Min.	6	12	60	83	17	108	
Lufkin	Average	48.4	67.1	233.5	179.9	201.1	163.8	
Yellow/seal coat	STD	25.06	27.57	58.14	54.85	75.42	68.26	
	Max.	104	146	435	343	479	381	
	Min.	8	19	140	85	67	49	
	% loss	0	0	0	0	0	0	

Table 29. Twelve-Month Retroreflectivity Values from Field Decks.

		Apex 921	Apex 9003	AD88	AD80	Ray-O-Lite	3M	AD80 with GulfStates
Houston	Average	12.5	Replaced	Replaced	13.8	29.6	24.1	9.5
White/concrete	STD	4.20			5.91	17.18	9.22	4.95
	Max.	17			20	57	38	13
	Min.	7			6	6	7	6
Laredo	Average	25.6	41.8	112.0	42.7	136.7	140.3	
White/asphalt	STD	6.50	11.92	57.96	8.24	32.94	61.62	
	Max.	35	67	208	56	189	316	
	Min.	14	25	20	27	52	29	
Laredo	Average	36.1	42.3	130.8	21.3	113.9	144.6	20.1
White/concrete	STD	13.54	8.99	56.16	4.04	15.56	59.23	5.59
	Max.	61	61	230	28	143	266	28
	Min.	7	24	59	11	85	33	11
Bryan	Average	16.7	25.2	92.8	34.9	35.8	105.4	
Yellow/seal coat	STD	4.25	11.29	37.53	10.38	29.71	22.39	
	Max.	25	61	149	50	116	137	
	Min.	10	13	38	22	13	55	
Lufkin	Average	33.4	29.3	166.4	47.0	128.8	184.7	
Yellow/seal coat	STD	21.92	15.95	66.41	21.21	49.05	85.16	
	Max.	84	80	347	111	303	357	
	Min.	7	10	44	16	55	49	

Table 30. Eighteen-Month Retroreflectivity Values from Field Decks.

		Apex 921	Apex 9003	AD88	AD80	Ray-O-Lite	3M	AD80 with GulfStates
Laredo White/asphalt	Average	13.1	11.3	57.1	12.9	72.2	61.9	
	STD	6.23	9.01	64.94	4.46	26.60	35.33	
	Max.	25	35	220	21	114	151	
	Min.	1	0	0	1	0	5	
Laredo White/concrete	Average	7.4	3.5	31.1	1.4	36.2	43.7	1.8
	STD	3.93	1.67	26.90	1.06	15.37	25.14	1.04
	Max.	14	7	96	3	60	99	3
	Min.	0	1	2	0	7	2	0
Bryan Yellow/seal coat	Average	4.4	5.2	34.8	11.5	10.2	24.4	
	STD	3.01	4.11	24.81	6.61	14.99	22.96	
	Max.	12	20	115	27	64	109	
	Min.	0	0	5	2	0	0	
Lufkin Yellow/seal coat	Average	10.4	10.5	127.5	47.0	146.2	121.8	
	STD	9.23	8.04	60.34	28.97	64.69	56.05	
	Max.	41	40	316	121	327	287	
	Min.	0	0	35	6	52	32	

Table 31. Twenty-Four-Month Retroreflectivity Values from Field Decks.

		Apex 921	Apex 9003	AD88	AD80	Ray-O-Lite	3M	AD80 with GulfStates
Laredo White/asphalt	Average	14.5	12.2	31.7	3.2	28.3	65.7	
	STD	15	13	15	3	30	66.5	
	Max.	6.19	9.34	38.91	1.56	11.72	28.33	
	Min.	26	38	131	7	46	120	
Laredo White/concrete	Average	14.5	14.0	19.0	0.6	8.7	45.9	0.5
	STD	9.39	4.63	11.26	0.65	3.49	15.13	0
	Max.	33	19	36	2	14	79	0.76
	Min.	0	2	0	0	2	26	2
Bryan Yellow/seal coat	Average	6.1	7.4	27.2	6.5	12.2	39.8	
	STD	4.15	4.76	18.51	3.12	10.36	17.38	
	Max.	15	19	80	11	41	68	
	Min.	0	1	6	1	1	15	
Lufkin Yellow/seal coat	Average	11.6	10.1	112.0	22.1	50.1	164.3	
	STD	11.24	12.05	63.92	13.40	28.26	66.23	
	Max.	44	53	270	51	119	297	
	Min.	0	0	17	0	8	47	

Table 32. Six-Month Marker Rating.

		Apex 921	Apex 9003	AD88	AD80	Ray-O-Lite	3M
Houston White/concrete	Marker case	3.69	3.94	4.44	3.69	4.48	3.94
	Lens surface	3.81	3.75	4.31	3.62	4.48	3.88
	Lens interior	3.81	3.88	4.25	3.77	4.52	4.00
	Average	3.77	3.85	4.33	3.69	4.49	3.94
Laredo White/asphalt	Marker case	3.78	3.97	3.81	4.00	4.94	4.28
	Lens surface	3.97	3.91	3.81	3.97	4.84	4.22
	Lens interior	4.06	4.03	4.00	3.97	4.97	4.19
	Average	3.94	3.97	3.88	3.98	4.92	4.23
Laredo White/concrete	Marker case	3.94	4.00	4.50	4.00	4.38	4.00
	Lens surface	3.81	3.94	4.42	4.00	4.38	4.19
	Lens interior	4.00	4.00	4.46	4.00	4.63	4.31
	Average	3.92	3.98	4.46	4.00	4.46	4.17
Bryan Yellow/seal coat	Marker case	3.97	4.00	4.75	3.94	4.81	4.00
	Lens surface	3.97	4.00	4.75	3.94	5.00	3.94
	Lens interior	4.00	4.00	4.94	3.94	5.00	4.00
	Average	3.98	4.00	4.81	3.94	4.94	3.98
Lufkin Yellow/seal coat	Marker case	4.03	4.44	4.72	4.75	4.97	5.00
	Lens surface	4.53	4.53	4.94	4.88	4.94	5.00
	Lens interior	4.53	4.53	4.97	4.97	4.97	5.00
	Average	4.36	4.50	4.88	4.86	4.96	5.00

Table 33. Twelve-Month Marker Rating.

		Apex 921	Apex 9003	AD88	AD80	Ray-O-Lite	3M
Houston	Marker case	3.00	Replaced	Replaced	3.50	4.46	3.94
White/concrete	Lens surface	3.25			3.50	4.08	3.94
	Lens interior	3.25			3.50	4.38	4.00
	Average	3.17			3.50	4.31	3.96
Laredo	Marker case	2.50	3.31	3.22	4.00	4.78	4.06
White/asphalt	Lens surface	3.50	3.84	3.47	3.97	4.81	3.88
	Lens interior	3.94	4.00	3.91	4.00	4.97	4.13
	Average	3.31	3.72	3.53	3.99	4.85	4.02
Laredo	Marker case	4.00	4.00	3.50	4.00	4.40	3.75
White/concrete	Lens surface	3.57	3.88	3.25	3.91	4.33	3.69
	Lens interior	3.86	4.00	3.92	4.00	4.60	3.69
	Average	3.81	3.96	3.56	3.97	4.44	3.71
Bryan	Marker case	3.85	4.07	4.38	3.81	4.14	4.00
Yellow/seal coat	Lens surface	3.85	4.07	4.38	3.88	4.29	4.00
	Lens interior	3.85	4.07	4.38	4.00	4.43	4.00
	Average	3.85	4.07	4.38	3.90	4.29	4.00
Lufkin	Marker case	3.81	4.00	4.00	4.00	4.81	5.00
Yellow/seal coat	Lens surface	3.81	4.00	4.00	4.00	4.91	5.00
	Lens interior	3.81	4.00	4.00	4.00	4.94	5.00
	Average	3.81	4.00	4.00	4.00	4.89	5.00

Table 34. Eighteen-Month Marker Rating.

		Apex 921	Apex 9003	AD88	AD80	Ray-O-Lite	3M
Laredo White/asphalt	Marker case	2.00	2.63	2.03	4.00	4.72	3.81
	Lens surface	3.38	3.31	2.56	3.67	4.19	3.38
	Lens interior	3.63	3.25	2.50	3.83	4.59	3.53
	Average	3.00	3.06	2.36	3.83	4.50	3.57
Laredo White/concrete	Marker case	3.08	4.00	3.75	4.00	4.47	3.50
	Lens surface	2.85	3.63	3.00	3.47	4.07	3.44
	Lens interior	2.85	3.81	3.17	3.80	4.40	3.69
	Average	2.92	3.81	3.31	3.76	4.31	3.54
Bryan Yellow/seal coat	Marker case	3.00	4.00	4.00	3.88	3.50	4.00
	Lens surface	3.41	4.00	4.00	3.81	3.75	4.00
	Lens interior	3.41	4.00	4.00	3.88	3.94	4.00
	Average	3.27	4.00	4.00	3.85	3.73	4.00
Lufkin Yellow/seal coat	Marker case	3.69	3.97	4.00	4.00	4.94	5.00
	Lens surface	3.72	3.97	4.00	4.00	4.94	5.00
	Lens interior	3.72	4.00	4.00	4.00	4.94	5.00
	Average	3.71	3.98	4.00	4.00	4.94	5.00

Table 35. Twenty-Four-Month Marker Rating.

		Apex 921	Apex 9003	AD88	AD80	Ray-O-Lite	3M
Laredo White/asphalt	Marker case	2.00	2.72	2.19	3.69	3.91	3.81
	Lens surface	3.00	2.91	2.69	2.72	3.59	3.44
	Lens interior	3.31	3.22	2.53	2.75	3.81	3.78
	Average	2.77	2.95	2.47	3.05	3.77	3.68
Laredo White/concrete	Marker case	2.63	3.75	3.75	3.73	4.06	3.44
	Lens surface	2.50	3.25	3.00	2.27	3.44	3.31
	Lens interior	2.50	3.31	2.92	2.13	3.50	3.38
	Average	2.54	3.44	3.22	2.71	3.67	3.38
Bryan Yellow/seal coat	Marker case	3.09	3.96	3.63	3.81	3.44	4.00
	Lens surface	3.41	4.00	3.69	3.75	3.69	4.00
	Lens interior	3.41	4.00	3.75	3.81	3.88	4.00
	Average	3.30	3.99	3.69	3.79	3.67	4.00
Lufkin Yellow/seal coat	Marker case	2.81	3.44	3.91	3.97	4.94	5.00
	Lens surface	3.66	3.88	3.97	4.00	4.94	5.00
	Lens interior	3.66	4.00	3.97	4.00	4.94	5.00
	Average	3.38	3.77	3.95	3.99	4.94	5.00